Global marine ecosystem response to a strong AMOC weakening under low and high future emission scenarios

Amber Adore Boot[1], Jeroen Gerhard Steenbeek[2], Marta Coll[3], Anna S. von der Heydt[4], and Henk A. Dijkstra[5]

[1]Institute for Marine and Atmospheric Research Utrecht
[2]Ecopath International Initiative (EII)
[3]Institute of Marine Science (ICM-CSIC), Barcelona, Spain
[4]Institute for Marine and Atmospheric research Utrecht, Utrecht University
[5]Institute for Marine and Atmospheric research Utrecht

April 15, 2024

Abstract

Marine ecosystems provide essential services to the Earth System and society. These ecosystems are threatened by anthropogenic activities and climate change. Climate change increases the risk of passing tipping points; for example, the Atlantic Meridional Overturning Circulation (AMOC) might tip under future global warming leading to additional changes in the climate system. Here, we look at the effect of an AMOC weakening on marine ecosystems by forcing the Community Earth System Model v2 (CESM2) with low (SSP1-2.6) and high (SSP5-8.5) emission scenarios from 2015 to 2100. An additional freshwater flux is added in the North Atlantic to induce extra weakening of the AMOC. In CESM2, the AMOC weakening has a large impact on phytoplankton biomass and temperature fields through various mechanisms that change the supply of nutrients to the surface ocean. We drive a marine ecosystem model, EcoOcean, with phytoplankton biomass and temperature fields from CESM2. In EcoOcean, we see negative impacts in Total System Biomass (TSB), which are larger for high trophic level organisms. The strongest net effect is seen in the high emission scenario, but the effect of the extra AMOC weakening on TSB is larger in the low emission scenario. On top of anthropogenic climate change, TSB decreases by -3.78% and -2.03% in SSP1-2.6 and SSP5-8.5, respectively due to the AMOC weakening. These results show that marine ecosystems will be under increased threat if the AMOC weakens which might put additional stresses on socio-economic systems that are dependent on marine biodiversity as a food and income source.

Global marine ecosystem response to a strong AMOC weakening under low and high future emission scenarios

A. A. Boot[1], J. Steenbeek[2], M. Coll[2,3], A. S. von der Heydt[1,4], and H. A. Dijkstra[1,4]

[1]Institute for Marine and Atmospheric research Utrecht, Department of Physics,Utrecht University, Utrecht, the Netherlands
[2]Ecopath International Initiative (EII) Research Association, Barcelona, Spain
[3]Department of Marine Renewal Resources, Institute of Marine Science (ICM-CSIC), Barcelona, Spain
[4]Center for Complex Systems Studies, Utrecht University, Utrecht, the Netherlands

Key Points:

- Marine ecosystems are negatively affected by a weakening of the Atlantic Meridional Overturning Circulation.
- Mechanisms involve changes in nutrient transport and subsequent phytoplankton response leading to changes in the food web.
- Regional responses depend strongly on shifts in phytoplankton dominance.

Corresponding author: Amber A. Boot, `a.a.boot@uu.nl`

Abstract

Marine ecosystems provide essential services to the Earth System and society. These ecosystems are threatened by anthropogenic activities and climate change. Climate change increases the risk of passing tipping points; for example, the Atlantic Meridional Overturning Circulation (AMOC) might tip under future global warming leading to additional changes in the climate system. Here, we look at the effect of an AMOC weakening on marine ecosystems by forcing the Community Earth System Model v2 (CESM2) with low (SSP1-2.6) and high (SSP5-8.5) emission scenarios from 2015 to 2100. An additional freshwater flux is added in the North Atlantic to induce an extra weakening the AMOC. In CESM2, the AMOC weakening has a large impact on phytoplankton biomass and temperature fields through various mechanisms that change the supply of nutrients to the surface ocean. We drive a marine ecosystem model, EcoOcean, with phytoplankton biomass and temperature fields from CESM2. In EcoOcean, we see negative impacts in Total System Biomass (TSB), which are larger for high trophic level organisms. The strongest net effect is seen in the high emission scenario, but the effect of the extra AMOC weakening on TSB is larger in the low emission scenario. On top of anthropogenic climate change, TSB decreases by -3.78% and -2.03% in SSP1-2.6 and SSP5-8.5, respectively due to the AMOC weakening. These results show that marine ecosystems will be under increased threat if the AMOC weakens which might put additional stresses on socio-economic systems that are dependent on marine biodiversity as a food and income source.

Plain Language Summary

Marine ecosystems provide essential services to the Earth System and society. These ecosystems are threatened by anthropogenic activities and climate change. Climate change might also lead to a strong weakening of the Atlantic Meridional Overturning Circulation (AMOC). Here, we use a complex Earth System Model and a Marine Ecosystem Model to study how marine ecosystems respond to a strong AMOC weakening in possible future climates (2015-2100) under low and high emission scenarios. The AMOC weakening affects the climate system through various mechanisms that change the supply of nutrients to the surface ocean, affecting the primary production by phytoplankton. We find that the AMOC weakening leads to a decrease in phytoplankton biomass that is larger higher up the food chain. In total, marine ecosystems lose -3.78% and -2.03% of biomass in the low and high emission scenarios respectively. These results show that marine ecosystems will be under increased threat if the AMOC weakens.

Keywords: Atlantic Meridional Overturning Circulation, Climate Change, Marine Ecosystems, Earth System Modelling, Marine Ecosystem Modelling, Tipping Points

1 Introduction

Anthropogenic climate change and other anthropogenic activities, such as overfishing and pollution, are a major threat for marine ecosystems and the services they provide. One of the services marine ecosystems provide is food for (human) consumption. It is estimated that the ocean provides 11% of animal protein that humans consume (Gattuso et al., 2015; FAO, 2022), and besides providing food, it also provides income through the fishery industry. Furthermore, marine ecosystems are estimated to export 11 Gigatonnes of carbon (GtC) each year from the surface to the deep ocean (Sanders et al., 2014), and without this export, atmospheric pCO_2 would be 200-400 ppm higher (Henson et al., 2022; Ito & Follows, 2005). Major changes in marine ecosystems can therefore have an important impact on both socio-economic systems and the climate system, making it very relevant to be able to make reliable projections on the future development of these ecosystems (Lotze et al., 2019; Tittensor et al., 2021).

Evidence of the impact of anthropogenic climate change on marine ecosystems is already apparent. Observations show, for example, a reduction in ocean productivity, changes in food webs, biogeographical shifts, and bleaching of warm water corals (Hoegh-Guldberg & Bruno, 2010; Doney et al., 2012; Gattuso et al., 2015; IPCC, 2022). The effects of climate change can propagate through the ecosystems in bottom-up and top-down direction, causing possible cascades in the ecosystem (Doney et al., 2012; Lotze et al., 2019). Another consequence of climate change is the expansion of hypoxic regions, especially those found along productive regions (Diaz & Rosenberg, 2008; Breitburg et al., 2018), which already has led to mass mortalities (Doney et al., 2012; Sampaio et al., 2021).

It has been suggested that many organisms in the ocean are at a very high risk of impact by climate change by 2100 (Gattuso et al., 2015; Coll et al., 2020), and the function of marine ecosystems is threatened by a possible loss of ecological resilience (Henson et al., 2021). As the climate warms, so does the probability of marine heat waves, which have been shown to have detrimental effects on ecosystems (Smale et al., 2019). Most CMIP6 (Eyring et al., 2016) Earth System Models (ESMs) project a future decrease in Net Primary Production (NPP). However, the intermodel spread in these projections is large and this spread has even increased compared to CMIP5 ESMs (Kwiatkowski et al., 2020; Tagliabue et al., 2021; Henson et al., 2022). Marine Ecosystem Models (MEMs) using input from two CMIP6 ESMs, project a decrease in Total System Biomass (TSB) in both a low and a high emission scenarios even though there is substantial spread in NPP in the ESMs (Tittensor et al., 2021).

Climate warming is not only a risk to marine ecosystems, it might also lead to tipping in the Earth System (Lenton et al., 2008; McKay et al., 2022). Passing a tipping point is a serious risk since the consequences of tipping are irreversible and can therefore be disastrous. A major tipping element in the ocean is the Atlantic Meridional Overturning Circulation (AMOC). The AMOC potentially has two stable states: an on-state reflecting the current AMOC regime with a strong circulation, and an off-state reflecting a weak or collapsed AMOC (Weijer et al., 2019). Tipping of the AMOC would lead to several changes in the Earth System affecting the entire globe. In the on-state the AMOC is responsible for a net transport of heat from the Southern Hemisphere across the equator to the Northern Hemisphere of 0.5 PW (Liu et al., 2017; Forget & Ferreira, 2019) thereby strongly influencing observed surface air temperature patterns. An AMOC collapse is expected to result in a cooling in the Northern Hemisphere and warming in the Southern Hemisphere, a southward shift of the Intertropical Convergene Zonce (ITCZ), and a strengthening of the trade winds (van Westen & Dijkstra, 2023a; Orihuela-Pinto et al., 2022; Caesar et al., 2018). As a response to the cooling, Arctic sea-ice extent is expected to increase under AMOC weakening or collapse. Besides the direct changes in advection due to an AMOC collapse, an AMOC weakening can also change important ocean characteristics such as the stratification and upwelling rates. Several studies have shown the impact this can have on the marine carbon cycle and the uptake capacity of the ocean (Zickfeld et al., 2008; Boot, von der Heydt, & Dijkstra, 2024). The changes in stratification and upwelling rates are specifically interesting for marine ecosystems, and through these processes, an AMOC weakening can impact marine primary productivity (Schmittner, 2005). The changes in ocean circulation also alter the connectivity in the ocean which can be relevant for environmental niches of plankton species, especially when their thermal constraints are taken into account (Manral et al., 2023). This provides a bottom-up control on marine ecosystems potentially threatening important ecosystem services and a pathway of cascading tipping from the physical climate system into marine ecosystems (Brovkin et al., 2021).

There are studies that suggest that the AMOC has been weakening over the past century (Caesar et al., 2018), and that the AMOC might tip between 2025 and 2095 (Ditlevsen & Ditlevsen, 2023). These studies are based on uncertain proxy data and are contested by some other studies (Worthington et al., 2021). However, a recent study using a physics based early warning signal shows that the AMOC is indeed on tipping course (van Westen et al., 2024). In CMIP6, the models show a consistent weakening of the AMOC across almost all emission scenarios, but no AMOC collapse is simulated up to 2100 (Weijer et al., 2020). However, this might be explained by the fact that the CMIP6 models are biased towards a too stable AMOC (van Westen & Dijkstra, 2023b) and might therefore underestimate the probability of a collapse.

In this study, we examine the impact of a strong AMOC weakening on marine ecosystems under anthropogenic climate change. We do this by analysing several simulations of the Community Earth System Model v2 (CESM2; Danabasoglu et al., 2020) where we use both a low and a high emission scenario, and simulations where we artificially weaken the AMOC by applying a surface freshwater flux to the North Atlantic Ocean. Since the ecosystem component in CESM2 is limited to three different phytoplankton groups and only one zooplankton group, we use the marine ecosystem model (MEM) EcoOcean (Coll et al., 2020) to simulate more detailed ecosystem dynamics. We force EcoOcean, a MEM part of FishMIP (Tittensor et al., 2018, 2021), with the output of the CESM2 simulations. Our results demonstrate the far reaching effects that a weakening of the AMOC can have on the marine ecosystem.

2 Methods

2.1 Earth System Model

The Community Earth System Model v2 (CESM2) is a state-of-the-art Earth System Model that is part of CMIP6. It has modules that represent the atmosphere (the Community Atmosphere Model v6), the land (the Community Land Model v5; Lawrence et al., 2019), sea ice (CICE5; Hunke et al., 2015), and the ocean (the Parallel Ocean Program v2, POP2; Smith et al., 2010) including ocean biogeochemistry (the Marine Biogeochemical Library, MARBL; Long et al., 2021). In this study we use the default CMIP6 version of CESM2, meaning that ice sheets and vegetation type are prescribed. All models are run on a nominal resolution of 1°, but the exact grid differs between the modules. Important for this study are the ocean modules POP2 and MARBL. These are both run on a displaced grid with a pole in Greenland. The vertical grid consists of 60 different layers with a thickness of 10 m in the top 150 m, after which the layer thickness increases to 250 m at 3500 m depth, staying constant up to the maximum ocean depth of 5500 m.

The ocean biogeochemistry module in CESM2 is MARBL (Long et al., 2021), which is an updated version of the Biogeochemical Elemental Cycling model (BEC; J. K. Moore et al., 2001, 2004, 2013; C. M. Moore et al., 2013). MARBL resolves three explicit phytoplankton types: diatoms, diazotrophs and small phytoplankton. Calcification is modelled implicitly as part of the small phytoplankton group using a variable rain ratio. Phytoplankton growth is co-limited by light and by silica (Si), phosphorus (P), nitrogen (N) and iron (Fe). Diatoms are the only group that can be limited by Si, and diazotrophs are nitrogen fixers and therefore not limited by N. However, diazotrophs are severely temperature limited if sea surface temperatures (SSTs) are below 15°C. The three phytoplankton types are grazed upon by one zooplankton group that, through differential grazing, implicitly represents multiple zooplankton groups (e.g. micro- and meso zooplankton). Both phyto- and zooplankton have a linear mortality formulation and for zooplankton a parametrized loss term is included that represents higher order trophic grazing. All primary production and consumption takes place in the top 150 m of the water column.

We use the same simulations that are presented in Boot, von der Heydt, and Dijkstra (2024) where the marine and terrestrial carbon cycle response to a strong AMOC weakening is studied. For a more thorough discussion on the simulations we refer the reader to Boot, von der Heydt, and Dijkstra (2024). We use emissions of two different scenarios: a low emission scenario SSP1-2.6 (from here on also referred to as 126), and a high emission scenario SSP5-8.5 (585). For each emission scenario there is a control (CTL) simulation where we force the model only with the emissions of the scenarios, and a simulation where we also apply a uniformly distributed freshwater flux in the North Atlantic Ocean between 50°N and 70°N at a constant rate of 0.5 Sv throughout the entire simulation (HOS simulations). We will refer to the simulations by combining the type and emission scenario, e.g. CTL-585 and HOS-126. All simulations are run from 2015 to 2100 and are initialized from the emission driven NCAR CMIP6 historical ('esm-hist') simulation (Danabasoglu, 2019).

2.2 Marine ecosystem model

We use EcoOcean v2 (Coll et al., 2020), an updated version of EcoOcean v1 (Christensen et al., 2015), which is one of the global, spatiotemporal explicit MEMs contributing to FishMIP (Tittensor et al., 2018, 2021). EcoOcean was originally developed to assess the impact of management strategies on the supply of seafood on a global scale. It is a 2D model with a horizontal resolution of 0.25 to 1° and simulates the time period 1950 to 2100 using monthly time steps. The EcoOcean framework combines several models which can be divided into three main components: (1) a component for marine biogeochemical processes and primary production, (2) a food web component that includes a dynamic niche model and species movement, and (3) a component simulating fisheries. Previously, EcoOcean was driven by simulations of the IPSL (using PISCES for ocean biogeochemistry; Boucher et al., 2020) and the GFDL (using COBALT for ocean biogeochemistry; Dunne et al., 2020) Earth System Models (Tittensor et al., 2018, 2021). In this study, we use the output of MARBL from the CESM2 simulations described in the previous section for component (1), and to match the resolution of CESM2, EcoOcean is used with a 1° resolution. We will not use active fisheries in this study and therefore component (3) is switched off. For a more thorough discussion on EcoOcean and the sensitivity of the model formulation, we refer the reader to Christensen et al. (2015) (v1) and Coll et al. (2020) (v2), and references therein.

The ecosystem module in EcoOcean simulates 52 different functional groups representing over 3400 individual species. Species are grouped together when biological and ecological traits are similar. The functional groups range from bacteria, plankton, different groups of fish, to marine mammals and birds. The different fish groups are differentiated on size (small: < 30 cm, medium: 30-90cm, large: > 90 cm), and grouped on, for example, where they live in the water column, i.e. pelagics, demersals, bathypelagics, bathydemersals, benthopelagics, reef fishes, sharks, rays and flat fishes. For a complete list of all functional groups, see the Supplementary Table 1 from Coll et al. (2020).

The food web model in EcoOcean is based on the 'Foraging Arena Theory' (Walters & Juanes, 1993; Ahrens et al., 2012), and the relative habitat capacity is determined using the Habitat Foraging Capacity Model (HFCM) (Christensen et al., 2014). Based on local predation risks and food availability, groups can move across spatial cells (Walters & Juanes, 1993; Martell et al., 2005; Christensen et al., 2014). The cell suitability in the HFCM is dependent on species native ranges, foraging capacity related to affinities for specific habitat distributions and types, and the response of the functional groups to environmental drivers.

The three phytoplankton groups simulated in the CESM2 are used to drive distributions and magnitude of corresponding planktonic groups in EcoOcean, and three different temperature fields in the CESM2 are used to drive the EcoOcean HFCM. One temperature field is averaged over the top 150 m, a second is depth averaged over the whole column, and the third represents bottom temperatures. Recall that the CESM2 simulations start in 2015 initialized from NCAR CMIP6 historical simulations (Danabasoglu, 2019). To run EcoOcean accurately, it needs to be calibrated to observations in the period 1950 to 2015. To be able to do this, we need also input variables for this period. The CESM2 simulations used in this study start at 2015 and are branched of from historical CMIP6 CESM2 simulations performed by NCAR. Unfortunately, not all necessary input variables to calibrate EcoOcean are available for the period 1950 to 2015 from these simulations and therefore we can not accurately calibrate EcoOcean to observations. We will therefore use relative changes in biomass B, defined as $\frac{B(t=2099)-B(t=2015)}{B(t=2015)} \times 100\%$, to assess the effect of the AMOC weakening on marine biomass. To spin up EcoOcean, we repeat the 2015 forcing of the CESM2 simulations in EcoOcean until a quasi-steady state is reached to replace the 1950-2015 calibration period. We look at three different aggregated groups of marine biomass: Total system biomass (TSB), total consumer biomass (TCB), and total commercial biomass (COM). For a definition of the three groups in EcoOcean see the supplementary material (Supplementary Table 1) of Coll et al. (2020).

3 Results

3.1 CESM2 Climate response

In both emission scenarios, the greenhouse gas emissions cause an increase in CO_2 concentration and warming. In CTL-585, CO_2 concentrations increase up to 1094 ppm in 2100, whereas CTL-126 has a maximum concentration in 2055 after which it decreases to 434 ppm due to negative emissions (Fig. 1a). The difference in atmospheric pCO_2 also result in a different Global Mean Surface Temperature (GMST), with around 5°C warming in CTL-585, and 1°C warming in CTL-126 (Fig. 1b). The forcing of the model causes a near linear weakening of the AMOC of around 50% for both emission scenarios, with a 2 Sv stronger weakening in CTL-585 (Fig. 1c). In the HOS simulations, the AMOC weakens much faster and stronger compared to the CTL simulations (Fig. 1c, f) as a response to the freshwater forcing. The maximum difference between the HOS and CTL simulations is around 8 Sv in the 2040's, and then decreases again (Fig. 1f). Due to the AMOC weakening, GMST warming is reduced following a similar trend as the reduction in AMOC strength (Fig. 1e). Also the spatial pattern of warming is affected by the AMOC weakening. The reduced northward heat transport in the HOS simulations causes relative cooling of both surface air temperature (SAT; Fig. S1) and sea surface temperature (SST; Fig. 2) in the Northern Hemisphere and relative warming in the Southern Hemisphere compared to the CTL simulations. The response in atmospheric pCO_2 to the hosing is small (Fig. 1d) related to many compensating effects within the carbon cycle (see Boot, von der Heydt, & Dijkstra, 2024).

The different temperature distribution in the HOS simulations compared to the CTL simulations causes atmospheric adjustments resulting in a southward shift of the ITCZ (Fig. S2), and a strengthening of the Northern Hemispheric trade winds (Fig. S3), both of which have an important influence on the surface stratification of the ocean (Fig. S4) and upwelling rates (Fig. S5). As a consequence to the relatively cooler Northern Hemisphere, Arctic sea-ice extent increases in both HOS simulations compared to their respective CTL simulations (Fig. S6). At the end of the simulation, the sea ice extent in HOS-126 is actually larger in 2100 compared to 2015, and also much larger compared to CTL-126 (Fig. S6c). In HOS-585 the strong warming still results in a much reduced Arctic sea-ice cover. However, the melting of the sea ice is much slower and, compared to CTL-585, HOS-585 also has more ice in 2100 (Fig.S6f).

3.2 CESM2 biogeochemical response

The changes in, for example, stratification and upwelling rates influence the nutrient concentrations in the euphotic zone of the ocean. In the CTL simulations, phosphate (PO_4^{3-}) concentrations decrease in the surface ocean almost everywhere (Fig. S7). The strongest responses are seen in the North Atlantic and Arctic Ocean, and in the East-

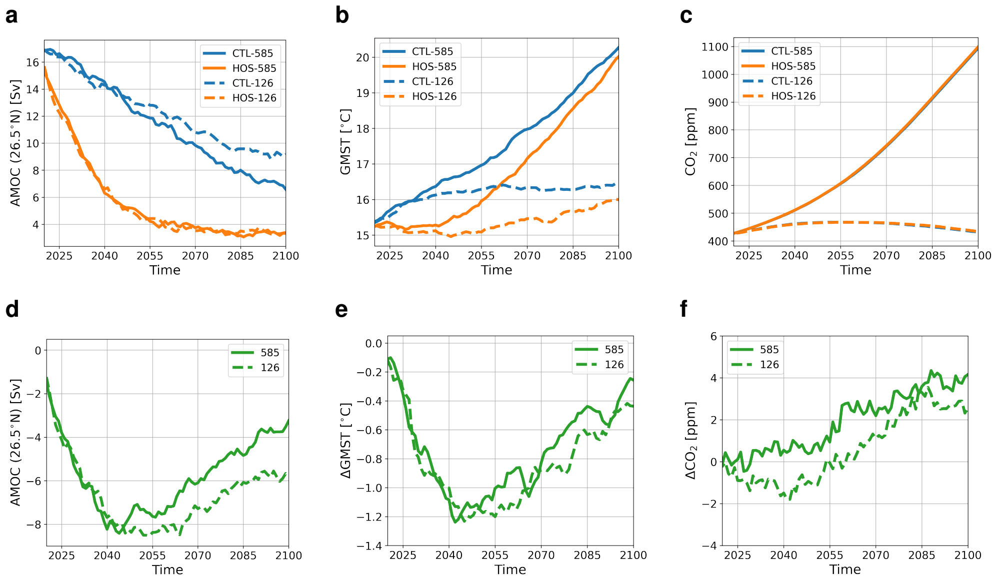

Figure 1. (a) Atmospheric CO_2 concentration in ppm. (b) GMST in °C. (c) AMOC strength at 26.5°N in Sv. In (a-c) blue lines represent the control (CTL) simulations, and orange lines the HOS simulations. (d-f) as in (a-c) but for the difference between the HOS simulations and the control simulations. In all subplots dashed lines represent SSP1-2.6 (126) and solid lines SSP5-8.5 (585). Results are smoothed with a 5 year moving average and represent the period 2020-2100.

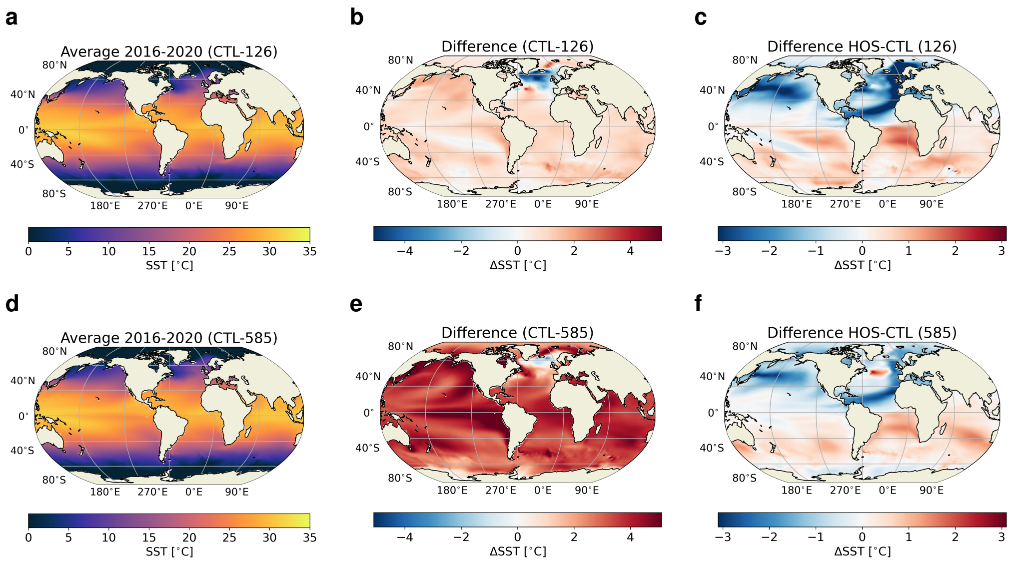

Figure 2. Sea Surface Temperature (SST) in °C for: (a) CTL-126 averaged over 2016-2020, (b) the average over 2016-2020 subtracted from the average over 2095-2099 in CTL-126, (c) CTL-126 subtracted from HOS-126 averaged over 2095-2099, and (d-f) as in (a-c) but for CTL-585 and HOS-585.

ern Equatorial and South Pacific Ocean, with in all regions a stronger response in CTL-585 compared to CTL-126. Nitrate (NO_3^-) concentrations do not decrease everywhere in the ocean in the CTL simulations, but just as with PO_4^{3-}, the strongest responses are seen in the North Atlantic, and Eastern Equatorial and South Pacific Ocean. (Fig. 3) There are also relatively strong decreases in the Northwestern Pacific Ocean. Just as for PO_4^{3-} the response is stronger in CTL-585 compared to CTL-126. Silicate (SiO_3^{2-}) shows a very similar response in the CTL simulations as NO_3^-, except in the Southern Ocean south of 40°S where a large decrease is simulated for both emission scenarios (Fig. S8). The response of iron (Fe) is slightly different compared to the other nutrients in the CTL simulations (Fig. S9). Large increases are seen in the Russian Arctic Ocean, along the equator, and in the subtropical North Atlantic Ocean. The largest descreases are seen in the rest of the Arctic Ocean, and the Northern Indian Ocean. The response in CTL-585 is typically a bit stronger compared to CTL-126, especially in the Eastern Equatorial Pacific, and south of Madagascar.

As a response to the AMOC weakening, there are additional large decreases in PO_4^{3-} concentrations for both scenarios in the North Equatorial Pacific, the Eastern Equatorial and Southern Atlantic, especially in the Benguela Upwelling System. Large increases are seen in the Canary Upwelling System (Fig. S7). The response to the AMOC weakening is very similar for NO_3^- compared to PO_4^{3-} except in the Arctic Ocean, where in the HOS simulations NO_3^- concentrations increase (Fig. 3). The response of SiO_3^{2-} to the AMOC weakening in the HOS simulations is also very similar to the responses in PO_4^{3-} and NO_3^- (Fig. S8). Again the response of Fe to the AMOC weakening in the HOS simulations compared to the CTL simulations differs from the other nutrients (Fig. S9). Most of the Southern Hemisphere sees a relative reduction in surface Fe concentrations except the South Atlantic and a small part of the South Pacific between 0 and 15°S, which actually sees some of the strongest increases relative to the CTL simulations. The North Pacific Ocean also sees relative increases, just as some parts of the North Atlantic and Arctic Ocean. In the Atlantic Ocean between 0 and 25°N, large relative decreases are seen. The two emission scenarios show very similar responses to the AMOC weakening except for some regional differences, such as in the Indian Ocean, and North Atlantic Ocean.

The response of the nutrients to the greenhouse gas emissions induced climate change in the CTL simulations result in changes in Net Primary Production (NPP; Fig. 4) and Export Production (EP; Fig. S10). NPP decreases in the North Atlantic Ocean (north of 30°N) as a response to the greenhouse gas emissions in both scenarios. In CTL-585 there are also large anomalies in the Eastern Equatorial Pacific (positive) and Western Equatorial Pacific (negative). In response to the AMOC weakening, we mostly see changes in the Atlantic basin (decrease) and in the Northeastern Equatorial Pacific (increase). In the Atlantic, the subtropical gyres (north and south) and the Benguela Upwelling System there is a large decrease in NPP, and in the Canary Upwelling System and along the North Equatorial Current there is a large increase in NPP in the HOS simulations compared to the CTL simulations.

The changes in primary productivity are also related to changes in biomass of the three phytoplankton groups. In the CTL simulations, the response of the diazotrophs (Fig. S13) can be mostly explained by the poleward shift of the 15°C isotherm (SST) as a response to the warming. We can see bands of strong increases of biomass along this isotherm with a stronger and more poleward increase in CTL-585 due to the larger warming in this simulation. In the HOS simulations, the 15°C isotherm shifts further poleward in the Southern Hemisphere due to the increased warming observed there compared to the CTL simulations. In the Northern Hemisphere, however, we see in the HOS simulations that this isotherm does not shift poleward, except for the North West Atlantic basin in HOS-585. Also diazotroph biomass decreases along the Iberian peninsula.

The diatoms show large decreases in the subpolar North Atlantic Ocean in the CTL simulations, and in CTL-585 areas with strong increases in the Southern Ocean (Fig. S14).

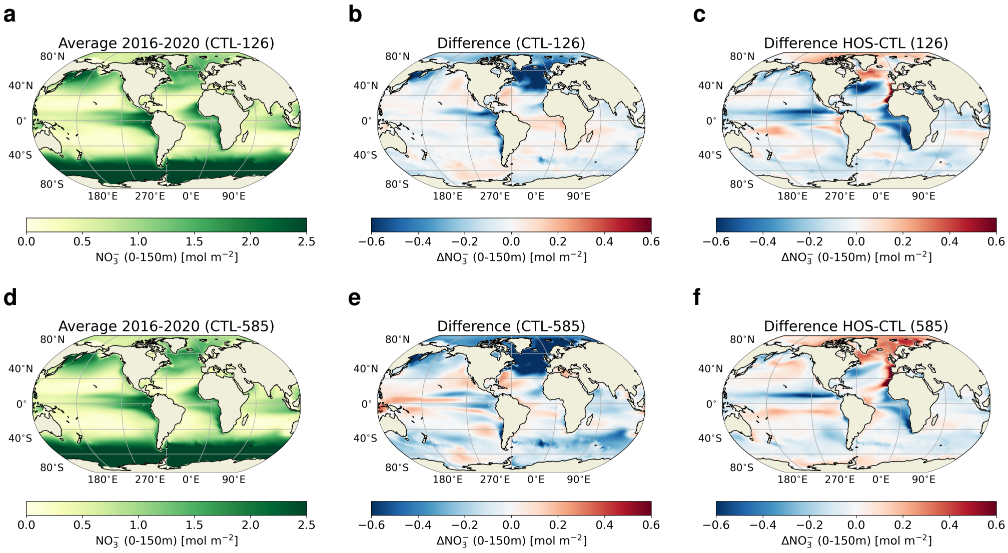

Figure 3. Nitrate (NO_3^-) concentrations integrated over the top 150 m in mol m^{-2} for: (a) CTL-126 averaged over 2016-2020, (b) the average over 2016-2020 subtracted from the average over 2095-2099 in CTL-126, (c) CTL-126 subtracted from HOS-126 averaged over 2095-2099, and (d-f) as in (a-c) but for CTL-585 and HOS-585.

This decrease in the subpolar North Atlantic can partly be explained by increased nutrient limitation due to reduced entrainment of nutrients from subsurface waters related to shallow mixed layer depth in this region. As the diatom biomass decreases, the light limitation for the small phytoplankton is lifted and they are able to outcompete the diatoms resulting in a shift of phytoplankton functional type in this region (Boot et al., 2023). In the HOS simulations, the largest changes in small phytoplankton occur very locally, i.e. between the subtropical and subpolar gyre in the North Atlantic, the Canary Upwelling System, the Benguela Upwelling System, around Tasmania and the equatorial West Pacific. In the CTL simulations, the small phytoplankton generally perform well in regions where diatom biomass decreases and vice versa, which is also the case in the HOS simulations (Fig. S15).

3.3 Role of AMOC weakening in CESM2

3.3.1 Temperature fields

The Habitat Foraging Capacipty Model (HFCM) in EcoOcean is driven by three different temperature fields: the temperature averaged over the top 150 m (Fig. S16), the temperature averaged over the entire water column (Fig. S17), and the bottom temperature (Fig. S18). The mean temperature of the top 150 m shows a different pattern than the SSTs (Fig. 2) as a response to the AMOC weakening. The top 150 m in the Subpolar North Atlantic and Arctic Ocean contains more heat in the HOS simulations compared to the CTL simulations. The Subtropical North Atlantic Ocean cools, whereas the South Atlantic warms. In the Indian and Southern Ocean, the northern Subtropical and southern Subpolar Pacific we see warming, and in the northern Subpolar and southern Subtropical Pacific we see cooling. Bottom temperatures show the largest response in the shallow regions. Generally these regions cool in the Northern Hemisphere and warm in the Southern Hemisphere. A major exception is the Arctic Ocean and some

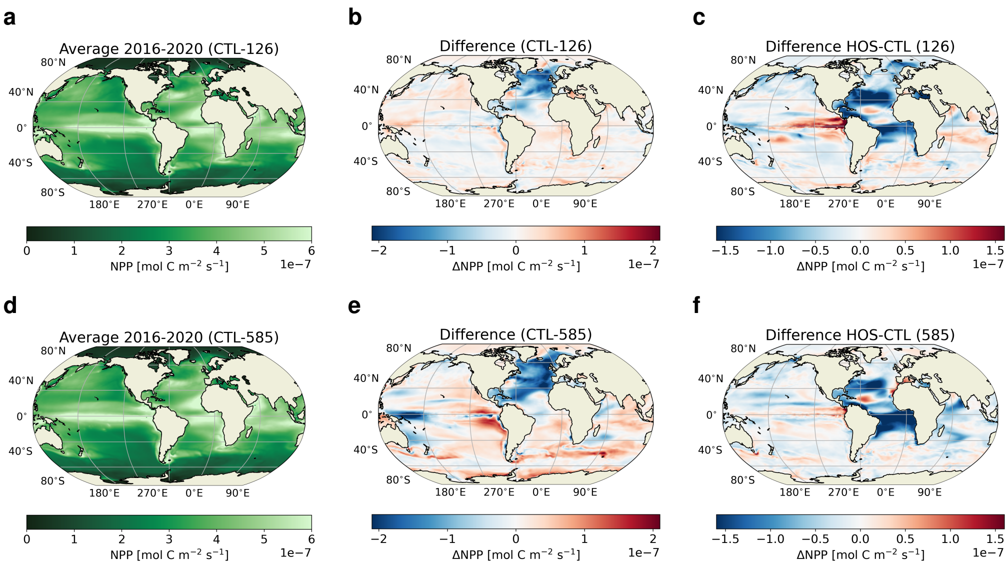

Figure 4. Net Primary Production integrated over the top 150 m in mol C m^{-2} s^{-1} for: (a) CTL-126 averaged over 2016-2020, (b) the average over 2016-2020 subtracted from the average over 2095-2099 in CTL-126, (c) CTL-126 subtracted from HOS-126 averaged over 2095-2099, and (d-f) as in (a-c) but for CTL-585 and HOS-585.

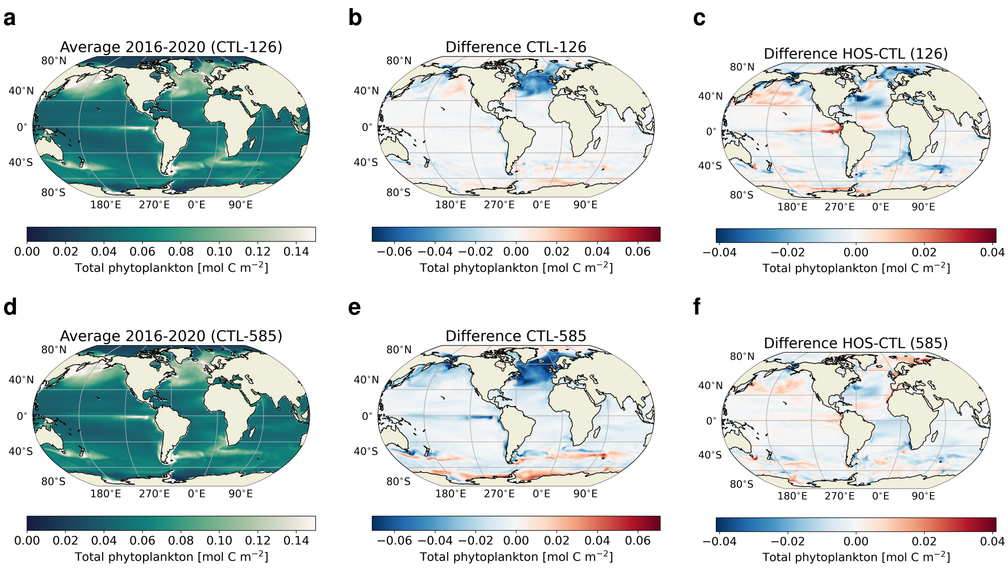

Figure 5. Total phytoplanktoon biomass integrated over the top 150 m in mol C m^{-2} for: (a) CTL-126 averaged over 2016-2020, (b) the average over 2016-2020 subtracted from the average over 2095-2099 in CTL-126, (c) CTL-126 subtracted from HOS-126 averaged over 2095-2099, and (d-f) as in (a-c) but for CTL-585 and HOS-585.

regions in the Subpolar North Atlantic Ocean that warm strongly. The column averaged water temperature follows generally the trend in the top temperature, except in the shallow regions. Here the trends are more similar to the trends seen in the bottom temperature. The warming in the Subpolar North Atlantic and Arctic Ocean are related to the insulating effects of sea ice. The warming in the Northern Subtropical and cooling in the Southern Subtropical Pacific Ocean are related to the stratification. Increased stratification north of the equator results in less upward mixing of cool subsurface waters while south of the equator the opposite occurs. The other regions follow the trends generally also observed in SSTs and SATs and are thus related to the forcing at the surface ocean.

3.3.2 Diazotrophs

The extent of the diazotrophs (Fig. S13) is limited by the 15°C SST (Fig. 2) isotherm as described earlier. The additional AMOC weakening in the HOS simulations affects the location of this isotherm on top of the climate change signal. In the HOS simulations in the Southern Hemisphere it shifts poleward due to the additional warming there, and in the North Pacific it shifts equatorward due to the relative cooling. In the North Atlantic the response is a bit different, and also differs between the emission scenarios. In the SSP1-2.6 scenario it shifts equatorward with a stronger response on the eastern side of the basin. On the eastern side of the basin water from the subpolar North Atlantic is advected southward. Since the subpolar region cools strongly due to the AMOC weakening, these water masses are relatively cool causing the relative cooling observed around the Iberian peninsula. In SSP5-8.5 this response on the eastern side of the basin is also seen, but on the western side we see a poleward increase of the diazotrophs because of a patch of surface ocean around 50°N that warms. This warming is caused by a southward shift of the North Atlantic Current in CTL-585 that is not found in to HOS-585 and the SSP1-2.6 simulations (Fig. S19).

3.3.3 Diatoms

For the diatoms (Fig. S14) there are a few regions that stand out in the HOS simulations compared to the CTL simulations. In the Western North Pacific Ocean, Eastern Equatorial Pacific Ocean, and North Subpolar Atlantic Ocean there are relative increases in diatom biomass for both emission scenarios over a relatively large area. Locally, there are also relative increases around Tasmania and in the Canary Upwelling System. The largest decreases are found in the extension of the Gulf Stream and in the Benguela Upwelling System.

The increases of diatoms in the Canary Upwelling System can be attributed to the strengthened trade winds (Fig. S3) in the HOS simulations which increase upwelling (Fig. S5) in this region. This upwelling supplies more nutrients to the surface ocean driving an increase in NPP in this region (Figs. 4 and S11). Also the increases in the Equatorial Pacific can be related to the AMOC weakening. The southward shift of the ITCZ decreases the stratification north of the equator (Fig. S4) because the freshwater flux at the surface ocean decreases (Fig. S3). The weaker stratification leads to deeper mixed layer depths (Fig. S20) and more entrainment of nutrients from the subsurface ocean. The increased availability of nutrients in the surface ocean drives an increase in diatom productivity and biomass (Figs. S11 and S14). The response in the North Subpolar Atlantic Ocean, where we see a region with a relative increase of diatoms biomass (in the gyre), and a region with a relative decrease of diatom biomass, can be explained by the NO_3^- concentrations (Fig. 3). In the CTL simulations, NO_3^- decreases in the subpolar region, increasing the nitrogen limitation of all phytoplankton in this region. Under increased nutrient stress, small phytoplankton are able to outcompete the diatoms (Boot et al., 2023). In the HOS simulations, the NO_3^- concentrations increase in the subpolar gyre, and decrease in the extension of the Gulf Stream, and the diatoms respond, by increasing their mass in the subpolar gyre, and decreasing their mass in the extension of the Gulf Stream compared to the CTL simulations. The NO_3^- concentrations in the extension of the Gulf Stream decrease because the weaker Gulf Stream transports less nutrients northwards, which is directly related to the weakening of the AMOC. Diatom

Table 1. Relative change in % of different total phytoplankton biomass, biomass of the three phytoplankton groups in CESM2, Total System Biomass, Total Consumer Biomass and total commercial biomass in EcoOcean in the year 2099 for the four different simulations and the difference between the HOS and CTL simulations (fourth column for SSP1-2.6 and last column for SSP5-8.5). Relative change is defined as the difference in biomass between 2099 and 2015 divided by the biomass in 2015.

Group	CTL-126	HOS-126	Δ-126	CTL-585	HOS-585	Δ-585
Total phytoplankton biomass	-3.99	-7.41	-3.42	-12.71	-13.56	-0.85
Small phytoplankton biomass	5.91	5.38	-0.53	-5.94	-9.00	-3.06
Diatom biomass	-13.96	-20.98	-7.02	-21.62	-20.44	1.18
Diazotroph biomass	3.81	3.03	-0.78	11.15	11.75	0.60
Total System Biomass	-1.41	-5.20	-3.78	-11.29	-13.33	-2.03
Total Consumer Biomass	-1.64	-5.92	-4.28	-12.49	-14.80	-2.31
Commercial species	-1.48	-4.92	-3.43	-12.75	-15.51	-2.76

biomass decreases in the Benguela Upwelling System because the advection of Si through the Aghulas leakage reduces.

3.3.4 Small Phytoplankton

Generally, small phytoplankton (Fig. S15) respond opposite to the diatoms in the HOS simulations compared to the CTL simulations. This is because the diatoms and small phytoplankton are generally competing for the same nutrients. Due to the AMOC weakening, locally the environmental conditions can change that can either favor the diatoms or the small phytoplankton. For example, the reduced Si concentrations in the Benguela Upwelling System (Fig. S8) causes the small phytoplankton to become dominant in this region since they are able to outcompete the diatoms.

3.3.5 Total phytoplankton biomass

The change in total phytoplankton biomass (Fig. 5) is generally the combined signal of the changes observed in diatom biomass and small phytoplankton biomass. There are, however, some regions where diatoms replace small phytoplankton or vice versa. In these regions the signal observed in the diatoms is generally dominant, but not everywhere (e.g. in the Fram Strait in SSP1-2.6). For each plankton type and the total phytoplankton biomass, the relative change over the simulation in % is shown in Table 1 for the entire ocean, and in Table S1 per region in the ocean.

3.4 EcoOcean: ecosystem response

There is a clear difference in the response in EcoOcean to the emission scenarios. In CTL-126, total system biomass (TSB) decreases by 1.41%, total consumer biomass (TCB) by 1.64% and commercial species by 1.48% (Table 1). In CTL-585, the decreases are much stronger: TSB decreases by 11.29%, TCB by 12.49% and commercial biomass by 12.75% (Table 1).

The response to the greenhouse gas emissions is different per region (Table 2). In both CTL-126 and CTL-585 the ocean around Antarctica (66°S – 90°) gain the most TSB (37.17% and 47.3%, respectively), and the subpolar North Atlantic and Pacific Ocean lose the most TSB (16.9% and 33.64% for the Atlantic and 12.92% and 25.98% for the

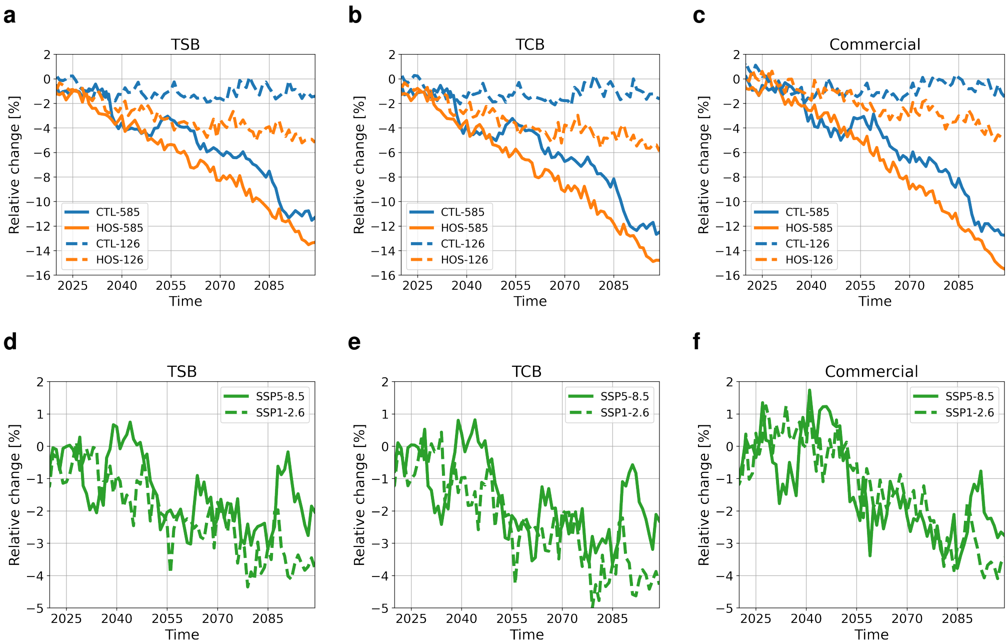

Figure 6. Relative changes in % in the CTL and HOS simulations (top row) and the difference between the two (bottom row) for Total System Biomass (TSB; a, d), Total Consumer Biomass (TCB; b, e), and Commercial species (c, f). Dashed lines represent SSP1-2.6 and solid lines SSP5-8.5. Blue represent the CTL simulations, orange the HOS simulations, and green the difference between the two (HOS minus CTL).

Pacific). An important difference between the emission scenarios is how the ecosystems develop in the Arctic Ocean (66°N – 90°N). In CTL-126 the Arctic Ocean loses 9.34% in TSB, while in CTL-585 we see an increase of 12.71%, which can be explained by looking at the sea-ice cover (Fig. S6). In CTL-585 most sea ice disappears which boosts NPP (Fig. 4) in this region providing the ecosystem with biomass to feed upon in a bottom up manner.

The effect of the strong AMOC weakening in HOS-126 results in a decrease in biomass with respect to CTL-126. TSB decreases with 3.78% with respect to CTL-126 and 5.20% in total (Table 1). The largest responses are seen in the Arctic Ocean, subpolar and subtropical (15°N-40°N) North Atlantic Ocean (30.45, 15.22, and 13.24% decrease in TSB with respect to CTL-126; Table 2). Compared to SSP1-2.6, the relative effect of the AMOC weakening is lower in SSP5-8.5 which is related to the much stronger climate forcing in the high emission scenario. TSB decreases with 2.03% with respect to CTL-585 and 13.33% in total. The largest response in TSB over time is seen in the Arctic Ocean and the subpolar North Atlantic, but, just as with the AMOC and GMST difference (Fig. 1), the difference becomes smaller over time. In 2100, the regions with the largest response in TSB are the oceans around Antarctica (an increase of 12.97% with respect to CTL-585), and in the Atlantic north of 15°S (a decrease of 6.38% around the equator, 5.9% in the subtropical gyre and 6.87% in the subpolar gyre (Fig. 7) with respect to CTL-585).

TCB and commercial species show similar results as for TSB, but the global response is slightly stronger (except for commercial species in HOS-126), i.e. there is a larger decrease in biomass of TCB and commercial species compared to TSB (Fig. 6). Regionally, the response is generally also similar to the results for TSB, but whether the response

Table 2. Relative change in % of Total System Biomass (TSB), Total Consumer Biomass (TCB) and total commercial biomass (COM) in 2099 for the difference between the HOS and CTL simulations for different regions in the ocean. Relative change is defined as in the main text as the difference in biomass between 2099 and 2015 divided by the biomass in 2015.

Region		TSB Δ-126	TSB Δ-585	TCB Δ-126	TCB Δ-585	COM Δ-126	COM Δ-585
Arctic Ocean	66°N - 90°N	-30.45	0.20	-31.58	0.19	-16.6	-1.18
Atlantic Ocean	40°N - 66°N	-15.22	-6.87	-15.88	-7.23	-17.1	-11.39
	15°N - 40°N	-13.24	-5.90	-14.46	-6.46	-15.04	-6.70
	15°S - 15°N	-5.82	-6.38	-7.25	-7.66	-7.93	-8.75
	15°S - 40°S	-2.15	-1.06	-3.04	-1.03	-4.77	-3.21
	40°S - 66°S	0.43	-2.78	0.86	-3.04	1.54	-5.03
Pacific Ocean	40°N - 66°N	-3.96	-4.87	-4.67	-5.18	4.73	1.02
	15°N - 40°N	2.33	2.04	2.33	2.03	3.17	1.71
	15°S - 15°N	-0.54	-0.88	0.94	-1.24	-0.14	-2.51
	15°S - 40°S	-7.93	-1.13	-8.26	-1.37	-7.13	-2.33
	40°S - 66°S	0.31	-3.06	0.86	-3.08	-0.36	-2.43
Indian Ocean	North of 15°S	0.09	-0.75	-0.09	-0.64	-0.41	-0.80
	15°N - 40°N	-2.03	-5.70	-2.57	-6.35	-2.89	-5.95
	40°N - 66°N	-5.37	4.97	-5.67	5.79	-4.31	5.95
Southern Ocean	66°S - 90°S	4.87	12.97	5.69	14.26	-13.58	14.05

is stronger or weaker differs per region (Table 2, Fig. 8 and Fig. 9). Interesting differences are, for example, that TSB increases in the subpolar North Pacific and decreases in the Antarctic Ocean as a response to the strong AMOC weakening, but that the biomass of commercial species show the opposite response (i.e. a decrease and an increase, respectively) in SSP1-2.6. This effect occurs in regions surrounding the sea-ice edge. This suggests that lower trophic levels respond faster to sea ice changes resulting in the decrease in TSB and TCB, while higher trophic levels respond slower resulting in a different response in total commercial biomass.

3.5 Role of AMOC weakening in EcoOcean

Total system (Fig. 7), consumer (Fig. 8), and commercial (Fig. 9), biomass all respond similar to the AMOC weakening (Fig. 6). Here we discuss the role of the AMOC weakening on total consumer biomass, and the mechanisms described also apply to total system and commercial biomass. Total consumer biomass (Fig. 8) follows in most regions the patterns seen in changes in total phytoplankton biomass. This means that to first order, the effects of an AMOC weakening on marine ecosystems follow the same mechanisms as for total phytoplankton biomass, which is the combined effect of the mechanisms present for the diazotrophs, diatoms and small phytoplankton. This means that the effects of an AMOC weakening affect marine ecosystems in a bottom up fashion by affecting the lowest trophic levels which through food web dynamics affect the entire ecosystem. There are a few regions that do not follow the patterns seen in total phytoplankton biomass, i.e. the Canary and Benguela Upwelling Systems, and the extension of the Gulf Stream. These are regions where a shift occurs in phytoplankton dominance, i.e. from small phytoplankton to diatoms in the Canary Upwelling System, and the other way around for the other two regions. These changes affect the food web dynamics in EcoOcean. In the Benguela Upwelling System and the surrounding ocean a decrease in total phytoplankton biomasss is simulated in CESM2 (Fig. 5), but the surrounding oceans in EcoOcean show an increase in TCB (Fig. 8). Besides an increase in TCB, the sur-

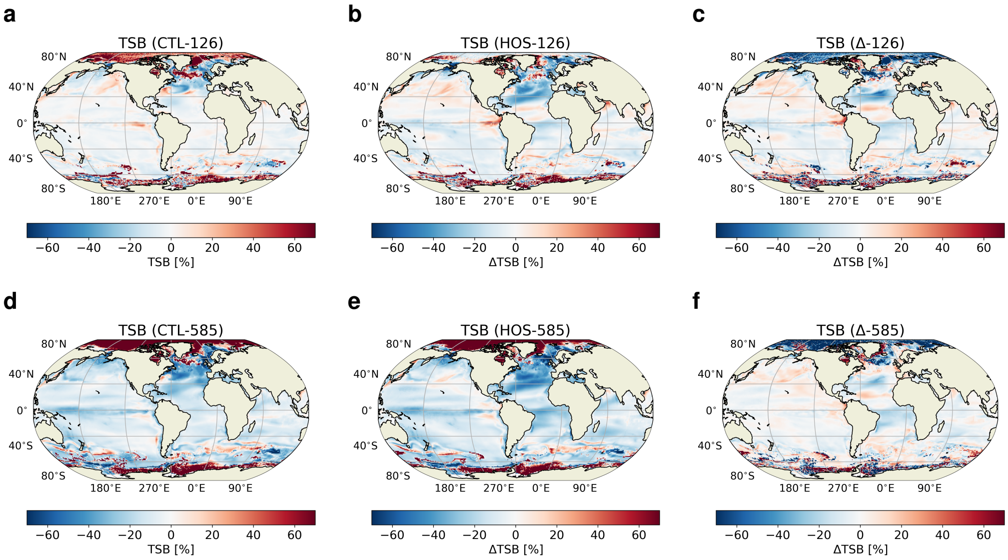

Figure 7. Relative changes averaged over 2095-2099 compared to 2016-2020 in % for Total System Biomass (TSB) in the CTL simulations (a, d), HOS simulations (b, e), and the difference between the two (c, f). (a-c) are for SSP1-2.6 and (d-f) are fore SSP5-8.5.

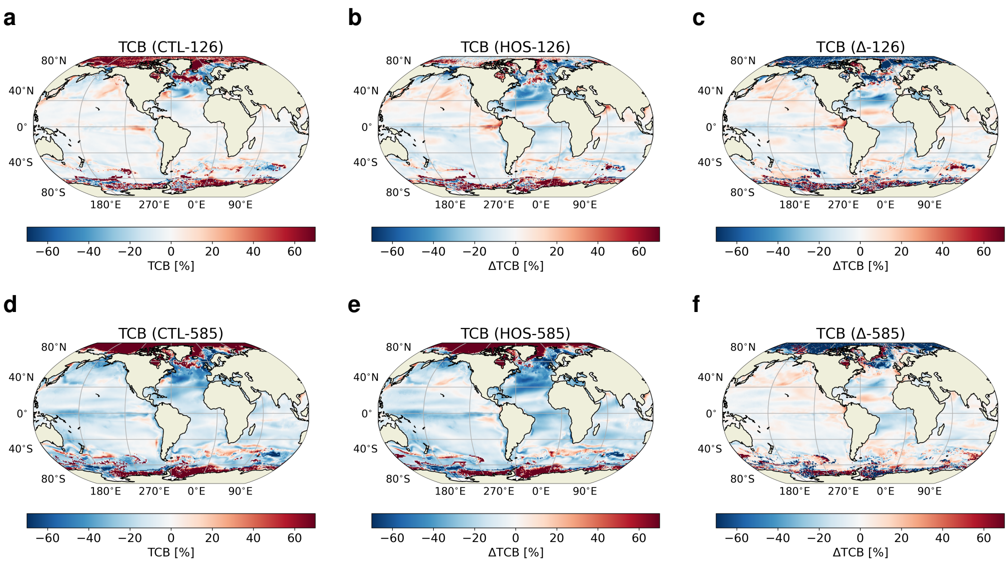

Figure 8. Relative changes averaged over 2095-2099 compared to 2016-2020 in % for Total Consumer Biomass (TCB) in the CTL simulations (a, d), HOS simulations (b, e), and the difference between the two (c, f). (a-c) are for SSP1-2.6 and (d-f) are fore SSP5-8.5.

rounding oceans also see an increase in both meso- and microzooplankton. Mesozooplankton (Fig. S22) are a central organism in the food web that feed on diatoms, diazotrophs and microzooplankton (Fig. S21) which predominantly feed on small phytoplankton. Since mesozooplankton have multiple food sources, they are able to increase their biomass even though diatom biomass is lost in this region. The reason why TCB follows mesozooplank-

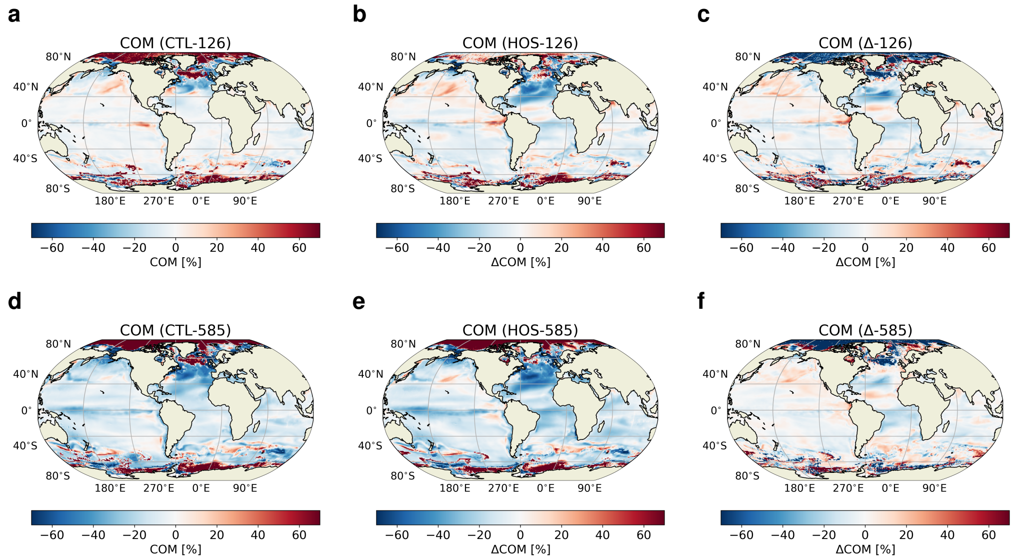

Figure 9. Relative changes averaged over 2095-2099 compared to 2016-2020 in % for commercial species (COM) in the CTL simulations (a, d), HOS simulations (b, e), and the difference between the two (c, f). (a-c) are for SSP1-2.6 and (d-f) are fore SSP5-8.5.

ton biomass closely is that mesozooplankton have a central role in the ecosystem since they are preyed upon by 26 different functional groups, and often are the most important food source for these groups in EcoOcean. In the Canary Upwelling System, we see a strong increase in phytoplankton biomass due to an increase in diatom biomass over a loss of small phytoplankton biomass. This leads to an increase in large zooplankton (krill; Fig. S23), a small decrease in mesozooplankton and a large decrease in microzooplankton. In the Benguela Upwelling System similar mechanisms with opposite effects are present, and the changes in the food web dynamics lead to reduced TCB in this region. In the extension of the Gulf Stream we find a strong decrease in diatom biomass in the HOS simulations, which is partly compensated for by small phytoplankton. However, the net effect in this region is a strong decrease in total phytoplankton biomass. TCB does not follow this strong decrease in total phytoplankton biomass. This is because the increase in small phytoplankton biomass, results in an increase in microzooplankton biomass. The mesozooplankton are consequently able to replace diatoms as a food source with microzooplankton as a food source.

4 Discussion

In this study we have looked at the effect of a strong weakening of the Atlantic Meridional Overturning Circulation (AMOC) on future global marine ecosystems under a low and high emission scenario. Fig. 10 provides an overview of how the AMOC weakening affects the climate system, ocean biogeochemistry and marine ecosystems. We see that the AMOC weakening has a large impact on the ocean state influencing ocean circulation, stratification and upwelling which leads to changes in the 3D nutrient fields. The changes in the nutrient fields directly affect the productivity and biomass of the three phytoplankton groups simulated in CESM2, i.e. the diazotrophs, diatoms and small phytoplankton. The effects of the AMOC weakening on the phytoplankton cascade through the food web leading to a similar response in total consumer biomass as the response in total phytoplankton biomass. There are some regions that deviate from this overall response. These regions typically see a shift in dominant phytoplankton group which causes an adjustment in the abundance of the three different zooplankton groups in EcoOcean. The mesozooplankton group is a central group in the food web that preys on both diatoms and microzooplankton that in turn prey on the small phytoplankton group. Through this differential feeding, mesozooplankton do not directly follow the trend of total phytoplankton biomass in regions that observe a phytoplankton composition shift.

Overall, climate change causes a reduction in both total system and total consumer biomass with a much stronger response in the high emission scenario. Similar changes are seen in the commercial species, suggesting that these effects will also be felt in socio-economic systems. The AMOC weakening leads to a stronger decrease in biomass in the aggregated groups mentioned above. The responses in total system, consumer and commercial biomass to an AMOC weakening are larger than the responses in total phytoplankton biomass, showing that the effect of the AMOC weakening is stronger on higher trophic levels.

EcoOcean has previously been coupled to Earth System Model (ESM) simulations using the GFDL and IPSL ESMs (Coll et al., 2020). Both ESMs show a different response for TSB to the climate change and the CESM2 simulations result in again a different response that lies between both the GFDL (relatively positive) and the IPSL (quite negative) responses. In FishMIP2 (Tittensor et al., 2021), EcoOcean is one of the more conservative marine ecosystem models and the only MEM with a complete, resilient food web. Compared to these two studies (Coll et al., 2020; Tittensor et al., 2021), the results presented here for TSB could be either more positive or negative when a different ESM is used, and more extreme in biomass loss when a different MEM is used.

There is quite some work based on Earth System Models of Intermediate Complexity (so-called EMICs) which generally focuses on longer timescales (i.e. multi-centennial to multi-millennial). These studies show a wide range of possible responses in the marine carbon cycle (Zickfeld et al., 2008), but no clear analysis has been performed on marine ecosystems. Schmittner (2005) looks at the ecosystem response to an AMOC weakening using a much simpler model than the models used in this study and suggests that on long timescales an AMOC weakening results in a suppression of NPP in the Atlantic, which is also what we find.

Since only one ESM and one MEM are used here, the results could be model dependent. The most important forcing in EcoOcean is the total phytoplankton biomass simulated in CESM2, and it would be very valuable to also use models with at least a different biogeochemical module, and preferably a different ESM with a different ocean component than CESM2. The spread in MEMs in FishMIP2 is generally smaller than that of ESMs in CMIP6 (Tittensor et al., 2021), and therefore additional simulations with different MEMs will provide less information than using different ESMs, but are valuable, nonetheless.

The results presented in this study hold implications for the efforts of mitigating climate change, the management of marine ecosystems, and socio-economic systems. If the AMOC strongly weakens, or even collapses in the coming century, marine ecosystems are negatively affected. This comes on top of the generally negative effects that anthropogenic climate change and other human activities such as fisheries have on these same ecosystems (Coll et al., 2020; Tittensor et al., 2021). We show that the AMOC weakening on top of anthropogenic climate change can result in basin wide depletion of high trophic level organisms, which can be also important for fisheries and food security. Previous studies have already stated that an AMOC weakening can affect societies through large regional climate changes (van Westen et al., 2024; Brovkin et al., 2021). We show here an additional pathway on how an AMOC weakening affects socio-economic systems through a reduction in abundance of commercial species. Since fish is an essential source of protein for millions of people (FAO, 2022), an AMOC weakening can have a disrup-

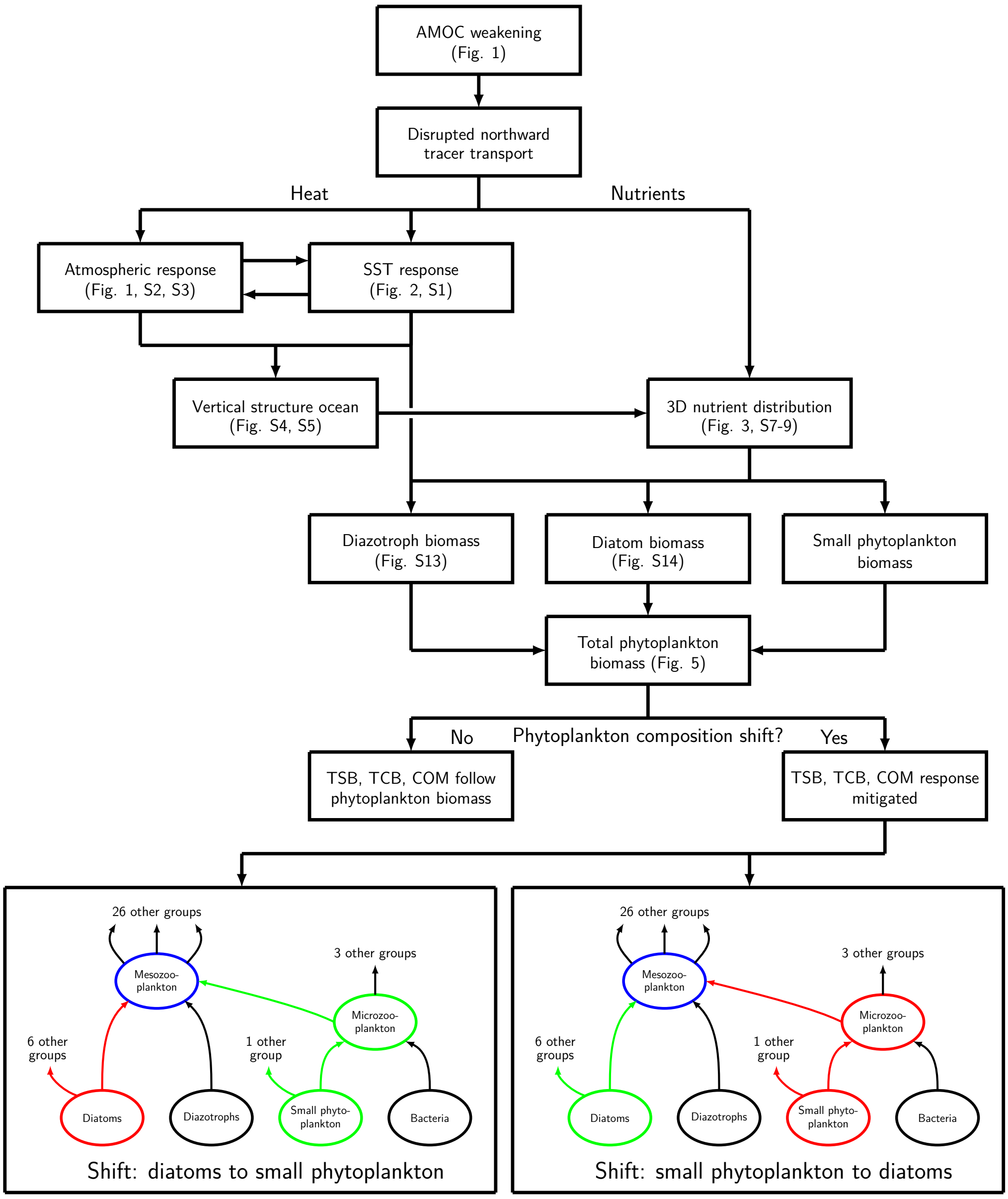

Figure 10. Summarizing figure showing in a simplified way how an AMOC weakening influences the climate system, ocean biogeochemistry and marine ecosystems. The diagrams at the bottom represent part of the food web in EcoOcean showing the response of the food web to a phytoplankton composition shift. The colors represent a decrease in biomass (red), an increase in biomass (green), and an unknown response (blue) in the mesozooplankton group.

tive effect on human societies. This is especially relevant since recent studies suggest we are approaching a tipping point for the AMOC (Ditlevsen & Ditlevsen, 2023; van Westen et al., 2024).

To conclude, in this study we have simulated a strong AMOC weakening using a low and high emission scenario in the CMIP6 state-of-the-art Earth System Model CESM2.

We forced a Marine Ecosystem Model, EcoOcean, with the CESM2 results to show the impact of an AMOC weakening on marine ecosystems. Both the low and high emission scenario show negative effects of the marine ecosystem, meaning that an AMOC weakening is an additional threat next to anthropogenic climate change. Another implication of our results is that tipping in the climate system can cascade over system boundaries to marine ecosystems, with possibly very negative effects on socio-economical systems.

5 Open Research

The scripts used for analysis and plotting, including the necessary datasets are saved in a repository: `https://doi.org/10.5281/zenodo.10891003` (Boot, Steenbeek, et al., 2024). In this repository also the most important output from the CESM2 and EcoOcean simulations is provided.

Acknowledgments
This study has been supported by the Netherlands Earth System Science Centre (NESSC), which is financially supported by the Ministry of Education, Culture and Science (OCW; Grant 024.002.001). A.A.B. and H.A.D. are also funded by the European Research Council through the ERC-AdG project TAOC (project 101055096). JS and MC acknowledge the European Union's Horizon 2020 research and innovation programme under grant agreement N°817578 (TRIATLAS) and the Spanish Ministry of Science and Innovation grant agreement N°PID2020-118097RB-I00 (ProOceans). MC acknowledges institutional support of the 'Severo Ochoa Centre of Excellence' accreditation (CEX2019-000928-S). The work of A.S.vdH. was also funded by the Dutch Research Council (NWO) through the NWO-Vici project 'Interacting climate tipping elements: When does tipping cause tipping?' (project VI.C.202.081). The authors want to thank Michael Kliphuis (IMAU, Utrecht University) for performing the CESM2 simulations, which were performed at SURFsara in Amsterdam on the Dutch Supercomputer Snellius under NWO-SURF project 17239.

References

Ahrens, R. N. M., Walters, C. J., & Christensen, V. (2012). Foraging arena theory. *Fish and Fisheries*, *13*(1), 41–59. doi: https://doi.org/10.1111/j.1467-2979.2011.00432.x

Boot, A. A., Steenbeek, J., Coll, M., von der Heydt, A. S., & Dijkstra, H. A. (2024, mar). *dboot0016/EF2024_CESM2_EcoOcean: v1.1.* Zenodo. doi: 10.5281/zenodo.10891003

Boot, A. A., von der Heydt, A. S., & Dijkstra, H. A. (2023). Effect of Plankton Composition Shifts in the North Atlantic on Atmospheric pCO2. *Geophysical Research Letters*, *50*(2), e2022GL100230. doi: https://doi.org/10.1029/2022GL100230

Boot, A. A., von der Heydt, A. S., & Dijkstra, H. A. (2024). Response of atmospheric pCO_2 to a strong AMOC weakening under low and high emission scenarios. *Under review at Climate Dynamics*.

Boucher, O., Servonnat, J., Albright, A. L., Aumont, O., Balkanski, Y., Bastrikov, V., . . . Vuichard, N. (2020). Presentation and Evaluation of the IPSL-CM6A-LR Climate Model. *Journal of Advances in Modeling Earth Systems*, *12*(7), e2019MS002010. doi: https://doi.org/10.1029/2019MS002010

Breitburg, D., Levin, L. A., Oschlies, A., Grégoire, M., Chavez, F. P., Conley, D. J., . . . Zhang, J. (2018). Declining oxygen in the global ocean and coastal waters. *Science*, *359*(6371), eaam7240. doi: 10.1126/science.aam7240

Brovkin, V., Brook, E., Williams, J. W., Bathiany, S., Lenton, T. M., Barton, M., . . . Yu, Z. (2021). Past abrupt changes, tipping points and cascading impacts in the Earth system. *Nature Geoscience*, *14*(8), 550–558. doi: 10.1038/s41561-021-00790-5

Caesar, L., Rahmstorf, S., Robinson, A., Feulner, G., & Saba, V. (2018). Observed fingerprint of a weakening Atlantic Ocean overturning circulation. *Nature*, *556*(7700), 191–196. doi: 10.1038/s41586-018-0006-5

Christensen, V., Coll, M., Buszowski, J., Cheung, W. W. L., Frölicher, T., Steenbeek, J., ... Walters, C. J. (2015). The global ocean is an ecosystem: simulating marine life and fisheries. *Global Ecology and Biogeography*, *24*(5), 507–517. doi: https://doi.org/10.1111/geb.12281

Christensen, V., Coll, M., Steenbeek, J., Buszowski, J., Chagaris, D., & Walters, C. J. (2014). Representing Variable Habitat Quality in a Spatial Food Web Model. *Ecosystems*, *17*(8), 1397–1412. doi: 10.1007/s10021-014-9803-3

Coll, M., Steenbeek, J., Pennino, M. G., Buszowski, J., Kaschner, K., Lotze, H. K., ... Christensen, V. (2020). Advancing Global Ecological Modeling Capabilities to Simulate Future Trajectories of Change in Marine Ecosystems. *Frontiers in Marine Science*, *7*. doi: 10.3389/fmars.2020.567877

Danabasoglu, G. (2019). *NCAR CESM2 model output prepared for CMIP6 CMIP esm-hist.* Earth System Grid Federation. doi: 10.22033/ESGF/CMIP6.7575

Danabasoglu, G., Lamarque, J.-F., Bacmeister, J., Bailey, D. A., DuVivier, A. K., Edwards, J., ... Strand, W. G. (2020). The Community Earth System Model Version 2 (CESM2). *Journal of Advances in Modeling Earth Systems*, *12*(2), e2019MS001916. doi: https://doi.org/10.1029/2019MS001916

Diaz, R. J., & Rosenberg, R. (2008). Spreading Dead Zones and Consequences for Marine Ecosystems. *Science*, *321*(5891), 926–929. doi: 10.1126/science.1156401

Ditlevsen, P., & Ditlevsen, S. (2023). Warning of a forthcoming collapse of the Atlantic meridional overturning circulation. *Nature Communications*, *14*(1), 4254.

Doney, S. C., Ruckelshaus, M., Emmett Duffy, J., Barry, J. P., Chan, F., English, C. A., ... Talley, L. D. (2012). Climate Change Impacts on Marine Ecosystems. *Annual Review of Marine Science*, *4*(1), 11–37. doi: 10.1146/annurev-marine-041911-111611

Dunne, J. P., Horowitz, L. W., Adcroft, A. J., Ginoux, P., Held, I. M., John, J. G., ... Zhao, M. (2020). The GFDL Earth System Model Version 4.1 (GFDL-ESM 4.1): Overall Coupled Model Description and Simulation Characteristics. *Journal of Advances in Modeling Earth Systems*, *12*(11), e2019MS002015. doi: https://doi.org/10.1029/2019MS002015

Eyring, V., Bony, S., Meehl, G. A., Senior, C. A., Stevens, B., Stouffer, R. J., & Taylor, K. E. (2016, may). Overview of the Coupled Model Intercomparison Project Phase 6 (CMIP6) experimental design and organization. *Geosci. Model Dev.*, *9*(5), 1937–1958. doi: 10.5194/gmd-9-1937-2016

FAO. (2022). *The state of world fisheries and aquaculture 2022.* FAO.

Forget, G., & Ferreira, D. (2019). Global ocean heat transport dominated by heat export from the tropical Pacific. *Nature Geoscience*, *12*(5), 351–354. doi: 10.1038/s41561-019-0333-7

Gattuso, J.-P., Magnan, A., Billé, R., Cheung, W. W. L., Howes, E. L., Joos, F., ... Turley, C. (2015). Contrasting futures for ocean and society from different anthropogenic CO₂ emissions scenarios. *Science*, *349*(6243), aac4722. doi: 10.1126/science.aac4722

Henson, S. A., Cael, B. B., Allen, S. R., & Dutkiewicz, S. (2021). Future phytoplankton diversity in a changing climate. *Nature Communications*, *12*(1), 5372. doi: 10.1038/s41467-021-25699-w

Henson, S. A., Laufkötter, C., Leung, S., Giering, S. L. C., Palevsky, H. I., & Cavan, E. L. (2022). Uncertain response of ocean biological carbon export in a changing world. *Nature Geoscience*, *15*(4), 248–254. doi:

10.1038/s41561-022-00927-0
Hoegh-Guldberg, O., & Bruno, J. F. (2010). The Impact of Climate Change on the World's Marine Ecosystems. *Science*, *328*(5985), 1523–1528. doi: 10.1126/science.1189930
Hunke, E. C., Lipscomb, W. H., Turner, A. K., Jeffrey, N., & Elliott, S. (2015). *CICE: The Los Alamos Sea Ice Model documentation and software user's manual, version 5.1. Doc* (Tech. Rep.). LA-CC-06-012, 116 pp., http://www. ccpo. odu. edu.
IPCC. (2022). *The ocean and cryosphere in a changing climate.* Cambridge, England: Cambridge University Press.
Ito, T., & Follows, M. J. (2005). Preformed phosphate, soft tissue pump and atmospheric CO2. *Journal of Marine Research*, *63*(4), 813–839. doi: doi:10.1357/0022240054663231
Kwiatkowski, L., Torres, O., Bopp, L., Aumont, O., Chamberlain, M., Christian, J. R., … Ziehn, T. (2020). Twenty-first century ocean warming, acidification, deoxygenation, and upper-ocean nutrient and primary production decline from CMIP6 model projections. *Biogeosciences*, *17*(13), 3439–3470. doi: 10.5194/bg-17-3439-2020
Lawrence, D. M., Fisher, R. A., Koven, C. D., Oleson, K. W., Swenson, S. C., Bonan, G., … Zeng, X. (2019, dec). The Community Land Model Version 5: Description of New Features, Benchmarking, and Impact of Forcing Uncertainty. *Journal of Advances in Modeling Earth Systems*, *11*(12), 4245–4287. doi: https://doi.org/10.1029/2018MS001583
Lenton, T. M., Held, H., Kriegler, E., Hall, J. W., Lucht, W., Rahmstorf, S., & Schellnhuber, H. J. (2008). Tipping elements in the Earth's climate system. *Proceedings of the National Academy of Sciences*, *105*(6), 1786–1793. doi: 10.1073/pnas.0705414105
Liu, X., Battisti, D. S., & Donohoe, A. (2017). Tropical Precipitation and Cross-Equatorial Ocean Heat Transport during the Mid-Holocene. *Journal of Climate*, *30*(10), 3529–3547. doi: https://doi.org/10.1175/JCLI-D-16-0502.1
Long, M. C., Moore, J. K., Lindsay, K., Levy, M., Doney, S. C., Luo, J. Y., … Sylvester, Z. T. (2021). Simulations With the Marine Biogeochemistry Library (MARBL). *Journal of Advances in Modeling Earth Systems*, *13*(12), e2021MS002647. doi: https://doi.org/10.1029/2021MS002647
Lotze, H. K., Tittensor, D. P., Bryndum-Buchholz, A., Eddy, T. D., Cheung, W. W. L., Galbraith, E. D., … Worm, B. (2019). Global ensemble projections reveal trophic amplification of ocean biomass declines with climate change. *Proceedings of the National Academy of Sciences*, *116*(26), 12907–12912. doi: 10.1073/pnas.1900194116
Manral, D., Iovino, D., Jaillon, O., Masina, S., Sarmento, H., Iudicone, D., … van Sebille, E. (2023). Computing marine plankton connectivity under thermal constraints. *Frontiers in Marine Science*, *10*. doi: 10.3389/fmars.2023.1066050
Martell, S. J. D., Essington, T. E., Lessard, B., Kitchell, J. F., Walters, C. J., & Boggs, C. H. (2005). Interactions of productivity, predation risk, and fishing effort in the efficacy of marine protected areas for the central Pacific. *Canadian Journal of Fisheries and Aquatic Sciences*, *62*(6), 1320–1336. doi: 10.1139/f05-114
McKay, D. I. A., Staal, A., Abrams, J. F., Winkelmann, R., Sakschewski, B., Loriani, S., … Lenton, T. M. (2022). Exceeding 1.5°C global warming could trigger multiple climate tipping points. *Science*, *377*(6611), eabn7950. doi: 10.1126/science.abn7950
Moore, C. M., Mills, M. M., Arrigo, K. R., Berman-Frank, I., Bopp, L., Boyd, P. W., … Ulloa, O. (2013). Processes and patterns of oceanic nutrient limitation. *Nature Geoscience*, *6*(9), 701–710. doi: 10.1038/ngeo1765

Moore, J. K., Doney, S. C., Kleypas, J. A., Glover, D. M., & Fung, I. Y. (2001). An intermediate complexity marine ecosystem model for the global domain. *Deep Sea Research Part II: Topical Studies in Oceanography*, *49*(1), 403–462. doi: https://doi.org/10.1016/S0967-0645(01)00108-4

Moore, J. K., Doney, S. C., & Lindsay, K. (2004, dec). Upper ocean ecosystem dynamics and iron cycling in a global three-dimensional model. *Global Biogeochemical Cycles*, *18*(4). doi: https://doi.org/10.1029/2004GB002220

Moore, J. K., Lindsay, K., Doney, S. C., Long, M. C., & Misumi, K. (2013). Marine Ecosystem Dynamics and Biogeochemical Cycling in the Community Earth System Model [CESM1(BGC)]: Comparison of the 1990s with the 2090s under the RCP4.5 and RCP8.5 Scenarios. *Journal of Climate*, *26*(23), 9291–9312. doi: https://doi.org/10.1175/JCLI-D-12-00566.1

Orihuela-Pinto, B., England, M. H., & Taschetto, A. S. (2022). Interbasin and interhemispheric impacts of a collapsed Atlantic Overturning Circulation. *Nature Climate Change*, *12*(6), 558–565. doi: 10.1038/s41558-022-01380-y

Sampaio, E., Santos, C., Rosa, I. C., Ferreira, V., Pörtner, H.-O., Duarte, C. M., … Rosa, R. (2021). Impacts of hypoxic events surpass those of future ocean warming and acidification. *Nature Ecology & Evolution*, *5*(3), 311–321. doi: 10.1038/s41559-020-01370-3

Sanders, R., Henson, S. A., Koski, M., De La Rocha, C. L., Painter, S. C., Poulton, A. J., … Martin, A. P. (2014). The Biological Carbon Pump in the North Atlantic. *Progress in Oceanography*, *129*, 200–218. doi: https://doi.org/10.1016/j.pocean.2014.05.005

Schmittner, A. (2005). Decline of the marine ecosystem caused by a reduction in the Atlantic overturning circulation. *Nature*, *434*(7033), 628–633. doi: 10.1038/nature03476

Smale, D. A., Wernberg, T., Oliver, E. C. J., Thomsen, M., Harvey, B. P., Straub, S. C., … Moore, P. J. (2019). Marine heatwaves threaten global biodiversity and the provision of ecosystem services. *Nature Climate Change*, *9*(4), 306–312. doi: 10.1038/s41558-019-0412-1

Smith, R., Jones, P. W., Briegleb, P. A., Bryan, O., Danabasoglu, G., Dennis, M. L., … Yeager, S. G. (2010). The Parallel Ocean Program (POP) reference manual: Ocean component of the Community Climate System Model (CCSM)..

Tagliabue, A., Kwiatkowski, L., Bopp, L., Butenschön, M., Cheung, W., Lengaigne, M., & Vialard, J. (2021). Persistent Uncertainties in Ocean Net Primary Production Climate Change Projections at Regional Scales Raise Challenges for Assessing Impacts on Ecosystem Services. *Frontiers in Climate*, *3*. doi: 10.3389/fclim.2021.738224

Tittensor, D. P., Eddy, T. D., Lotze, H. K., Galbraith, E. D., Cheung, W., Barange, M., … Walker, N. D. (2018). A protocol for the intercomparison of marine fishery\hack{\break} and ecosystem models: Fish-MIP v1.0. *Geoscientific Model Development*, *11*(4), 1421–1442. doi: 10.5194/gmd-11-1421-2018

Tittensor, D. P., Novaglio, C., Harrison, C. S., Heneghan, R. F., Barrier, N., Bianchi, D., … Blanchard, J. L. (2021). Next-generation ensemble projections reveal higher climate risks for marine ecosystems. *Nature Climate Change*, *11*(11), 973–981. doi: 10.1038/s41558-021-01173-9

van Westen, R. M., & Dijkstra, H. A. (2023a). Asymmetry of AMOC Hysteresis in a State-Of-The-Art Global Climate Model. *Geophysical Research Letters*, *50*(22), e2023GL106088. doi: https://doi.org/10.1029/2023GL106088

van Westen, R. M., & Dijkstra, H. A. (2023b). Persistent Climate Model Biases in the Atlantic Ocean's Freshwater Transport. *EGUsphere*, *2023*, 1–29. doi: 10.5194/egusphere-2023-1502

van Westen, R. M., Kliphuis, M., & Dijkstra, H. A. (2024). Physics-based early warning signal shows that AMOC is on tipping course. *Science Advances*, *10*(6), eadk1189. doi: 10.1126/sciadv.adk1189

Walters, C. J., & Juanes, F. (1993). Recruitment Limitation as a Consequence of Natural Selection for Use of Restricted Feeding Habitats and Predation Risk Taking by Juvenile Fishes. *Canadian Journal of Fisheries and Aquatic Sciences*, *50*(10), 2058–2070. doi: 10.1139/f93-229

Weijer, W., Cheng, W., Drijfhout, S. S., Fedorov, A. V., Hu, A., Jackson, L. C., ... Zhang, J. (2019, aug). Stability of the Atlantic Meridional Overturning Circulation: A Review and Synthesis. *Journal of Geophysical Research: Oceans*, *124*(8), 5336–5375. doi: https://doi.org/10.1029/2019JC015083

Weijer, W., Cheng, W., Garuba, O. A., Hu, A., & Nadiga, B. T. (2020, jun). CMIP6 Models Predict Significant 21st Century Decline of the Atlantic Meridional Overturning Circulation. *Geophysical Research Letters*, *47*(12), e2019GL086075. doi: https://doi.org/10.1029/2019GL086075

Worthington, E. L., Moat, B. I., Smeed, D. A., Mecking, J. V., Marsh, R., & McCarthy, G. D. (2021). A 30-year reconstruction of the Atlantic meridional overturning circulation shows no decline. *Ocean Science*, *17*(1), 285–299. doi: 10.5194/os-17-285-2021

Zickfeld, K., Eby, M., & Weaver, A. J. (2008, sep). Carbon-cycle feedbacks of changes in the Atlantic meridional overturning circulation under future atmospheric CO2. *Global Biogeochemical Cycles*, *22*(3). doi: https://doi.org/10.1029/2007GB003118

Global marine ecosystem response to a strong AMOC weakening under low and high future emission scenarios

A. A. Boot[1], J. Steenbeek[2], M. Coll[2,3], A. S. von der Heydt[1,4], and H. A. Dijkstra[1,4]

[1]Institute for Marine and Atmospheric research Utrecht, Department of Physics,Utrecht University, Utrecht, the Netherlands
[2]Ecopath International Initiative (EII) Research Association, Barcelona, Spain
[3]Department of Marine Renewal Resources, Institute of Marine Science (ICM-CSIC), Barcelona, Spain
[4]Center for Complex Systems Studies, Utrecht University, Utrecht, the Netherlands

Key Points:

- Marine ecosystems are negatively affected by a weakening of the Atlantic Meridional Overturning Circulation.
- Mechanisms involve changes in nutrient transport and subsequent phytoplankton response leading to changes in the food web.
- Regional responses depend strongly on shifts in phytoplankton dominance.

Corresponding author: Amber A. Boot, `a.a.boot@uu.nl`

Abstract

Marine ecosystems provide essential services to the Earth System and society. These ecosystems are threatened by anthropogenic activities and climate change. Climate change increases the risk of passing tipping points; for example, the Atlantic Meridional Overturning Circulation (AMOC) might tip under future global warming leading to additional changes in the climate system. Here, we look at the effect of an AMOC weakening on marine ecosystems by forcing the Community Earth System Model v2 (CESM2) with low (SSP1-2.6) and high (SSP5-8.5) emission scenarios from 2015 to 2100. An additional freshwater flux is added in the North Atlantic to induce an extra weakening the AMOC. In CESM2, the AMOC weakening has a large impact on phytoplankton biomass and temperature fields through various mechanisms that change the supply of nutrients to the surface ocean. We drive a marine ecosystem model, EcoOcean, with phytoplankton biomass and temperature fields from CESM2. In EcoOcean, we see negative impacts in Total System Biomass (TSB), which are larger for high trophic level organisms. The strongest net effect is seen in the high emission scenario, but the effect of the extra AMOC weakening on TSB is larger in the low emission scenario. On top of anthropogenic climate change, TSB decreases by -3.78% and -2.03% in SSP1-2.6 and SSP5-8.5, respectively due to the AMOC weakening. These results show that marine ecosystems will be under increased threat if the AMOC weakens which might put additional stresses on socio-economic systems that are dependent on marine biodiversity as a food and income source.

Plain Language Summary

Marine ecosystems provide essential services to the Earth System and society. These ecosystems are threatened by anthropogenic activities and climate change. Climate change might also lead to a strong weakening of the Atlantic Meridional Overturning Circulation (AMOC). Here, we use a complex Earth System Model and a Marine Ecosystem Model to study how marine ecosystems respond to a strong AMOC weakening in possible future climates (2015-2100) under low and high emission scenarios. The AMOC weakening affects the climate system through various mechanisms that change the supply of nutrients to the surface ocean, affecting the primary production by phytoplankton. We find that the AMOC weakening leads to a decrease in phytoplankton biomass that is larger higher up the food chain. In total, marine ecosystems lose -3.78% and -2.03% of biomass in the low and high emission scenarios respectively. These results show that marine ecosystems will be under increased threat if the AMOC weakens.

Keywords: Atlantic Meridional Overturning Circulation, Climate Change, Marine Ecosystems, Earth System Modelling, Marine Ecosystem Modelling, Tipping Points

1 Introduction

Anthropogenic climate change and other anthropogenic activities, such as overfishing and pollution, are a major threat for marine ecosystems and the services they provide. One of the services marine ecosystems provide is food for (human) consumption. It is estimated that the ocean provides 11% of animal protein that humans consume (Gattuso et al., 2015; FAO, 2022), and besides providing food, it also provides income through the fishery industry. Furthermore, marine ecosystems are estimated to export 11 Gigatonnes of carbon (GtC) each year from the surface to the deep ocean (Sanders et al., 2014), and without this export, atmospheric pCO_2 would be 200-400 ppm higher (Henson et al., 2022; Ito & Follows, 2005). Major changes in marine ecosystems can therefore have an important impact on both socio-economic systems and the climate system, making it very relevant to be able to make reliable projections on the future development of these ecosystems (Lotze et al., 2019; Tittensor et al., 2021).

Evidence of the impact of anthropogenic climate change on marine ecosystems is already apparent. Observations show, for example, a reduction in ocean productivity, changes in food webs, biogeographical shifts, and bleaching of warm water corals (Hoegh-Guldberg & Bruno, 2010; Doney et al., 2012; Gattuso et al., 2015; IPCC, 2022). The effects of climate change can propagate through the ecosystems in bottom-up and top-down direction, causing possible cascades in the ecosystem (Doney et al., 2012; Lotze et al., 2019). Another consequence of climate change is the expansion of hypoxic regions, especially those found along productive regions (Diaz & Rosenberg, 2008; Breitburg et al., 2018), which already has led to mass mortalities (Doney et al., 2012; Sampaio et al., 2021).

It has been suggested that many organisms in the ocean are at a very high risk of impact by climate change by 2100 (Gattuso et al., 2015; Coll et al., 2020), and the function of marine ecosystems is threatened by a possible loss of ecological resilience (Henson et al., 2021). As the climate warms, so does the probability of marine heat waves, which have been shown to have detrimental effects on ecosystems (Smale et al., 2019). Most CMIP6 (Eyring et al., 2016) Earth System Models (ESMs) project a future decrease in Net Primary Production (NPP). However, the intermodel spread in these projections is large and this spread has even increased compared to CMIP5 ESMs (Kwiatkowski et al., 2020; Tagliabue et al., 2021; Henson et al., 2022). Marine Ecosystem Models (MEMs) using input from two CMIP6 ESMs, project a decrease in Total System Biomass (TSB) in both a low and a high emission scenarios even though there is substantial spread in NPP in the ESMs (Tittensor et al., 2021).

Climate warming is not only a risk to marine ecosystems, it might also lead to tipping in the Earth System (Lenton et al., 2008; McKay et al., 2022). Passing a tipping point is a serious risk since the consequences of tipping are irreversible and can therefore be disastrous. A major tipping element in the ocean is the Atlantic Meridional Overturning Circulation (AMOC). The AMOC potentially has two stable states: an on-state reflecting the current AMOC regime with a strong circulation, and an off-state reflecting a weak or collapsed AMOC (Weijer et al., 2019). Tipping of the AMOC would lead to several changes in the Earth System affecting the entire globe. In the on-state the AMOC is responsible for a net transport of heat from the Southern Hemisphere across the equator to the Northern Hemisphere of 0.5 PW (Liu et al., 2017; Forget & Ferreira, 2019) thereby strongly influencing observed surface air temperature patterns. An AMOC collapse is expected to result in a cooling in the Northern Hemisphere and warming in the Southern Hemisphere, a southward shift of the Intertropical Convergene Zonce (ITCZ), and a strengthening of the trade winds (van Westen & Dijkstra, 2023a; Orihuela-Pinto et al., 2022; Caesar et al., 2018). As a response to the cooling, Arctic sea-ice extent is expected to increase under AMOC weakening or collapse. Besides the direct changes in advection due to an AMOC collapse, an AMOC weakening can also change important ocean characteristics such as the stratification and upwelling rates. Several studies have shown the impact this can have on the marine carbon cycle and the uptake capacity of the ocean (Zickfeld et al., 2008; Boot, von der Heydt, & Dijkstra, 2024). The changes in stratification and upwelling rates are specifically interesting for marine ecosystems, and through these processes, an AMOC weakening can impact marine primary productivity (Schmittner, 2005). The changes in ocean circulation also alter the connectivity in the ocean which can be relevant for environmental niches of plankton species, especially when their thermal constraints are taken into account (Manral et al., 2023). This provides a bottom-up control on marine ecosystems potentially threatening important ecosystem services and a pathway of cascading tipping from the physical climate system into marine ecosystems (Brovkin et al., 2021).

There are studies that suggest that the AMOC has been weakening over the past century (Caesar et al., 2018), and that the AMOC might tip between 2025 and 2095 (Ditlevsen & Ditlevsen, 2023). These studies are based on uncertain proxy data and are contested by some other studies (Worthington et al., 2021). However, a recent study using a physics based early warning signal shows that the AMOC is indeed on tipping course (van Westen et al., 2024). In CMIP6, the models show a consistent weakening of the AMOC across almost all emission scenarios, but no AMOC collapse is simulated up to 2100 (Weijer et al., 2020). However, this might be explained by the fact that the CMIP6 models are biased towards a too stable AMOC (van Westen & Dijkstra, 2023b) and might therefore underestimate the probability of a collapse.

In this study, we examine the impact of a strong AMOC weakening on marine ecosystems under anthropogenic climate change. We do this by analysing several simulations of the Community Earth System Model v2 (CESM2; Danabasoglu et al., 2020) where we use both a low and a high emission scenario, and simulations where we artificially weaken the AMOC by applying a surface freshwater flux to the North Atlantic Ocean. Since the ecosystem component in CESM2 is limited to three different phytoplankton groups and only one zooplankton group, we use the marine ecosystem model (MEM) EcoOcean (Coll et al., 2020) to simulate more detailed ecosystem dynamics. We force EcoOcean, a MEM part of FishMIP (Tittensor et al., 2018, 2021), with the output of the CESM2 simulations. Our results demonstrate the far reaching effects that a weakening of the AMOC can have on the marine ecosystem.

2 Methods

2.1 Earth System Model

The Community Earth System Model v2 (CESM2) is a state-of-the-art Earth System Model that is part of CMIP6. It has modules that represent the atmosphere (the Community Atmosphere Model v6), the land (the Community Land Model v5; Lawrence et al., 2019), sea ice (CICE5; Hunke et al., 2015), and the ocean (the Parallel Ocean Program v2, POP2; Smith et al., 2010) including ocean biogeochemistry (the Marine Biogeochemical Library, MARBL; Long et al., 2021). In this study we use the default CMIP6 version of CESM2, meaning that ice sheets and vegetation type are prescribed. All models are run on a nominal resolution of 1°, but the exact grid differs between the modules. Important for this study are the ocean modules POP2 and MARBL. These are both run on a displaced grid with a pole in Greenland. The vertical grid consists of 60 different layers with a thickness of 10 m in the top 150 m, after which the layer thickness increases to 250 m at 3500 m depth, staying constant up to the maximum ocean depth of 5500 m.

The ocean biogeochemistry module in CESM2 is MARBL (Long et al., 2021), which is an updated version of the Biogeochemical Elemental Cycling model (BEC; J. K. Moore et al., 2001, 2004, 2013; C. M. Moore et al., 2013). MARBL resolves three explicit phytoplankton types: diatoms, diazotrophs and small phytoplankton. Calcification is modelled implicitly as part of the small phytoplankton group using a variable rain ratio. Phytoplankton growth is co-limited by light and by silica (Si), phosphorus (P), nitrogen (N) and iron (Fe). Diatoms are the only group that can be limited by Si, and diazotrophs are nitrogen fixers and therefore not limited by N. However, diazotrophs are severely temperature limited if sea surface temperatures (SSTs) are below 15°C. The three phytoplankton types are grazed upon by one zooplankton group that, through differential grazing, implicitly represents multiple zooplankton groups (e.g. micro- and meso zooplankton). Both phyto- and zooplankton have a linear mortality formulation and for zooplankton a parametrized loss term is included that represents higher order trophic grazing. All primary production and consumption takes place in the top 150 m of the water column.

We use the same simulations that are presented in Boot, von der Heydt, and Dijkstra (2024) where the marine and terrestrial carbon cycle response to a strong AMOC weakening is studied. For a more thorough discussion on the simulations we refer the reader to Boot, von der Heydt, and Dijkstra (2024). We use emissions of two different scenarios: a low emission scenario SSP1-2.6 (from here on also referred to as 126), and a high emission scenario SSP5-8.5 (585). For each emission scenario there is a control (CTL) simulation where we force the model only with the emissions of the scenarios, and a simulation where we also apply a uniformly distributed freshwater flux in the North Atlantic Ocean between 50°N and 70°N at a constant rate of 0.5 Sv throughout the entire simulation (HOS simulations). We will refer to the simulations by combining the type and emission scenario, e.g. CTL-585 and HOS-126. All simulations are run from 2015 to 2100 and are initialized from the emission driven NCAR CMIP6 historical ('esm-hist') simulation (Danabasoglu, 2019).

2.2 Marine ecosystem model

We use EcoOcean v2 (Coll et al., 2020), an updated version of EcoOcean v1 (Christensen et al., 2015), which is one of the global, spatiotemporal explicit MEMs contributing to FishMIP (Tittensor et al., 2018, 2021). EcoOcean was originally developed to assess the impact of management strategies on the supply of seafood on a global scale. It is a 2D model with a horizontal resolution of 0.25 to 1° and simulates the time period 1950 to 2100 using monthly time steps. The EcoOcean framework combines several models which can be divided into three main components: (1) a component for marine biogeochemical processes and primary production, (2) a food web component that includes a dynamic niche model and species movement, and (3) a component simulating fisheries. Previously, EcoOcean was driven by simulations of the IPSL (using PISCES for ocean biogeochemistry; Boucher et al., 2020) and the GFDL (using COBALT for ocean biogeochemistry; Dunne et al., 2020) Earth System Models (Tittensor et al., 2018, 2021). In this study, we use the output of MARBL from the CESM2 simulations described in the previous section for component (1), and to match the resolution of CESM2, EcoOcean is used with a 1° resolution. We will not use active fisheries in this study and therefore component (3) is switched off. For a more thorough discussion on EcoOcean and the sensitivity of the model formulation, we refer the reader to Christensen et al. (2015) (v1) and Coll et al. (2020) (v2), and references therein.

The ecosystem module in EcoOcean simulates 52 different functional groups representing over 3400 individual species. Species are grouped together when biological and ecological traits are similar. The functional groups range from bacteria, plankton, different groups of fish, to marine mammals and birds. The different fish groups are differentiated on size (small: $<$ 30 cm, medium: 30-90cm, large: $>$ 90 cm), and grouped on, for example, where they live in the water column, i.e. pelagics, demersals, bathypelagics, bathydemersals, benthopelagics, reef fishes, sharks, rays and flat fishes. For a complete list of all functional groups, see the Supplementary Table 1 from Coll et al. (2020).

The food web model in EcoOcean is based on the 'Foraging Arena Theory' (Walters & Juanes, 1993; Ahrens et al., 2012), and the relative habitat capacity is determined using the Habitat Foraging Capacity Model (HFCM) (Christensen et al., 2014). Based on local predation risks and food availability, groups can move across spatial cells (Walters & Juanes, 1993; Martell et al., 2005; Christensen et al., 2014). The cell suitability in the HFCM is dependent on species native ranges, foraging capacity related to affinities for specific habitat distributions and types, and the response of the functional groups to environmental drivers.

The three phytoplankton groups simulated in the CESM2 are used to drive distributions and magnitude of corresponding planktonic groups in EcoOcean, and three different temperature fields in the CESM2 are used to drive the EcoOcean HFCM. One temperature field is averaged over the top 150 m, a second is depth averaged over the whole column, and the third represents bottom temperatures. Recall that the CESM2 simulations start in 2015 initialized from NCAR CMIP6 historical simulations (Danabasoglu, 2019). To run EcoOcean accurately, it needs to be calibrated to observations in the period 1950 to 2015. To be able to do this, we need also input variables for this period. The CESM2 simulations used in this study start at 2015 and are branched of from historical CMIP6 CESM2 simulations performed by NCAR. Unfortunately, not all necessary input variables to calibrate EcoOcean are available for the period 1950 to 2015 from these simulations and therefore we can not accurately calibrate EcoOcean to observations. We will therefore use relative changes in biomass B, defined as $\frac{B(t=2099)-B(t=2015)}{B(t=2015)} \times 100\%$, to assess the effect of the AMOC weakening on marine biomass. To spin up EcoOcean, we repeat the 2015 forcing of the CESM2 simulations in EcoOcean until a quasi-steady state is reached to replace the 1950-2015 calibration period. We look at three different aggregated groups of marine biomass: Total system biomass (TSB), total consumer biomass (TCB), and total commercial biomass (COM). For a definition of the three groups in EcoOcean see the supplementary material (Supplementary Table 1) of Coll et al. (2020).

3 Results

3.1 CESM2 Climate response

In both emission scenarios, the greenhouse gas emissions cause an increase in CO_2 concentration and warming. In CTL-585, CO_2 concentrations increase up to 1094 ppm in 2100, whereas CTL-126 has a maximum concentration in 2055 after which it decreases to 434 ppm due to negative emissions (Fig. 1a). The difference in atmospheric pCO_2 also result in a different Global Mean Surface Temperature (GMST), with around 5°C warming in CTL-585, and 1°C warming in CTL-126 (Fig. 1b). The forcing of the model causes a near linear weakening of the AMOC of around 50% for both emission scenarios, with a 2 Sv stronger weakening in CTL-585 (Fig. 1c). In the HOS simulations, the AMOC weakens much faster and stronger compared to the CTL simulations (Fig. 1c, f) as a response to the freshwater forcing. The maximum difference between the HOS and CTL simulations is around 8 Sv in the 2040's, and then decreases again (Fig. 1f). Due to the AMOC weakening, GMST warming is reduced following a similar trend as the reduction in AMOC strength (Fig. 1e). Also the spatial pattern of warming is affected by the AMOC weakening. The reduced northward heat transport in the HOS simulations causes relative cooling of both surface air temperature (SAT; Fig. S1) and sea surface temperature (SST; Fig. 2) in the Northern Hemisphere and relative warming in the Southern Hemisphere compared to the CTL simulations. The response in atmospheric pCO_2 to the hosing is small (Fig. 1d) related to many compensating effects within the carbon cycle (see Boot, von der Heydt, & Dijkstra, 2024).

The different temperature distribution in the HOS simulations compared to the CTL simulations causes atmospheric adjustments resulting in a southward shift of the ITCZ (Fig. S2), and a strengthening of the Northern Hemispheric trade winds (Fig. S3), both of which have an important influence on the surface stratification of the ocean (Fig. S4) and upwelling rates (Fig. S5). As a consequence to the relatively cooler Northern Hemisphere, Arctic sea-ice extent increases in both HOS simulations compared to their respective CTL simulations (Fig. S6). At the end of the simulation, the sea ice extent in HOS-126 is actually larger in 2100 compared to 2015, and also much larger compared to CTL-126 (Fig. S6c). In HOS-585 the strong warming still results in a much reduced Arctic sea-ice cover. However, the melting of the sea ice is much slower and, compared to CTL-585, HOS-585 also has more ice in 2100 (Fig.S6f).

3.2 CESM2 biogeochemical response

The changes in, for example, stratification and upwelling rates influence the nutrient concentrations in the euphotic zone of the ocean. In the CTL simulations, phosphate (PO_4^{3-}) concentrations decrease in the surface ocean almost everywhere (Fig. S7). The strongest responses are seen in the North Atlantic and Arctic Ocean, and in the East-

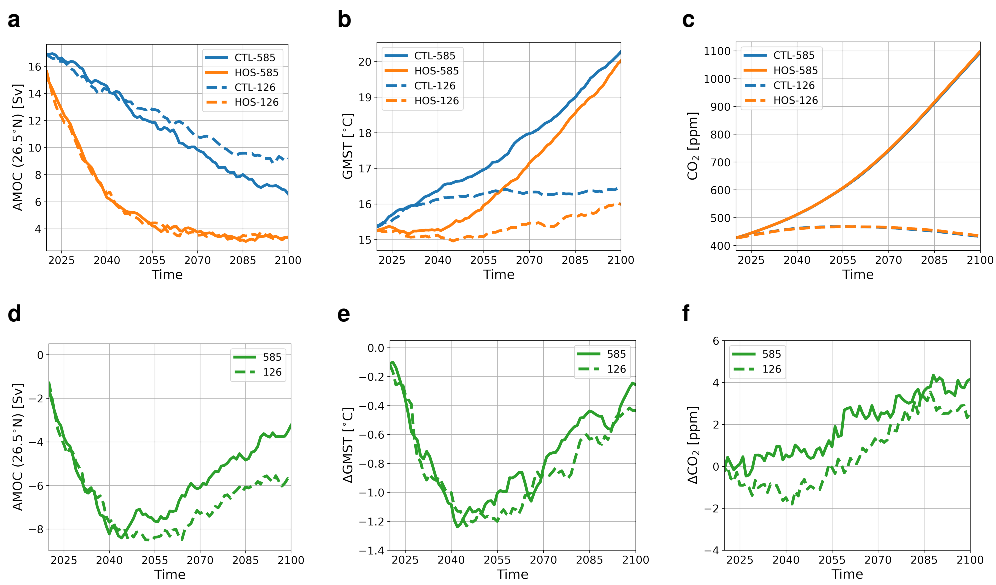

Figure 1. (a) Atmospheric CO_2 concentration in ppm. (b) GMST in °C. (c) AMOC strength at 26.5°N in Sv. In (a-c) blue lines represent the control (CTL) simulations, and orange lines the HOS simulations. (d-f) as in (a-c) but for the difference between the HOS simulations and the control simulations. In all subplots dashed lines represent SSP1-2.6 (126) and solid lines SSP5-8.5 (585). Results are smoothed with a 5 year moving average and represent the period 2020-2100.

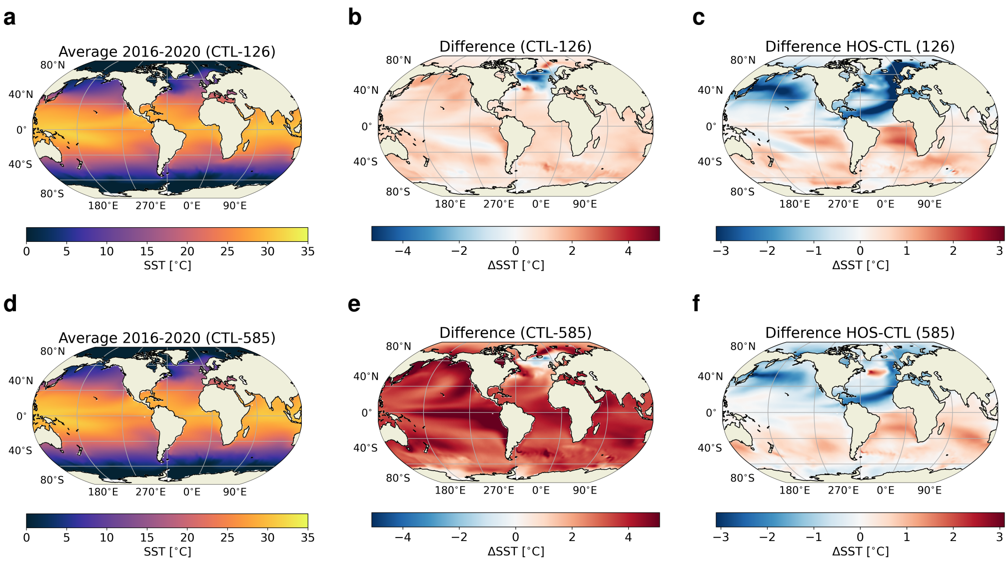

Figure 2. Sea Surface Temperature (SST) in °C for: (a) CTL-126 averaged over 2016-2020, (b) the average over 2016-2020 subtracted from the average over 2095-2099 in CTL-126, (c) CTL-126 subtracted from HOS-126 averaged over 2095-2099, and (d-f) as in (a-c) but for CTL-585 and HOS-585.

ern Equatorial and South Pacific Ocean, with in all regions a stronger response in CTL-585 compared to CTL-126. Nitrate (NO_3^-) concentrations do not decrease everywhere in the ocean in the CTL simulations, but just as with PO_4^{3-}, the strongest responses are seen in the North Atlantic, and Eastern Equatorial and South Pacific Ocean. (Fig. 3) There are also relatively strong decreases in the Northwestern Pacific Ocean. Just as for PO_4^{3-} the response is stronger in CTL-585 compared to CTL-126. Silicate (SiO_3^{2-}) shows a very similar response in the CTL simulations as NO_3^-, except in the Southern Ocean south of 40°S where a large decrease is simulated for both emission scenarios (Fig. S8). The response of iron (Fe) is slightly different compared to the other nutrients in the CTL simulations (Fig. S9). Large increases are seen in the Russian Arctic Ocean, along the equator, and in the subtropical North Atlantic Ocean. The largest descreases are seen in the rest of the Arctic Ocean, and the Northern Indian Ocean. The response in CTL-585 is typically a bit stronger compared to CTL-126, especially in the Eastern Equatorial Pacific, and south of Madagascar.

As a response to the AMOC weakening, there are additional large decreases in PO_4^{3-} concentrations for both scenarios in the North Equatorial Pacific, the Eastern Equatorial and Southern Atlantic, especially in the Benguela Upwelling System. Large increases are seen in the Canary Upwelling System (Fig. S7). The response to the AMOC weakening is very similar for NO_3^- compared to PO_4^{3-} except in the Arctic Ocean, where in the HOS simulations NO_3^- concentrations increase (Fig. 3). The response of SiO_3^{2-} to the AMOC weakening in the HOS simulations is also very similar to the responses in PO_4^{3-} and NO_3^- (Fig. S8). Again the response of Fe to the AMOC weakening in the HOS simulations compared to the CTL simulations differs from the other nutrients (Fig. S9). Most of the Southern Hemisphere sees a relative reduction in surface Fe concentrations except the South Atlantic and a small part of the South Pacific between 0 and 15°S, which actually sees some of the strongest increases relative to the CTL simulations. The North Pacific Ocean also sees relative increases, just as some parts of the North Atlantic and Arctic Ocean. In the Atlantic Ocean between 0 and 25°N, large relative decreases are seen. The two emission scenarios show very similar responses to the AMOC weakening except for some regional differences, such as in the Indian Ocean, and North Atlantic Ocean.

The response of the nutrients to the greenhouse gas emissions induced climate change in the CTL simulations result in changes in Net Primary Production (NPP; Fig. 4) and Export Production (EP; Fig. S10). NPP decreases in the North Atlantic Ocean (north of 30°N) as a response to the greenhouse gas emissions in both scenarios. In CTL-585 there are also large anomalies in the Eastern Equatorial Pacific (positive) and Western Equatorial Pacific (negative). In response to the AMOC weakening, we mostly see changes in the Atlantic basin (decrease) and in the Northeastern Equatorial Pacific (increase). In the Atlantic, the subtropical gyres (north and south) and the Benguela Upwelling System there is a large decrease in NPP, and in the Canary Upwelling System and along the North Equatorial Current there is a large increase in NPP in the HOS simulations compared to the CTL simulations.

The changes in primary productivity are also related to changes in biomass of the three phytoplankton groups. In the CTL simulations, the response of the diazotrophs (Fig. S13) can be mostly explained by the poleward shift of the 15°C isotherm (SST) as a response to the warming. We can see bands of strong increases of biomass along this isotherm with a stronger and more poleward increase in CTL-585 due to the larger warming in this simulation. In the HOS simulations, the 15°C isotherm shifts further poleward in the Southern Hemisphere due to the increased warming observed there compared to the CTL simulations. In the Northern Hemisphere, however, we see in the HOS simulations that this isotherm does not shift poleward, except for the North West Atlantic basin in HOS-585. Also diazotroph biomass decreases along the Iberian peninsula.

The diatoms show large decreases in the subpolar North Atlantic Ocean in the CTL simulations, and in CTL-585 areas with strong increases in the Southern Ocean (Fig. S14).

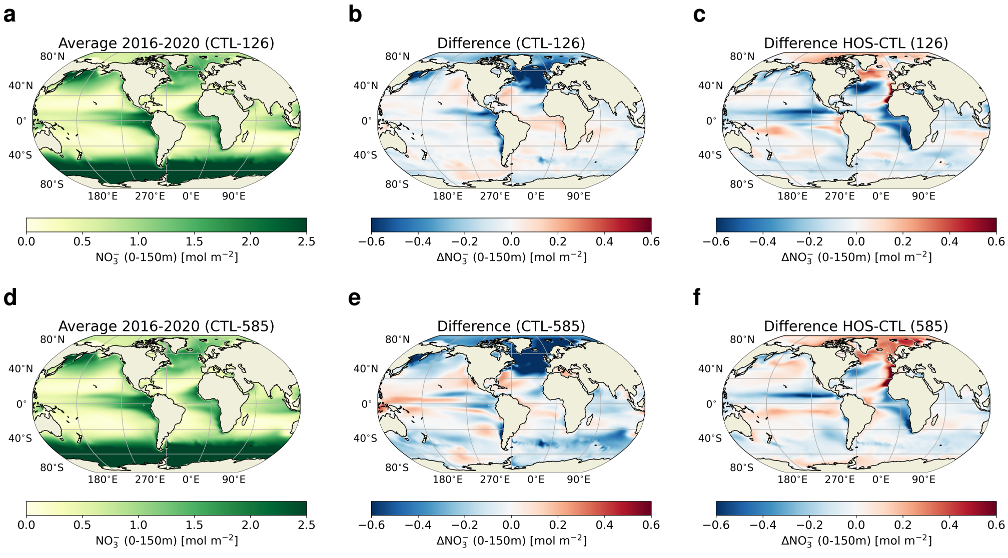

Figure 3. Nitrate (NO_3^-) concentrations integrated over the top 150 m in mol m^{-2} for: (a) CTL-126 averaged over 2016-2020, (b) the average over 2016-2020 subtracted from the average over 2095-2099 in CTL-126, (c) CTL-126 subtracted from HOS-126 averaged over 2095-2099, and (d-f) as in (a-c) but for CTL-585 and HOS-585.

This decrease in the subpolar North Atlantic can partly be explained by increased nutrient limitation due to reduced entrainment of nutrients from subsurface waters related to shallow mixed layer depth in this region. As the diatom biomass decreases, the light limitation for the small phytoplankton is lifted and they are able to outcompete the diatoms resulting in a shift of phytoplankton functional type in this region (Boot et al., 2023). In the HOS simulations, the largest changes in small phytoplankton occur very locally, i.e. between the subtropical and subpolar gyre in the North Atlantic, the Canary Upwelling System, the Benguela Upwelling System, around Tasmania and the equatorial West Pacific. In the CTL simulations, the small phytoplankton generally perform well in regions where diatom biomass decreases and vice versa, which is also the case in the HOS simulations (Fig. S15).

3.3 Role of AMOC weakening in CESM2

3.3.1 Temperature fields

The Habitat Foraging Capacipty Model (HFCM) in EcoOcean is driven by three different temperature fields: the temperature averaged over the top 150 m (Fig. S16), the temperature averaged over the entire water column (Fig. S17), and the bottom temperature (Fig. S18). The mean temperature of the top 150 m shows a different pattern than the SSTs (Fig. 2) as a response to the AMOC weakening. The top 150 m in the Subpolar North Atlantic and Arctic Ocean contains more heat in the HOS simulations compared to the CTL simulations. The Subtropical North Atlantic Ocean cools, whereas the South Atlantic warms. In the Indian and Southern Ocean, the northern Subtropical and southern Subpolar Pacific we see warming, and in the northern Subpolar and southern Subtropical Pacific we see cooling. Bottom temperatures show the largest response in the shallow regions. Generally these regions cool in the Northern Hemisphere and warm in the Southern Hemisphere. A major exception is the Arctic Ocean and some

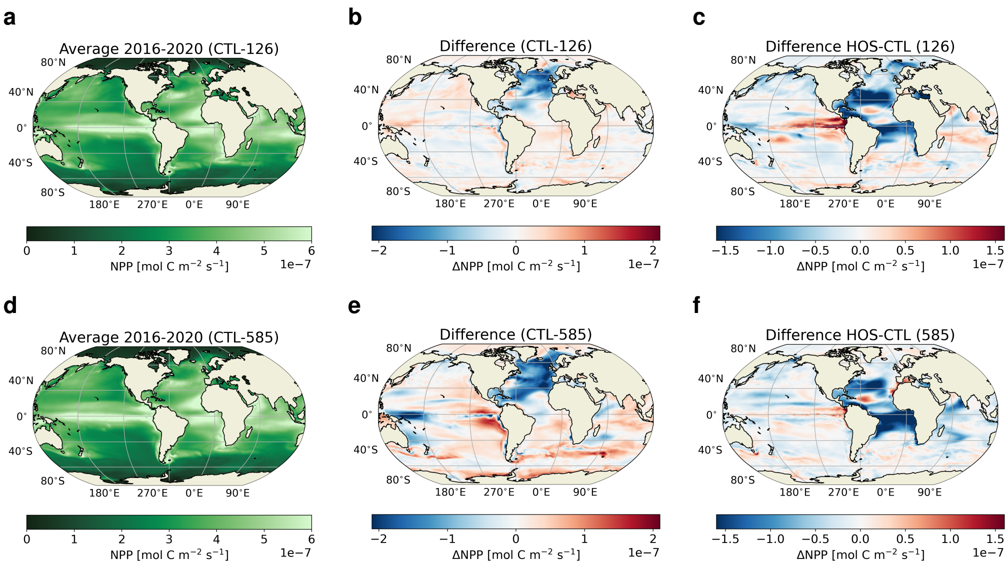

Figure 4. Net Primary Production integrated over the top 150 m in mol C m^{-2} s^{-1} for: (a) CTL-126 averaged over 2016-2020, (b) the average over 2016-2020 subtracted from the average over 2095-2099 in CTL-126, (c) CTL-126 subtracted from HOS-126 averaged over 2095-2099, and (d-f) as in (a-c) but for CTL-585 and HOS-585.

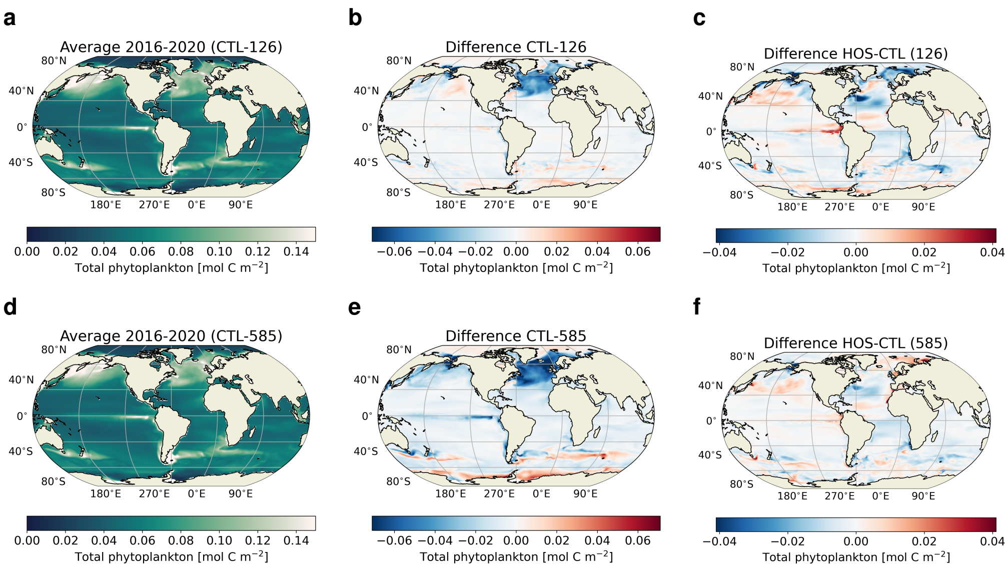

Figure 5. Total phytoplanktoon biomass integrated over the top 150 m in mol C m^{-2} for: (a) CTL-126 averaged over 2016-2020, (b) the average over 2016-2020 subtracted from the average over 2095-2099 in CTL-126, (c) CTL-126 subtracted from HOS-126 averaged over 2095-2099, and (d-f) as in (a-c) but for CTL-585 and HOS-585.

regions in the Subpolar North Atlantic Ocean that warm strongly. The column averaged water temperature follows generally the trend in the top temperature, except in the shallow regions. Here the trends are more similar to the trends seen in the bottom temperature. The warming in the Subpolar North Atlantic and Arctic Ocean are related to the insulating effects of sea ice. The warming in the Northern Subtropical and cooling in the Southern Subtropical Pacific Ocean are related to the stratification. Increased stratification north of the equator results in less upward mixing of cool subsurface waters while south of the equator the opposite occurs. The other regions follow the trends generally also observed in SSTs and SATs and are thus related to the forcing at the surface ocean.

3.3.2 Diazotrophs

The extent of the diazotrophs (Fig. S13) is limited by the 15°C SST (Fig. 2) isotherm as described earlier. The additional AMOC weakening in the HOS simulations affects the location of this isotherm on top of the climate change signal. In the HOS simulations in the Southern Hemisphere it shifts poleward due to the additional warming there, and in the North Pacific it shifts equatorward due to the relative cooling. In the North Atlantic the response is a bit different, and also differs between the emission scenarios. In the SSP1-2.6 scenario it shifts equatorward with a stronger response on the eastern side of the basin. On the eastern side of the basin water from the subpolar North Atlantic is advected southward. Since the subpolar region cools strongly due to the AMOC weakening, these water masses are relatively cool causing the relative cooling observed around the Iberian peninsula. In SSP5-8.5 this response on the eastern side of the basin is also seen, but on the western side we see a poleward increase of the diazotrophs because of a patch of surface ocean around 50°N that warms. This warming is caused by a southward shift of the North Atlantic Current in CTL-585 that is not found in to HOS-585 and the SSP1-2.6 simulations (Fig. S19).

3.3.3 Diatoms

For the diatoms (Fig. S14) there are a few regions that stand out in the HOS simulations compared to the CTL simulations. In the Western North Pacific Ocean, Eastern Equatorial Pacific Ocean, and North Subpolar Atlantic Ocean there are relative increases in diatom biomass for both emission scenarios over a relatively large area. Locally, there are also relative increases around Tasmania and in the Canary Upwelling System. The largest decreases are found in the extension of the Gulf Stream and in the Benguela Upwelling System.

The increases of diatoms in the Canary Upwelling System can be attributed to the strengthened trade winds (Fig. S3) in the HOS simulations which increase upwelling (Fig. S5) in this region. This upwelling supplies more nutrients to the surface ocean driving an increase in NPP in this region (Figs. 4 and S11). Also the increases in the Equatorial Pacific can be related to the AMOC weakening. The southward shift of the ITCZ decreases the stratification north of the equator (Fig. S4) because the freshwater flux at the surface ocean decreases (Fig. S3). The weaker stratification leads to deeper mixed layer depths (Fig. S20) and more entrainment of nutrients from the subsurface ocean. The increased availability of nutrients in the surface ocean drives an increase in diatom productivity and biomass (Figs. S11 and S14). The response in the North Subpolar Atlantic Ocean, where we see a region with a relative increase of diatoms biomass (in the gyre), and a region with a relative decrease of diatom biomass, can be explained by the NO_3^- concentrations (Fig. 3). In the CTL simulations, NO_3^- decreases in the subpolar region, increasing the nitrogen limitation of all phytoplankton in this region. Under increased nutrient stress, small phytoplankton are able to outcompete the diatoms (Boot et al., 2023). In the HOS simulations, the NO_3^- concentrations increase in the subpolar gyre, and decrease in the extension of the Gulf Stream, and the diatoms respond, by increasing their mass in the subpolar gyre, and decreasing their mass in the extension of the Gulf Stream compared to the CTL simulations. The NO_3^- concentrations in the extension of the Gulf Stream decrease because the weaker Gulf Stream transports less nutrients northwards, which is directly related to the weakening of the AMOC. Diatom

Table 1. Relative change in % of different total phytoplankton biomass, biomass of the three phytoplankton groups in CESM2, Total System Biomass, Total Consumer Biomass and total commercial biomass in EcoOcean in the year 2099 for the four different simulations and the difference between the HOS and CTL simulations (fourth column for SSP1-2.6 and last column for SSP5-8.5). Relative change is defined as the difference in biomass between 2099 and 2015 divided by the biomass in 2015.

Group	CTL-126	HOS-126	Δ-126	CTL-585	HOS-585	Δ-585
Total phytoplankton biomass	-3.99	-7.41	-3.42	-12.71	-13.56	-0.85
Small phytoplankton biomass	5.91	5.38	-0.53	-5.94	-9.00	-3.06
Diatom biomass	-13.96	-20.98	-7.02	-21.62	-20.44	1.18
Diazotroph biomass	3.81	3.03	-0.78	11.15	11.75	0.60
Total System Biomass	-1.41	-5.20	-3.78	-11.29	-13.33	-2.03
Total Consumer Biomass	-1.64	-5.92	-4.28	-12.49	-14.80	-2.31
Commercial species	-1.48	-4.92	-3.43	-12.75	-15.51	-2.76

biomass decreases in the Benguela Upwelling System because the advection of Si through the Aghulas leakage reduces.

3.3.4 Small Phytoplankton

Generally, small phytoplankton (Fig. S15) respond opposite to the diatoms in the HOS simulations compared to the CTL simulations. This is because the diatoms and small phytoplankton are generally competing for the same nutrients. Due to the AMOC weakening, locally the environmental conditions can change that can either favor the diatoms or the small phytoplankton. For example, the reduced Si concentrations in the Benguela Upwelling System (Fig. S8) causes the small phytoplankton to become dominant in this region since they are able to outcompete the diatoms.

3.3.5 Total phytoplankton biomass

The change in total phytoplankton biomass (Fig. 5) is generally the combined signal of the changes observed in diatom biomass and small phytoplankton biomass. There are, however, some regions where diatoms replace small phytoplankton or vice versa. In these regions the signal observed in the diatoms is generally dominant, but not everywhere (e.g. in the Fram Strait in SSP1-2.6). For each plankton type and the total phytoplankton biomass, the relative change over the simulation in % is shown in Table 1 for the entire ocean, and in Table S1 per region in the ocean.

3.4 EcoOcean: ecosystem response

There is a clear difference in the response in EcoOcean to the emission scenarios. In CTL-126, total system biomass (TSB) decreases by 1.41%, total consumer biomass (TCB) by 1.64% and commercial species by 1.48% (Table 1). In CTL-585, the decreases are much stronger: TSB decreases by 11.29%, TCB by 12.49% and commercial biomass by 12.75% (Table 1).

The response to the greenhouse gas emissions is different per region (Table 2). In both CTL-126 and CTL-585 the ocean around Antarctica (66°S – 90°) gain the most TSB (37.17% and 47.3%, respectively), and the subpolar North Atlantic and Pacific Ocean lose the most TSB (16.9% and 33.64% for the Atlantic and 12.92% and 25.98% for the

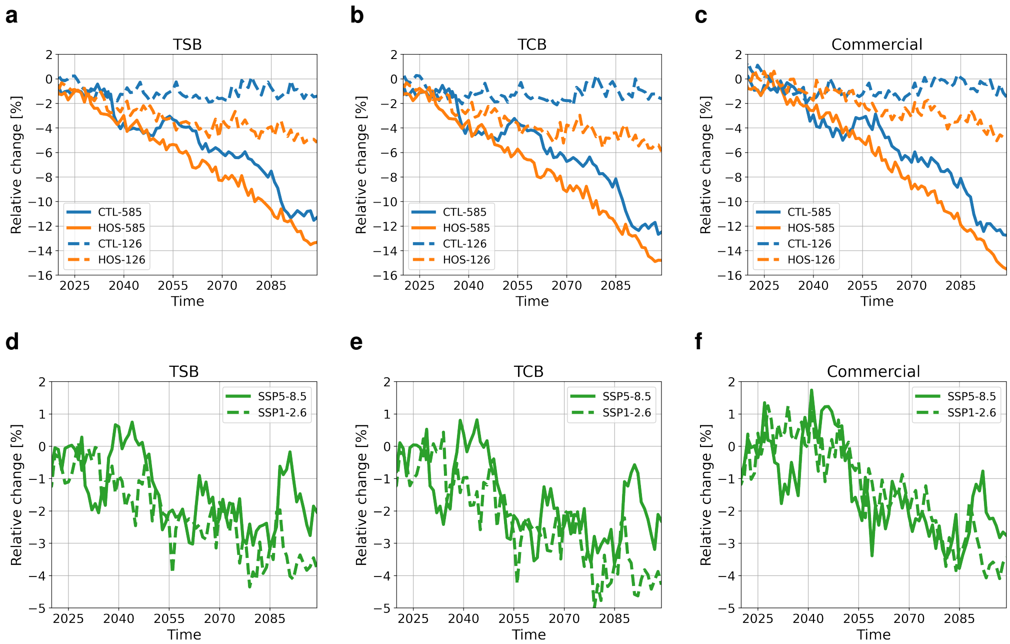

Figure 6. Relative changes in % in the CTL and HOS simulations (top row) and the difference between the two (bottom row) for Total System Biomass (TSB; a, d), Total Consumer Biomass (TCB; b, e), and Commercial species (c, f). Dashed lines represent SSP1-2.6 and solid lines SSP5-8.5. Blue represent the CTL simulations, orange the HOS simulations, and green the difference between the two (HOS minus CTL).

Pacific). An important difference between the emission scenarios is how the ecosystems develop in the Arctic Ocean (66°N – 90°N). In CTL-126 the Arctic Ocean loses 9.34% in TSB, while in CTL-585 we see an increase of 12.71%, which can be explained by looking at the sea-ice cover (Fig. S6). In CTL-585 most sea ice disappears which boosts NPP (Fig. 4) in this region providing the ecosystem with biomass to feed upon in a bottom up manner.

The effect of the strong AMOC weakening in HOS-126 results in a decrease in biomass with respect to CTL-126. TSB decreases with 3.78% with respect to CTL-126 and 5.20% in total (Table 1). The largest responses are seen in the Arctic Ocean, subpolar and subtropical (15°N-40°N) North Atlantic Ocean (30.45, 15.22, and 13.24% decrease in TSB with respect to CTL-126; Table 2). Compared to SSP1-2.6, the relative effect of the AMOC weakening is lower in SSP5-8.5 which is related to the much stronger climate forcing in the high emission scenario. TSB decreases with 2.03% with respect to CTL-585 and 13.33% in total. The largest response in TSB over time is seen in the Arctic Ocean and the subpolar North Atlantic, but, just as with the AMOC and GMST difference (Fig. 1), the difference becomes smaller over time. In 2100, the regions with the largest response in TSB are the oceans around Antarctica (an increase of 12.97% with respect to CTL-585), and in the Atlantic north of 15°S (a decrease of 6.38% around the equator, 5.9% in the subtropical gyre and 6.87% in the subpolar gyre (Fig. 7) with respect to CTL-585).

TCB and commercial species show similar results as for TSB, but the global response is slightly stronger (except for commercial species in HOS-126), i.e. there is a larger decrease in biomass of TCB and commercial species compared to TSB (Fig. 6). Regionally, the response is generally also similar to the results for TSB, but whether the response

Table 2. Relative change in % of Total System Biomass (TSB), Total Consumer Biomass (TCB) and total commercial biomass (COM) in 2099 for the difference between the HOS and CTL simulations for different regions in the ocean. Relative change is defined as in the main text as the difference in biomass between 2099 and 2015 divided by the biomass in 2015.

Region		TSB Δ-126	TSB Δ-585	TCB Δ-126	TCB Δ-585	COM Δ-126	COM Δ-585
Arctic Ocean	66°N - 90°N	-30.45	0.20	-31.58	0.19	-16.6	-1.18
Atlantic Ocean	40°N - 66°N	-15.22	-6.87	-15.88	-7.23	-17.1	-11.39
	15°N - 40°N	-13.24	-5.90	-14.46	-6.46	-15.04	-6.70
	15°S - 15°N	-5.82	-6.38	-7.25	-7.66	-7.93	-8.75
	15°S - 40°S	-2.15	-1.06	-3.04	-1.03	-4.77	-3.21
	40°S - 66°S	0.43	-2.78	0.86	-3.04	1.54	-5.03
Pacific Ocean	40°N - 66°N	-3.96	-4.87	-4.67	-5.18	4.73	1.02
	15°N - 40°N	2.33	2.04	2.33	2.03	3.17	1.71
	15°S - 15°N	-0.54	-0.88	0.94	-1.24	-0.14	-2.51
	15°S - 40°S	-7.93	-1.13	-8.26	-1.37	-7.13	-2.33
	40°S - 66°S	0.31	-3.06	0.86	-3.08	-0.36	-2.43
Indian Ocean	North of 15°S	0.09	-0.75	-0.09	-0.64	-0.41	-0.80
	15°N - 40°N	-2.03	-5.70	-2.57	-6.35	-2.89	-5.95
	40°N - 66°N	-5.37	4.97	-5.67	5.79	-4.31	5.95
Southern Ocean	66°S - 90°S	4.87	12.97	5.69	14.26	-13.58	14.05

is stronger or weaker differs per region (Table 2, Fig. 8 and Fig. 9). Interesting differences are, for example, that TSB increases in the subpolar North Pacific and decreases in the Antarctic Ocean as a response to the strong AMOC weakening, but that the biomass of commercial species show the opposite response (i.e. a decrease and an increase, respectively) in SSP1-2.6. This effect occurs in regions surrounding the sea-ice edge. This suggests that lower trophic levels respond faster to sea ice changes resulting in the decrease in TSB and TCB, while higher trophic levels respond slower resulting in a different response in total commercial biomass.

3.5 Role of AMOC weakening in EcoOcean

Total system (Fig. 7), consumer (Fig. 8), and commercial (Fig. 9), biomass all respond similar to the AMOC weakening (Fig. 6). Here we discuss the role of the AMOC weakening on total consumer biomass, and the mechanisms described also apply to total system and commercial biomass. Total consumer biomass (Fig. 8) follows in most regions the patterns seen in changes in total phytoplankton biomass. This means that to first order, the effects of an AMOC weakening on marine ecosystems follow the same mechanisms as for total phytoplankton biomass, which is the combined effect of the mechanisms present for the diazotrophs, diatoms and small phytoplankton. This means that the effects of an AMOC weakening affect marine ecosystems in a bottom up fashion by affecting the lowest trophic levels which through food web dynamics affect the entire ecosystem. There are a few regions that do not follow the patterns seen in total phytoplankton biomass, i.e. the Canary and Benguela Upwelling Systems, and the extension of the Gulf Stream. These are regions where a shift occurs in phytoplankton dominance, i.e. from small phytoplankton to diatoms in the Canary Upwelling System, and the other way around for the other two regions. These changes affect the food web dynamics in EcoOcean. In the Benguela Upwelling System and the surrounding ocean a decrease in total phytoplankton biomasss is simulated in CESM2 (Fig. 5), but the surrounding oceans in EcoOcean show an increase in TCB (Fig. 8). Besides an increase in TCB, the sur-

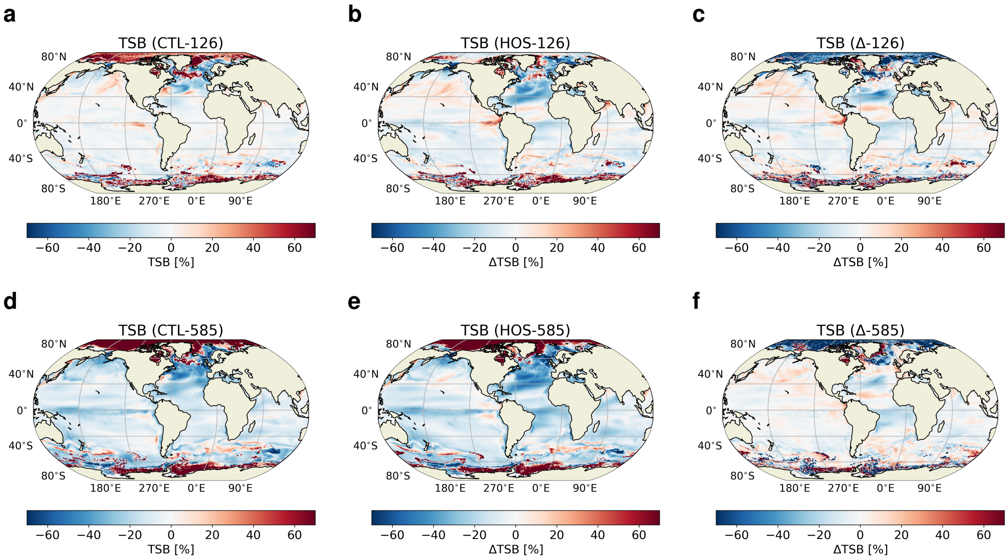

Figure 7. Relative changes averaged over 2095-2099 compared to 2016-2020 in % for Total System Biomass (TSB) in the CTL simulations (a, d), HOS simulations (b, e), and the difference between the two (c, f). (a-c) are for SSP1-2.6 and (d-f) are fore SSP5-8.5.

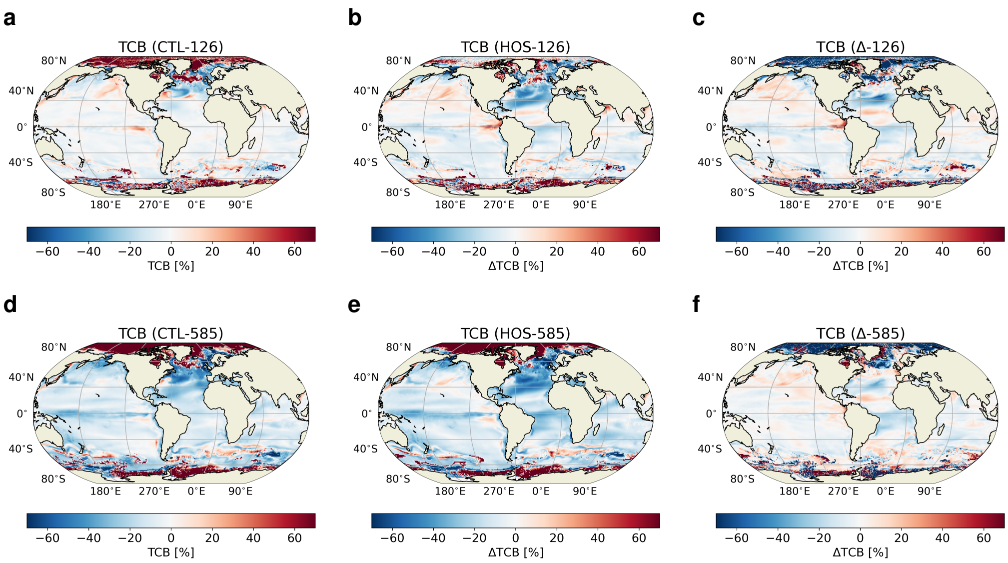

Figure 8. Relative changes averaged over 2095-2099 compared to 2016-2020 in % for Total Consumer Biomass (TCB) in the CTL simulations (a, d), HOS simulations (b, e), and the difference between the two (c, f). (a-c) are for SSP1-2.6 and (d-f) are fore SSP5-8.5.

rounding oceans also see an increase in both meso- and microzooplankton. Mesozooplankton (Fig. S22) are a central organism in the food web that feed on diatoms, diazotrophs and microzooplankton (Fig. S21) which predominantly feed on small phytoplankton. Since mesozooplankton have multiple food sources, they are able to increase their biomass even though diatom biomass is lost in this region. The reason why TCB follows mesozooplank-

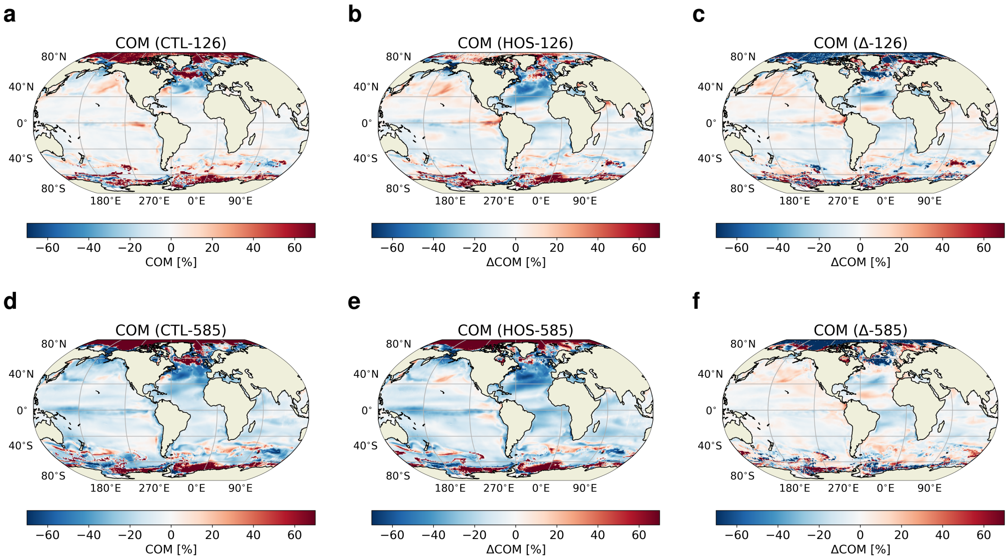

Figure 9. Relative changes averaged over 2095-2099 compared to 2016-2020 in % for commercial species (COM) in the CTL simulations (a, d), HOS simulations (b, e), and the difference between the two (c, f). (a-c) are for SSP1-2.6 and (d-f) are fore SSP5-8.5.

ton biomass closely is that mesozooplankton have a central role in the ecosystem since they are preyed upon by 26 different functional groups, and often are the most important food source for these groups in EcoOcean. In the Canary Upwelling System, we see a strong increase in phytoplankton biomass due to an increase in diatom biomass over a loss of small phytoplankton biomass. This leads to an increase in large zooplankton (krill; Fig. S23), a small decrease in mesozooplankton and a large decrease in microzooplankton. In the Benguela Upwelling System similar mechanisms with opposite effects are present, and the changes in the food web dynamics lead to reduced TCB in this region. In the extension of the Gulf Stream we find a strong decrease in diatom biomass in the HOS simulations, which is partly compensated for by small phytoplankton. However, the net effect in this region is a strong decrease in total phytoplankton biomass. TCB does not follow this strong decrease in total phytoplankton biomass. This is because the increase in small phytoplankton biomass, results in an increase in microzooplankton biomass. The mesozooplankton are consequently able to replace diatoms as a food source with microzooplankton as a food source.

4 Discussion

In this study we have looked at the effect of a strong weakening of the Atlantic Meridional Overturning Circulation (AMOC) on future global marine ecosystems under a low and high emission scenario. Fig. 10 provides an overview of how the AMOC weakening affects the climate system, ocean biogeochemistry and marine ecosystems. We see that the AMOC weakening has a large impact on the ocean state influencing ocean circulation, stratification and upwelling which leads to changes in the 3D nutrient fields. The changes in the nutrient fields directly affect the productivity and biomass of the three phytoplankton groups simulated in CESM2, i.e. the diazotrophs, diatoms and small phytoplankton. The effects of the AMOC weakening on the phytoplankton cascade through the food web leading to a similar response in total consumer biomass as the response in total phytoplankton biomass. There are some regions that deviate from this overall response. These regions typically see a shift in dominant phytoplankton group which causes an adjustment in the abundance of the three different zooplankton groups in EcoOcean. The mesozooplankton group is a central group in the food web that preys on both diatoms and microzooplankton that in turn prey on the small phytoplankton group. Through this differential feeding, mesozooplankton do not directly follow the trend of total phytoplankton biomass in regions that observe a phytoplankton composition shift.

Overall, climate change causes a reduction in both total system and total consumer biomass with a much stronger response in the high emission scenario. Similar changes are seen in the commercial species, suggesting that these effects will also be felt in socio-economic systems. The AMOC weakening leads to a stronger decrease in biomass in the aggregated groups mentioned above. The responses in total system, consumer and commercial biomass to an AMOC weakening are larger than the responses in total phytoplankton biomass, showing that the effect of the AMOC weakening is stronger on higher trophic levels.

EcoOcean has previously been coupled to Earth System Model (ESM) simulations using the GFDL and IPSL ESMs (Coll et al., 2020). Both ESMs show a different response for TSB to the climate change and the CESM2 simulations result in again a different response that lies between both the GFDL (relatively positive) and the IPSL (quite negative) responses. In FishMIP2 (Tittensor et al., 2021), EcoOcean is one of the more conservative marine ecosystem models and the only MEM with a complete, resilient food web. Compared to these two studies (Coll et al., 2020; Tittensor et al., 2021), the results presented here for TSB could be either more positive or negative when a different ESM is used, and more extreme in biomass loss when a different MEM is used.

There is quite some work based on Earth System Models of Intermediate Complexity (so-called EMICs) which generally focuses on longer timescales (i.e. multi-centennial to multi-millennial). These studies show a wide range of possible responses in the marine carbon cycle (Zickfeld et al., 2008), but no clear analysis has been performed on marine ecosystems. Schmittner (2005) looks at the ecosystem response to an AMOC weakening using a much simpler model than the models used in this study and suggests that on long timescales an AMOC weakening results in a suppression of NPP in the Atlantic, which is also what we find.

Since only one ESM and one MEM are used here, the results could be model dependent. The most important forcing in EcoOcean is the total phytoplankton biomass simulated in CESM2, and it would be very valuable to also use models with at least a different biogeochemical module, and preferably a different ESM with a different ocean component than CESM2. The spread in MEMs in FishMIP2 is generally smaller than that of ESMs in CMIP6 (Tittensor et al., 2021), and therefore additional simulations with different MEMs will provide less information than using different ESMs, but are valuable, nonetheless.

The results presented in this study hold implications for the efforts of mitigating climate change, the management of marine ecosystems, and socio-economic systems. If the AMOC strongly weakens, or even collapses in the coming century, marine ecosystems are negatively affected. This comes on top of the generally negative effects that anthropogenic climate change and other human activities such as fisheries have on these same ecosystems (Coll et al., 2020; Tittensor et al., 2021). We show that the AMOC weakening on top of anthropogenic climate change can result in basin wide depletion of high trophic level organisms, which can be also important for fisheries and food security. Previous studies have already stated that an AMOC weakening can affect societies through large regional climate changes (van Westen et al., 2024; Brovkin et al., 2021). We show here an additional pathway on how an AMOC weakening affects socio-economic systems through a reduction in abundance of commercial species. Since fish is an essential source of protein for millions of people (FAO, 2022), an AMOC weakening can have a disrup-

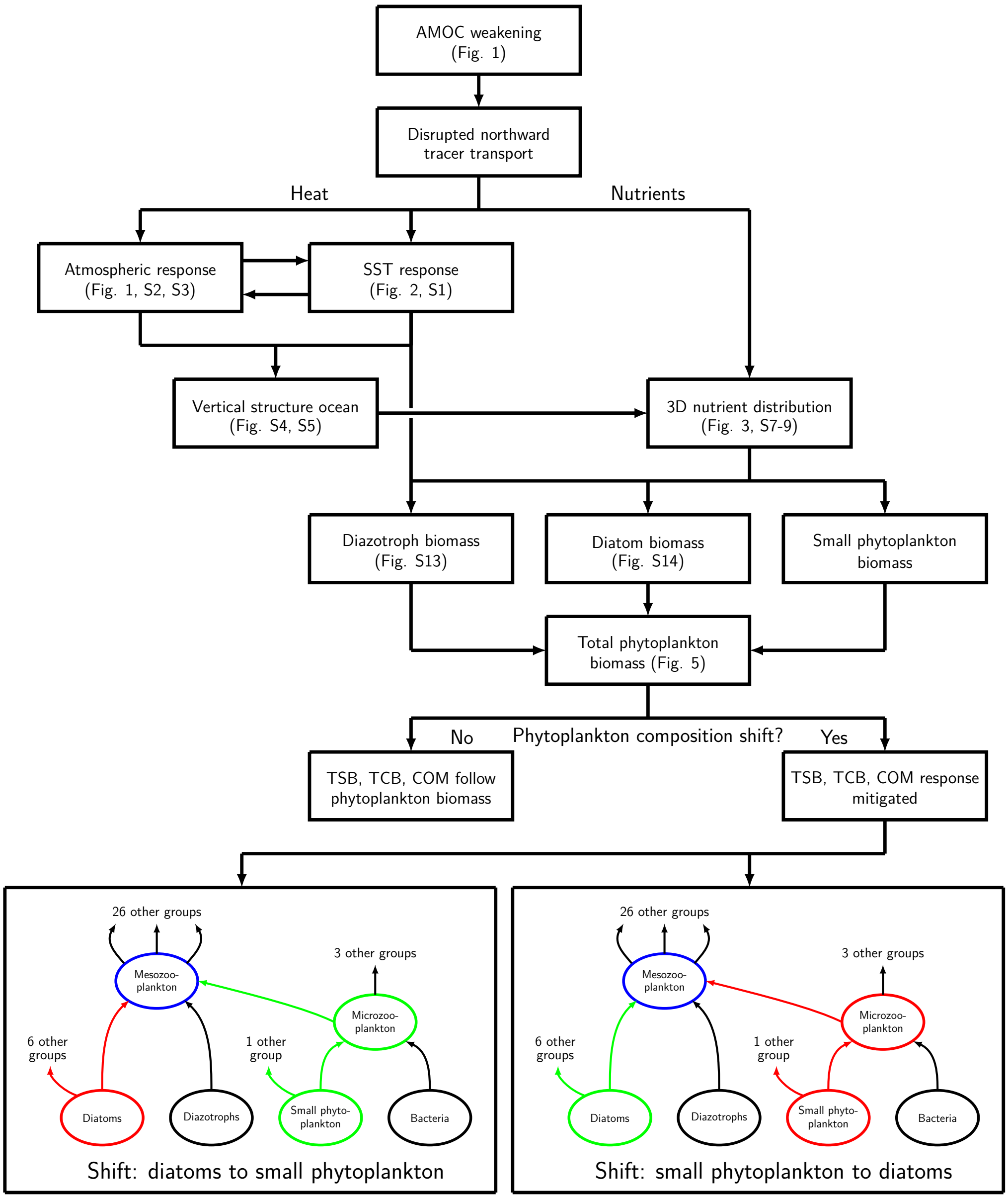

Figure 10. Summarizing figure showing in a simplified way how an AMOC weakening influences the climate system, ocean biogeochemistry and marine ecosystems. The diagrams at the bottom represent part of the food web in EcoOcean showing the response of the food web to a phytoplankton composition shift. The colors represent a decrease in biomass (red), an increase in biomass (green), and an unknown response (blue) in the mesozooplankton group.

tive effect on human societies. This is especially relevant since recent studies suggest we are approaching a tipping point for the AMOC (Ditlevsen & Ditlevsen, 2023; van Westen et al., 2024).

To conclude, in this study we have simulated a strong AMOC weakening using a low and high emission scenario in the CMIP6 state-of-the-art Earth System Model CESM2.

We forced a Marine Ecosystem Model, EcoOcean, with the CESM2 results to show the impact of an AMOC weakening on marine ecosystems. Both the low and high emission scenario show negative effects of the marine ecosystem, meaning that an AMOC weakening is an additional threat next to anthropogenic climate change. Another implication of our results is that tipping in the climate system can cascade over system boundaries to marine ecosystems, with possibly very negative effects on socio-economical systems.

5 Open Research

The scripts used for analysis and plotting, including the necessary datasets are saved in a repository: `https://doi.org/10.5281/zenodo.10891003` (Boot, Steenbeek, et al., 2024). In this repository also the most important output from the CESM2 and EcoOcean simulations is provided.

Acknowledgments

This study has been supported by the Netherlands Earth System Science Centre (NESSC), which is financially supported by the Ministry of Education, Culture and Science (OCW; Grant 024.002.001). A.A.B. and H.A.D. are also funded by the European Research Council through the ERC-AdG project TAOC (project 101055096). JS and MC acknowledge the European Union's Horizon 2020 research and innovation programme under grant agreement N°817578 (TRIATLAS) and the Spanish Ministry of Science and Innovation grant agreement N°PID2020-118097RB-I00 (ProOceans). MC acknowledges institutional support of the 'Severo Ochoa Centre of Excellence' accreditation (CEX2019-000928-S). The work of A.S.vdH. was also funded by the Dutch Research Council (NWO) through the NWO-Vici project 'Interacting climate tipping elements: When does tipping cause tipping?' (project VI.C.202.081). The authors want to thank Michael Kliphuis (IMAU, Utrecht University) for performing the CESM2 simulations, which were performed at SURFsara in Amsterdam on the Dutch Supercomputer Snellius under NWO-SURF project 17239.

References

Ahrens, R. N. M., Walters, C. J., & Christensen, V. (2012). Foraging arena theory. *Fish and Fisheries*, *13*(1), 41–59. doi: https://doi.org/10.1111/j.1467-2979.2011.00432.x

Boot, A. A., Steenbeek, J., Coll, M., von der Heydt, A. S., & Dijkstra, H. A. (2024, mar). *dboot0016/EF2024_CESM2_EcoOcean: v1.1.* Zenodo. doi: 10.5281/zenodo.10891003

Boot, A. A., von der Heydt, A. S., & Dijkstra, H. A. (2023). Effect of Plankton Composition Shifts in the North Atlantic on Atmospheric pCO2. *Geophysical Research Letters*, *50*(2), e2022GL100230. doi: https://doi.org/10.1029/2022GL100230

Boot, A. A., von der Heydt, A. S., & Dijkstra, H. A. (2024). Response of atmospheric pCO_2 to a strong AMOC weakening under low and high emission scenarios. *Under review at Climate Dynamics*.

Boucher, O., Servonnat, J., Albright, A. L., Aumont, O., Balkanski, Y., Bastrikov, V., ... Vuichard, N. (2020). Presentation and Evaluation of the IPSL-CM6A-LR Climate Model. *Journal of Advances in Modeling Earth Systems*, *12*(7), e2019MS002010. doi: https://doi.org/10.1029/2019MS002010

Breitburg, D., Levin, L. A., Oschlies, A., Grégoire, M., Chavez, F. P., Conley, D. J., ... Zhang, J. (2018). Declining oxygen in the global ocean and coastal waters. *Science*, *359*(6371), eaam7240. doi: 10.1126/science.aam7240

Brovkin, V., Brook, E., Williams, J. W., Bathiany, S., Lenton, T. M., Barton, M., ... Yu, Z. (2021). Past abrupt changes, tipping points and cascading impacts in the Earth system. *Nature Geoscience*, *14*(8), 550–558. doi: 10.1038/s41561-021-00790-5

Caesar, L., Rahmstorf, S., Robinson, A., Feulner, G., & Saba, V. (2018). Observed fingerprint of a weakening Atlantic Ocean overturning circulation. *Nature*, *556*(7700), 191–196. doi: 10.1038/s41586-018-0006-5

Christensen, V., Coll, M., Buszowski, J., Cheung, W. W. L., Frölicher, T., Steenbeek, J., … Walters, C. J. (2015). The global ocean is an ecosystem: simulating marine life and fisheries. *Global Ecology and Biogeography*, *24*(5), 507–517. doi: https://doi.org/10.1111/geb.12281

Christensen, V., Coll, M., Steenbeek, J., Buszowski, J., Chagaris, D., & Walters, C. J. (2014). Representing Variable Habitat Quality in a Spatial Food Web Model. *Ecosystems*, *17*(8), 1397–1412. doi: 10.1007/s10021-014-9803-3

Coll, M., Steenbeek, J., Pennino, M. G., Buszowski, J., Kaschner, K., Lotze, H. K., … Christensen, V. (2020). Advancing Global Ecological Modeling Capabilities to Simulate Future Trajectories of Change in Marine Ecosystems. *Frontiers in Marine Science*, *7*. doi: 10.3389/fmars.2020.567877

Danabasoglu, G. (2019). *NCAR CESM2 model output prepared for CMIP6 CMIP esm-hist.* Earth System Grid Federation. doi: 10.22033/ESGF/CMIP6.7575

Danabasoglu, G., Lamarque, J.-F., Bacmeister, J., Bailey, D. A., DuVivier, A. K., Edwards, J., … Strand, W. G. (2020). The Community Earth System Model Version 2 (CESM2). *Journal of Advances in Modeling Earth Systems*, *12*(2), e2019MS001916. doi: https://doi.org/10.1029/2019MS001916

Diaz, R. J., & Rosenberg, R. (2008). Spreading Dead Zones and Consequences for Marine Ecosystems. *Science*, *321*(5891), 926–929. doi: 10.1126/science.1156401

Ditlevsen, P., & Ditlevsen, S. (2023). Warning of a forthcoming collapse of the Atlantic meridional overturning circulation. *Nature Communications*, *14*(1), 4254.

Doney, S. C., Ruckelshaus, M., Emmett Duffy, J., Barry, J. P., Chan, F., English, C. A., … Talley, L. D. (2012). Climate Change Impacts on Marine Ecosystems. *Annual Review of Marine Science*, *4*(1), 11–37. doi: 10.1146/annurev-marine-041911-111611

Dunne, J. P., Horowitz, L. W., Adcroft, A. J., Ginoux, P., Held, I. M., John, J. G., … Zhao, M. (2020). The GFDL Earth System Model Version 4.1 (GFDL-ESM 4.1): Overall Coupled Model Description and Simulation Characteristics. *Journal of Advances in Modeling Earth Systems*, *12*(11), e2019MS002015. doi: https://doi.org/10.1029/2019MS002015

Eyring, V., Bony, S., Meehl, G. A., Senior, C. A., Stevens, B., Stouffer, R. J., & Taylor, K. E. (2016, may). Overview of the Coupled Model Intercomparison Project Phase 6 (CMIP6) experimental design and organization. *Geosci. Model Dev.*, *9*(5), 1937–1958. doi: 10.5194/gmd-9-1937-2016

FAO. (2022). *The state of world fisheries and aquaculture 2022.* FAO.

Forget, G., & Ferreira, D. (2019). Global ocean heat transport dominated by heat export from the tropical Pacific. *Nature Geoscience*, *12*(5), 351–354. doi: 10.1038/s41561-019-0333-7

Gattuso, J.-P., Magnan, A., Billé, R., Cheung, W. W. L., Howes, E. L., Joos, F., … Turley, C. (2015). Contrasting futures for ocean and society from different anthropogenic CO₂ emissions scenarios. *Science*, *349*(6243), aac4722. doi: 10.1126/science.aac4722

Henson, S. A., Cael, B. B., Allen, S. R., & Dutkiewicz, S. (2021). Future phytoplankton diversity in a changing climate. *Nature Communications*, *12*(1), 5372. doi: 10.1038/s41467-021-25699-w

Henson, S. A., Laufkötter, C., Leung, S., Giering, S. L. C., Palevsky, H. I., & Cavan, E. L. (2022). Uncertain response of ocean biological carbon export in a changing world. *Nature Geoscience*, *15*(4), 248–254. doi:

10.1038/s41561-022-00927-0

Hoegh-Guldberg, O., & Bruno, J. F. (2010). The Impact of Climate Change on the World's Marine Ecosystems. *Science*, *328*(5985), 1523–1528. doi: 10.1126/science.1189930

Hunke, E. C., Lipscomb, W. H., Turner, A. K., Jeffrey, N., & Elliott, S. (2015). *CICE: The Los Alamos Sea Ice Model documentation and software user's manual, version 5.1. Doc* (Tech. Rep.). LA-CC-06-012, 116 pp., http://www. ccpo. odu. edu.

IPCC. (2022). *The ocean and cryosphere in a changing climate.* Cambridge, England: Cambridge University Press.

Ito, T., & Follows, M. J. (2005). Preformed phosphate, soft tissue pump and atmospheric CO2. *Journal of Marine Research*, *63*(4), 813–839. doi: doi:10.1357/0022240054663231

Kwiatkowski, L., Torres, O., Bopp, L., Aumont, O., Chamberlain, M., Christian, J. R., ... Ziehn, T. (2020). Twenty-first century ocean warming, acidification, deoxygenation, and upper-ocean nutrient and primary production decline from CMIP6 model projections. *Biogeosciences*, *17*(13), 3439–3470. doi: 10.5194/bg-17-3439-2020

Lawrence, D. M., Fisher, R. A., Koven, C. D., Oleson, K. W., Swenson, S. C., Bonan, G., ... Zeng, X. (2019, dec). The Community Land Model Version 5: Description of New Features, Benchmarking, and Impact of Forcing Uncertainty. *Journal of Advances in Modeling Earth Systems*, *11*(12), 4245–4287. doi: https://doi.org/10.1029/2018MS001583

Lenton, T. M., Held, H., Kriegler, E., Hall, J. W., Lucht, W., Rahmstorf, S., & Schellnhuber, H. J. (2008). Tipping elements in the Earth's climate system. *Proceedings of the National Academy of Sciences*, *105*(6), 1786–1793. doi: 10.1073/pnas.0705414105

Liu, X., Battisti, D. S., & Donohoe, A. (2017). Tropical Precipitation and Cross-Equatorial Ocean Heat Transport during the Mid-Holocene. *Journal of Climate*, *30*(10), 3529–3547. doi: https://doi.org/10.1175/JCLI-D-16-0502.1

Long, M. C., Moore, J. K., Lindsay, K., Levy, M., Doney, S. C., Luo, J. Y., ... Sylvester, Z. T. (2021). Simulations With the Marine Biogeochemistry Library (MARBL). *Journal of Advances in Modeling Earth Systems*, *13*(12), e2021MS002647. doi: https://doi.org/10.1029/2021MS002647

Lotze, H. K., Tittensor, D. P., Bryndum-Buchholz, A., Eddy, T. D., Cheung, W. W. L., Galbraith, E. D., ... Worm, B. (2019). Global ensemble projections reveal trophic amplification of ocean biomass declines with climate change. *Proceedings of the National Academy of Sciences*, *116*(26), 12907–12912. doi: 10.1073/pnas.1900194116

Manral, D., Iovino, D., Jaillon, O., Masina, S., Sarmento, H., Iudicone, D., ... van Sebille, E. (2023). Computing marine plankton connectivity under thermal constraints. *Frontiers in Marine Science*, *10*. doi: 10.3389/fmars.2023.1066050

Martell, S. J. D., Essington, T. E., Lessard, B., Kitchell, J. F., Walters, C. J., & Boggs, C. H. (2005). Interactions of productivity, predation risk, and fishing effort in the efficacy of marine protected areas for the central Pacific. *Canadian Journal of Fisheries and Aquatic Sciences*, *62*(6), 1320–1336. doi: 10.1139/f05-114

McKay, D. I. A., Staal, A., Abrams, J. F., Winkelmann, R., Sakschewski, B., Loriani, S., ... Lenton, T. M. (2022). Exceeding 1.5°C global warming could trigger multiple climate tipping points. *Science*, *377*(6611), eabn7950. doi: 10.1126/science.abn7950

Moore, C. M., Mills, M. M., Arrigo, K. R., Berman-Frank, I., Bopp, L., Boyd, P. W., ... Ulloa, O. (2013). Processes and patterns of oceanic nutrient limitation. *Nature Geoscience*, *6*(9), 701–710. doi: 10.1038/ngeo1765

Moore, J. K., Doney, S. C., Kleypas, J. A., Glover, D. M., & Fung, I. Y. (2001). An intermediate complexity marine ecosystem model for the global domain. *Deep Sea Research Part II: Topical Studies in Oceanography*, *49*(1), 403–462. doi: https://doi.org/10.1016/S0967-0645(01)00108-4

Moore, J. K., Doney, S. C., & Lindsay, K. (2004, dec). Upper ocean ecosystem dynamics and iron cycling in a global three-dimensional model. *Global Biogeochemical Cycles*, *18*(4). doi: https://doi.org/10.1029/2004GB002220

Moore, J. K., Lindsay, K., Doney, S. C., Long, M. C., & Misumi, K. (2013). Marine Ecosystem Dynamics and Biogeochemical Cycling in the Community Earth System Model [CESM1(BGC)]: Comparison of the 1990s with the 2090s under the RCP4.5 and RCP8.5 Scenarios. *Journal of Climate*, *26*(23), 9291–9312. doi: https://doi.org/10.1175/JCLI-D-12-00566.1

Orihuela-Pinto, B., England, M. H., & Taschetto, A. S. (2022). Interbasin and interhemispheric impacts of a collapsed Atlantic Overturning Circulation. *Nature Climate Change*, *12*(6), 558–565. doi: 10.1038/s41558-022-01380-y

Sampaio, E., Santos, C., Rosa, I. C., Ferreira, V., Pörtner, H.-O., Duarte, C. M., … Rosa, R. (2021). Impacts of hypoxic events surpass those of future ocean warming and acidification. *Nature Ecology & Evolution*, *5*(3), 311–321. doi: 10.1038/s41559-020-01370-3

Sanders, R., Henson, S. A., Koski, M., De La Rocha, C. L., Painter, S. C., Poulton, A. J., … Martin, A. P. (2014). The Biological Carbon Pump in the North Atlantic. *Progress in Oceanography*, *129*, 200–218. doi: https://doi.org/10.1016/j.pocean.2014.05.005

Schmittner, A. (2005). Decline of the marine ecosystem caused by a reduction in the Atlantic overturning circulation. *Nature*, *434*(7033), 628–633. doi: 10.1038/nature03476

Smale, D. A., Wernberg, T., Oliver, E. C. J., Thomsen, M., Harvey, B. P., Straub, S. C., … Moore, P. J. (2019). Marine heatwaves threaten global biodiversity and the provision of ecosystem services. *Nature Climate Change*, *9*(4), 306–312. doi: 10.1038/s41558-019-0412-1

Smith, R., Jones, P. W., Briegleb, P. A., Bryan, O., Danabasoglu, G., Dennis, M. L., … Yeager, S. G. (2010). The Parallel Ocean Program (POP) reference manual: Ocean component of the Community Climate System Model (CCSM)..

Tagliabue, A., Kwiatkowski, L., Bopp, L., Butenschön, M., Cheung, W., Lengaigne, M., & Vialard, J. (2021). Persistent Uncertainties in Ocean Net Primary Production Climate Change Projections at Regional Scales Raise Challenges for Assessing Impacts on Ecosystem Services. *Frontiers in Climate*, *3*. doi: 10.3389/fclim.2021.738224

Tittensor, D. P., Eddy, T. D., Lotze, H. K., Galbraith, E. D., Cheung, W., Barange, M., … Walker, N. D. (2018). A protocol for the intercomparison of marine fishery\hack{\break} and ecosystem models: Fish-MIP v1.0. *Geoscientific Model Development*, *11*(4), 1421–1442. doi: 10.5194/gmd-11-1421-2018

Tittensor, D. P., Novaglio, C., Harrison, C. S., Heneghan, R. F., Barrier, N., Bianchi, D., … Blanchard, J. L. (2021). Next-generation ensemble projections reveal higher climate risks for marine ecosystems. *Nature Climate Change*, *11*(11), 973–981. doi: 10.1038/s41558-021-01173-9

van Westen, R. M., & Dijkstra, H. A. (2023a). Asymmetry of AMOC Hysteresis in a State-Of-The-Art Global Climate Model. *Geophysical Research Letters*, *50*(22), e2023GL106088. doi: https://doi.org/10.1029/2023GL106088

van Westen, R. M., & Dijkstra, H. A. (2023b). Persistent Climate Model Biases in the Atlantic Ocean's Freshwater Transport. *EGUsphere*, *2023*, 1–29. doi: 10.5194/egusphere-2023-1502

van Westen, R. M., Kliphuis, M., & Dijkstra, H. A. (2024). Physics-based early warning signal shows that AMOC is on tipping course. *Science Advances*, *10*(6), eadk1189. doi: 10.1126/sciadv.adk1189

Walters, C. J., & Juanes, F. (1993). Recruitment Limitation as a Consequence of Natural Selection for Use of Restricted Feeding Habitats and Predation Risk Taking by Juvenile Fishes. *Canadian Journal of Fisheries and Aquatic Sciences*, *50*(10), 2058–2070. doi: 10.1139/f93-229

Weijer, W., Cheng, W., Drijfhout, S. S., Fedorov, A. V., Hu, A., Jackson, L. C., ... Zhang, J. (2019, aug). Stability of the Atlantic Meridional Overturning Circulation: A Review and Synthesis. *Journal of Geophysical Research: Oceans*, *124*(8), 5336–5375. doi: https://doi.org/10.1029/2019JC015083

Weijer, W., Cheng, W., Garuba, O. A., Hu, A., & Nadiga, B. T. (2020, jun). CMIP6 Models Predict Significant 21st Century Decline of the Atlantic Meridional Overturning Circulation. *Geophysical Research Letters*, *47*(12), e2019GL086075. doi: https://doi.org/10.1029/2019GL086075

Worthington, E. L., Moat, B. I., Smeed, D. A., Mecking, J. V., Marsh, R., & McCarthy, G. D. (2021). A 30-year reconstruction of the Atlantic meridional overturning circulation shows no decline. *Ocean Science*, *17*(1), 285–299. doi: 10.5194/os-17-285-2021

Zickfeld, K., Eby, M., & Weaver, A. J. (2008, sep). Carbon-cycle feedbacks of changes in the Atlantic meridional overturning circulation under future atmospheric CO2. *Global Biogeochemical Cycles*, *22*(3). doi: https://doi.org/10.1029/2007GB003118

Supporting Information for "Global marine ecosystem response to a strong AMOC weakening under low and high future emission scenarios"

A. A. Boot[1], J. Steenbeek[2], M. Coll[2,3], A. S. von der Heydt[1,4], and H. A. Dijkstra[1,4]

[1]Institute for Marine and Atmospheric research Utrecht, Department of Physics,Utrecht University, Utrecht, the Netherlands

[2]Ecopath International Initiative (EII) Research Association, Barcelona, Spain

[3]Department of Marine Renewal Resources, Institute of Marine Science (ICM-CSIC), Barcelona, Spain

[4]Center for Complex Systems Studies, Utrecht University, Utrecht, the Netherlands

Contents of this file

Corresponding author: Amber A. Boot, Institute for Marine and Atmospheric Research Utrecht, Utrecht University, Princetonplein 8, 35844CC Utrecht, the Netherlands. (a.a.boot@uu.nl)

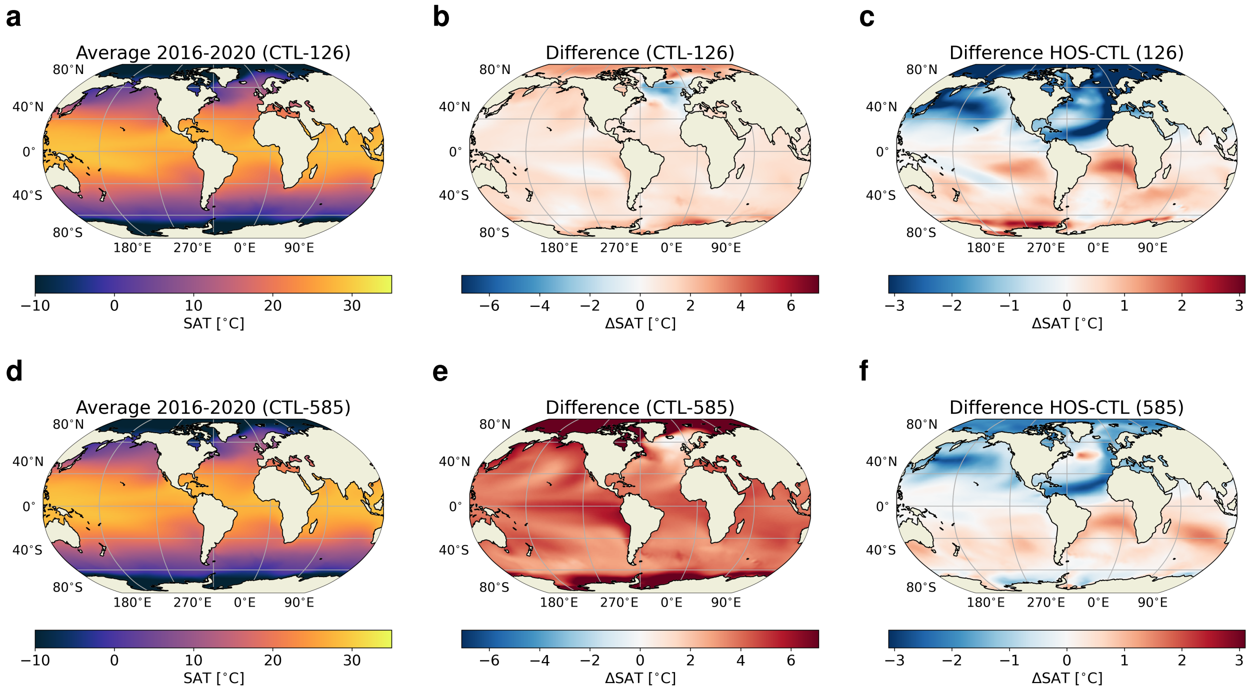

Figure S1. Surface Air Temperature (SAT) in °C for: (a) CTL-126 averaged over 2016-2020, (b) the average over 2016-2020 subtracted from the average over 2095-2099 in CTL-126, (c) CTL-126 subtracted from HOS-126 averaged over 2095-2099, and (d-f) as in (a-c) but for CTL-585 and HOS-585.

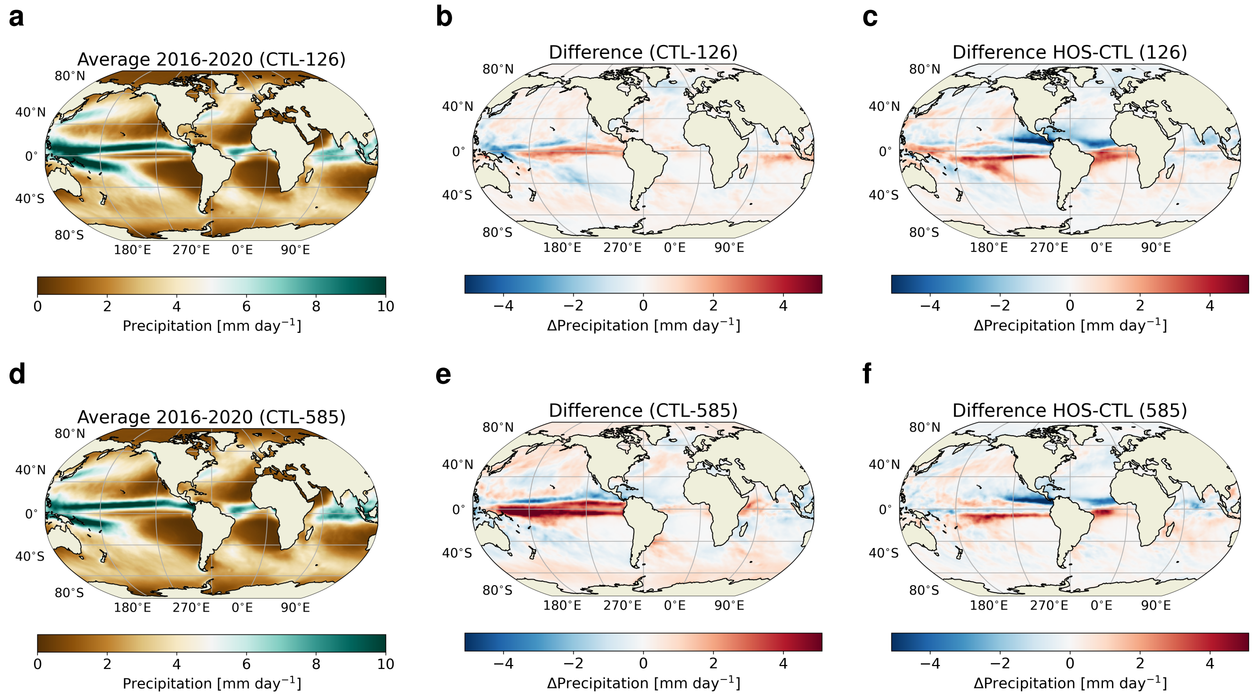

Figure S2. Precipitation in mm day^{-1} for: (a) CTL-126 averaged over 2016-2020, (b) the average over 2016-2020 subtracted from the average over 2095-2099 in CTL-126, (c) CTL-126 subtracted from HOS-126 averaged over 2095-2099, and (d-f) as in (a-c) but for CTL-585 and HOS-585.

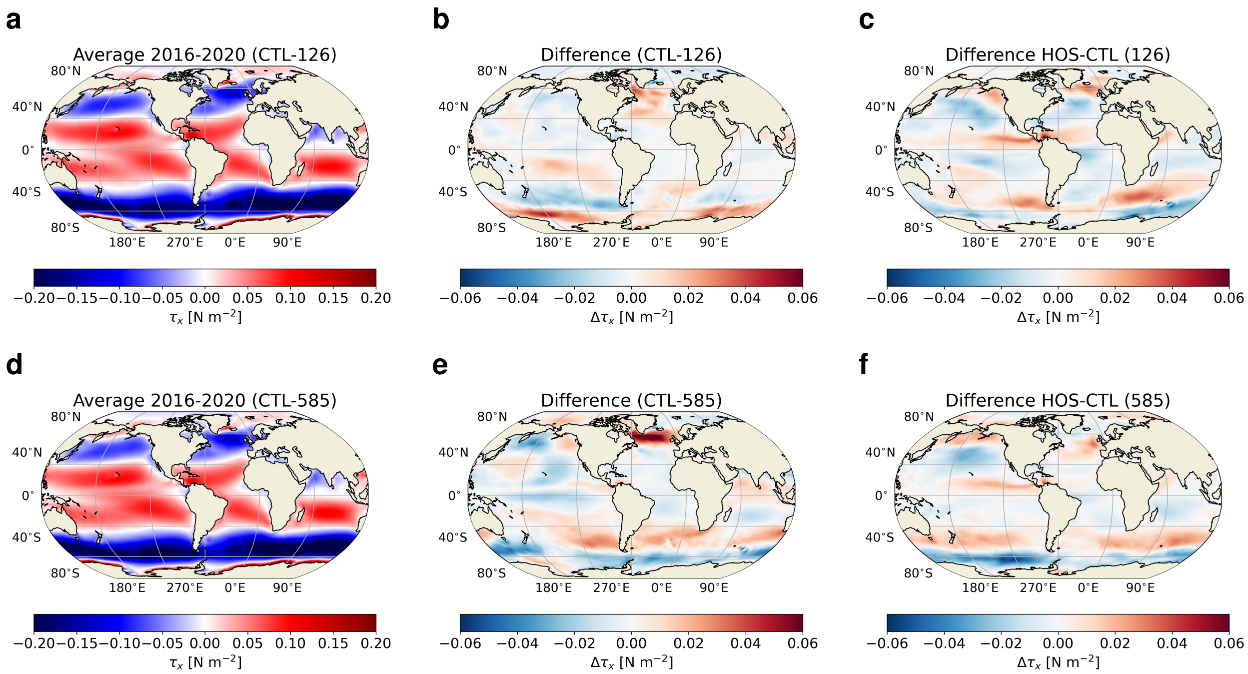

Figure S3. Zonal surface wind stress in N m^{-2} for: (a) CTL-126 averaged over 2016-2020, (b) the average over 2016-2020 subtracted from the average over 2095-2099 in CTL-126, (c) CTL-126 subtracted from HOS-126 averaged over 2095-2099, and (d-f) as in (a-c) but for CTL-585 and HOS-585.

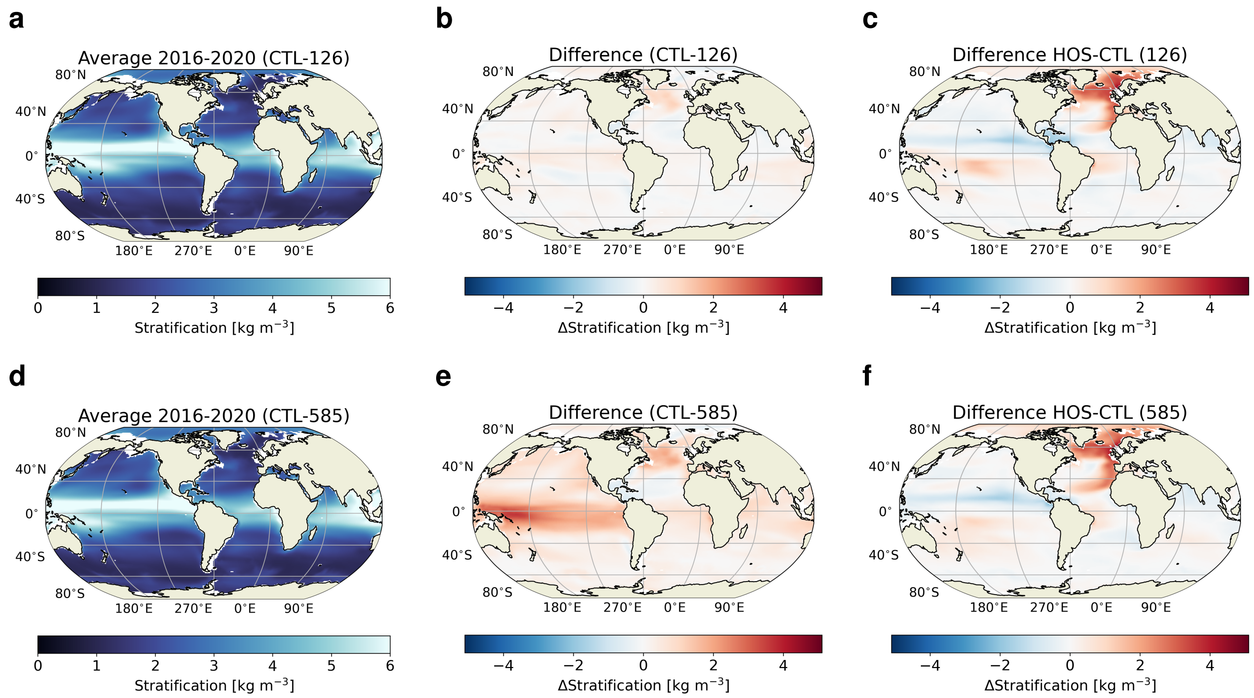

Figure S4. Stratification, defined as the density difference between 200 m depth and the surface, in kg m^{-3} for: (a) CTL-126 averaged over 2016-2020, (b) the average over 2016-2020 subtracted from the average over 2095-2099 in CTL-126, (c) CTL-126 subtracted from HOS-126 averaged over 2095-2099, and (d-f) as in (a-c) but for CTL-585 and HOS-585.

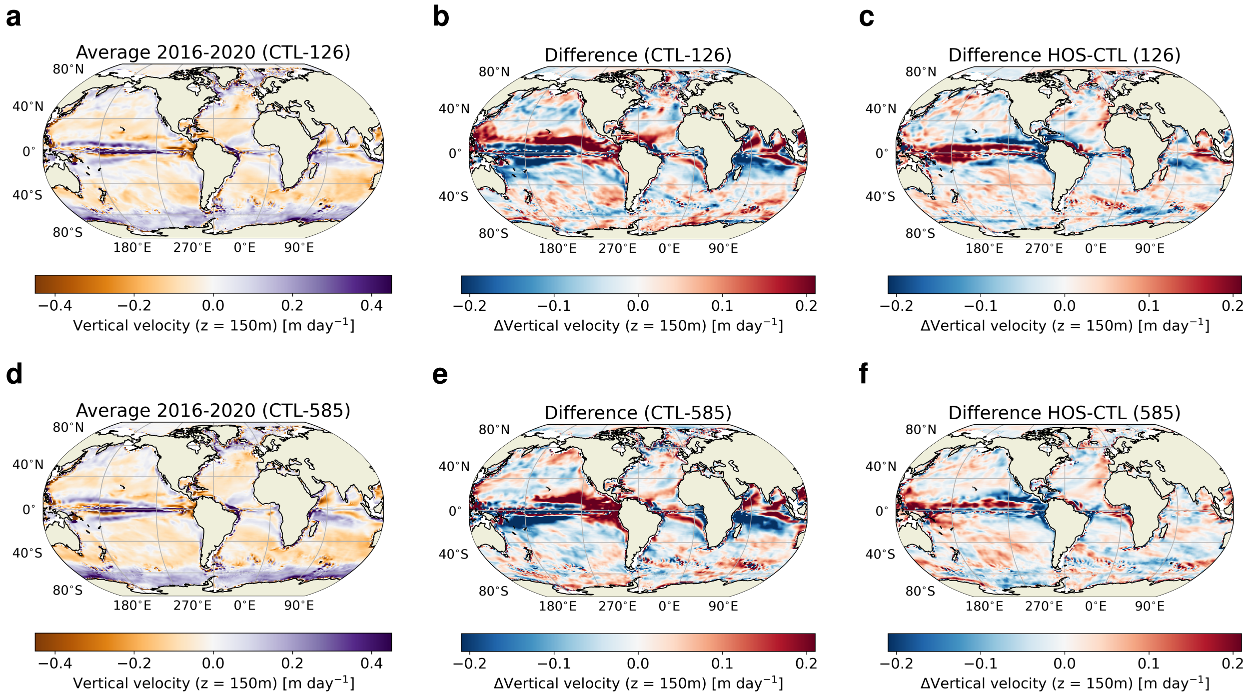

Figure S5. Upwelling velocity at 150 m in m day^{-1} for: (a) CTL-126 averaged over 2016-2020, (b) the average over 2016-2020 subtracted from the average over 2095-2099 in CTL-126, (c) CTL-126 subtracted from HOS-126 averaged over 2095-2099, and (d-f) as in (a-c) but for CTL-585 and HOS-585.

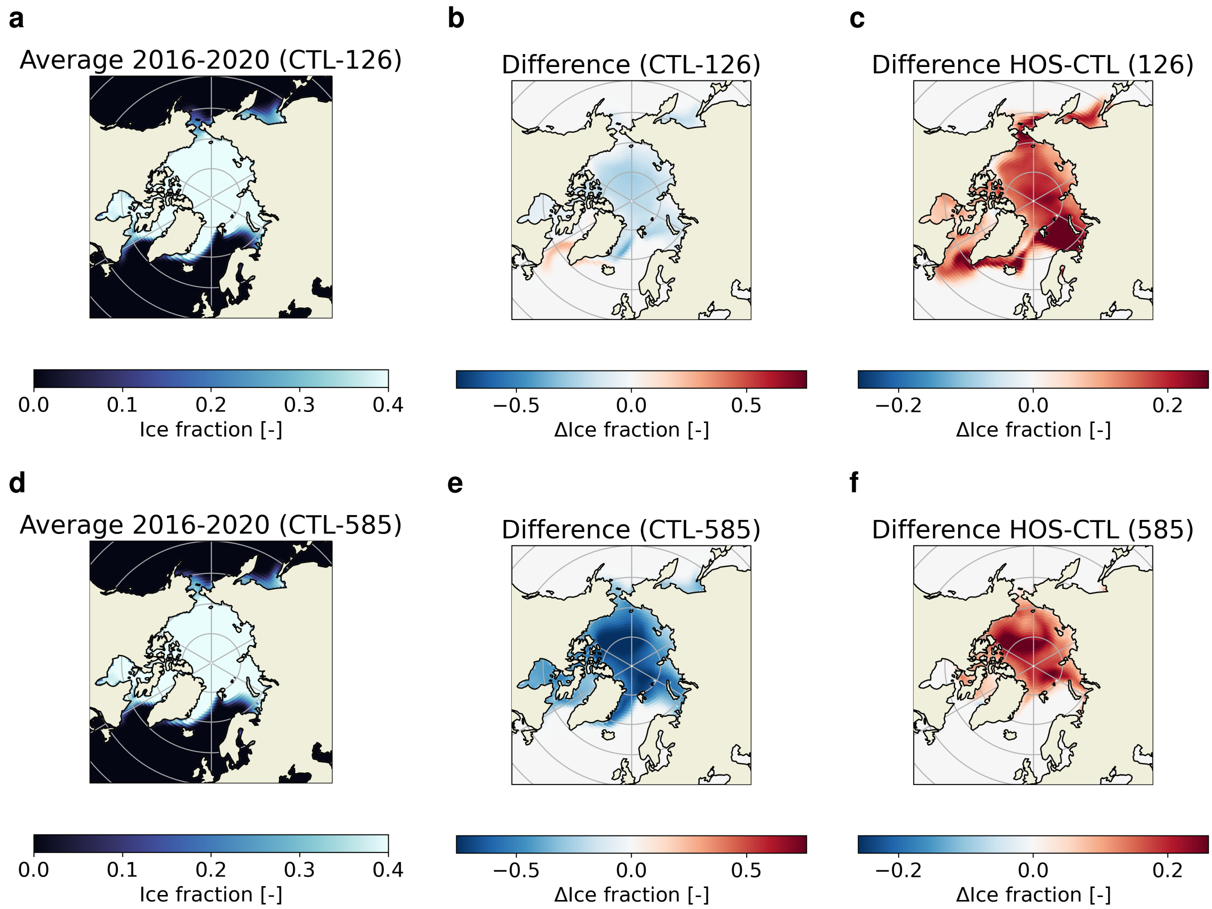

Figure S6. Arctic sea-ice fraction (unitless) for: (a) CTL-126 averaged over 2016-2020, (b) the average over 2016-2020 subtracted from the average over 2095-2099 in CTL-126, (c) CTL-126 subtracted from HOS-126 averaged over 2095-2099, and (d-f) as in (a-c) but for CTL-585 and HOS-585.

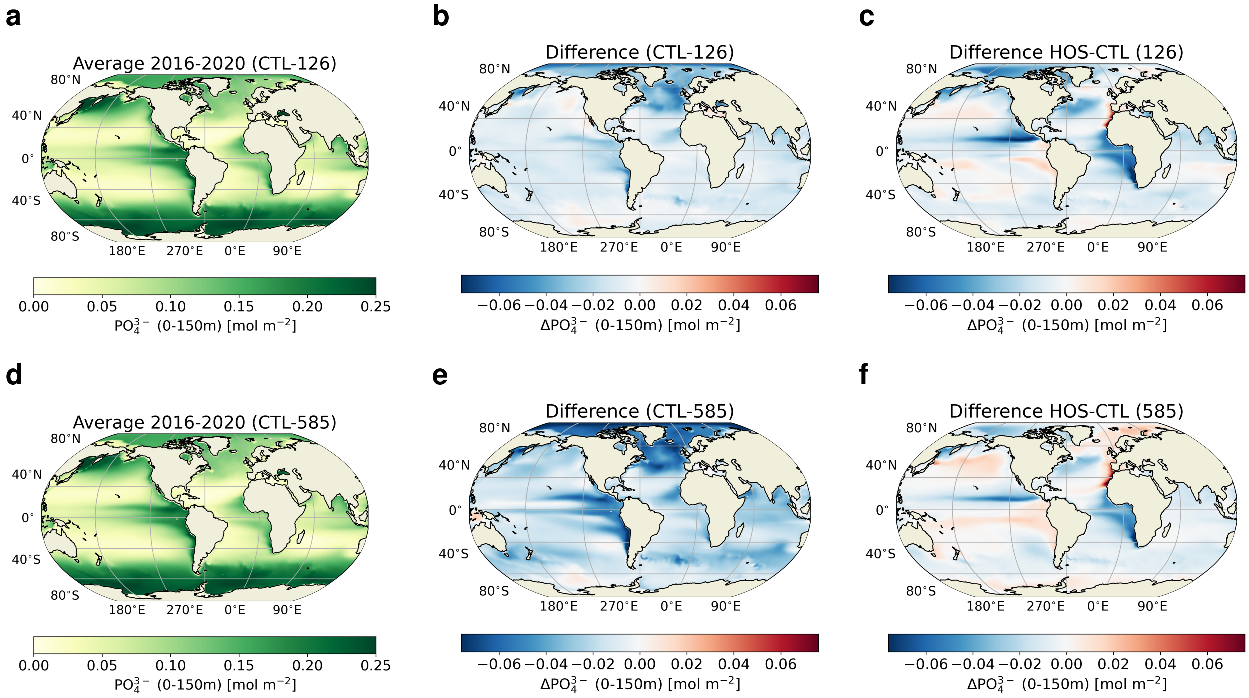

Figure S7. Phosphate (PO_4^{3-}) concentrations integrated over the top 150 m in mol m^{-2} for: (a) CTL-126 averaged over 2016-2020, (b) the average over 2016-2020 subtracted from the average over 2095-2099 in CTL-126, (c) CTL-126 subtracted from HOS-126 averaged over 2095-2099, and (d-f) as in (a-c) but for CTL-585 and HOS-585.

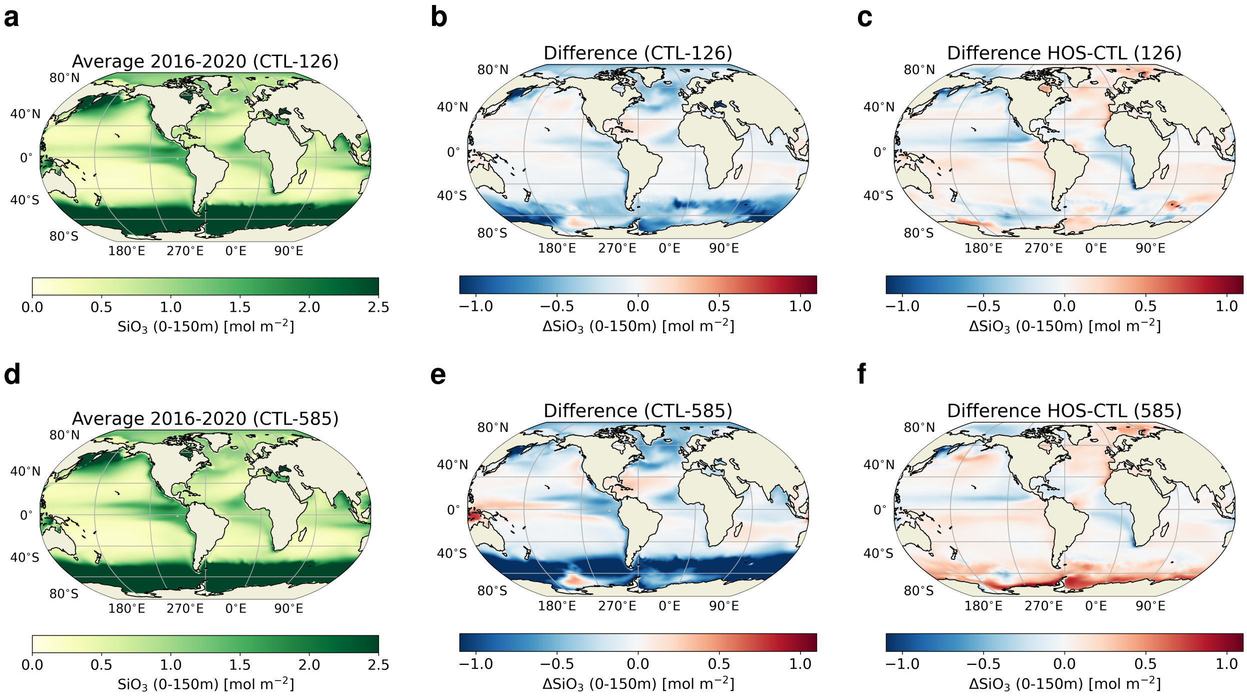

Figure S8. Silicate (SiO_3^{2-}) concentrations integrated over the top 150 m in mol m^{-2} for: (a) CTL-126 averaged over 2016-2020, (b) the average over 2016-2020 subtracted from the average over 2095-2099 in CTL-126, (c) CTL-126 subtracted from HOS-126 averaged over 2095-2099, and (d-f) as in (a-c) but for CTL-585 and HOS-585.

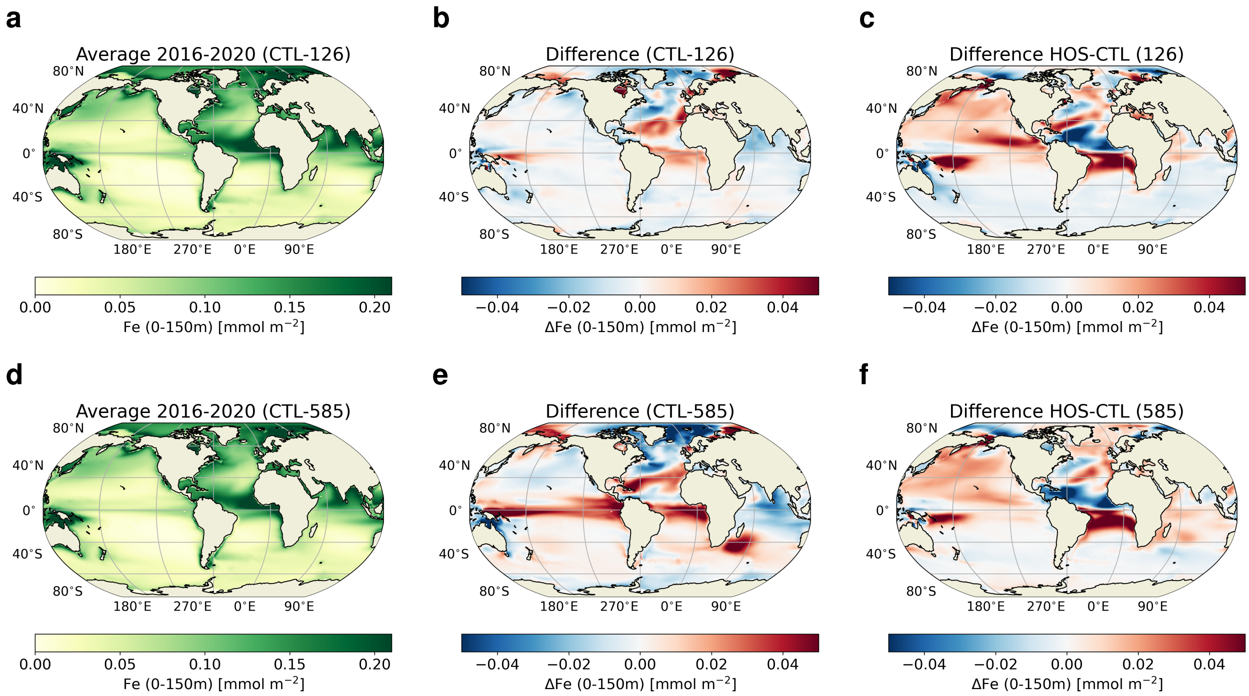

Figure S9. Iron (Fe) concentrations integrated over the top 150 m in mmol m^{-2} for: (a) CTL-126 averaged over 2016-2020, (b) the average over 2016-2020 subtracted from the average over 2095-2099 in CTL-126, (c) CTL-126 subtracted from HOS-126 averaged over 2095-2099, and (d-f) as in (a-c) but for CTL-585 and HOS-585.

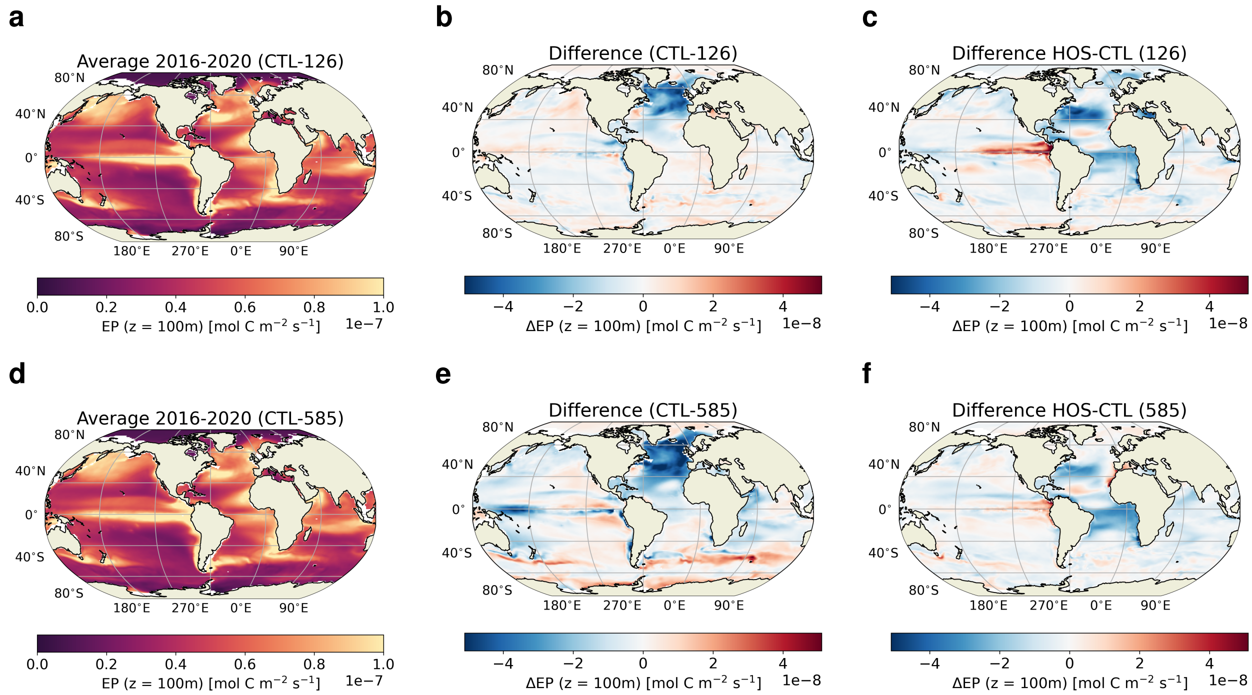

Figure S10. Export production at 100 m depth in mol C m^{-2} s^{-1} for: (a) CTL-126 averaged over 2016-2020, (b) the average over 2016-2020 subtracted from the average over 2095-2099 in CTL-126, (c) CTL-126 subtracted from HOS-126 averaged over 2095-2099, and (d-f) as in (a-c) but for CTL-585 and HOS-585.

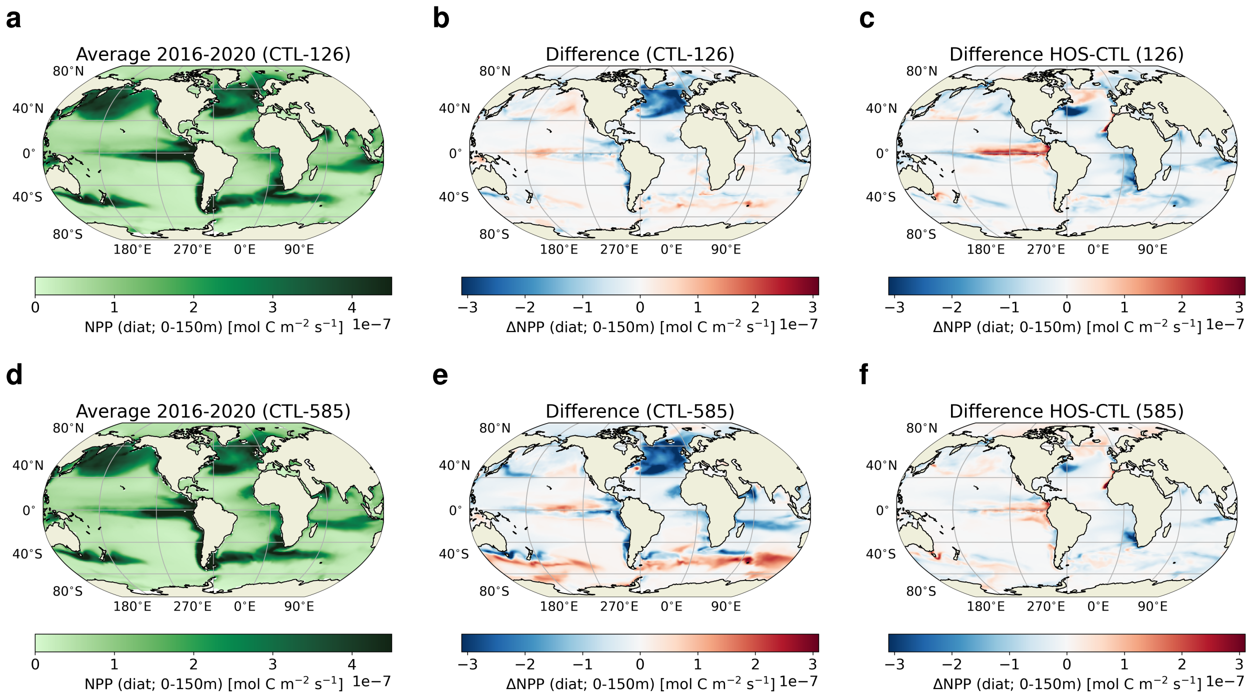

Figure S11. Net Primary Production of diatoms integrated over the top 150 m in mol C m^{-2} s^{-1} for: (a) CTL-126 averaged over 2016-2020, (b) the average over 2016-2020 subtracted from the average over 2095-2099 in CTL-126, (c) CTL-126 subtracted from HOS-126 averaged over 2095-2099, and (d-f) as in (a-c) but for CTL-585 and HOS-585.

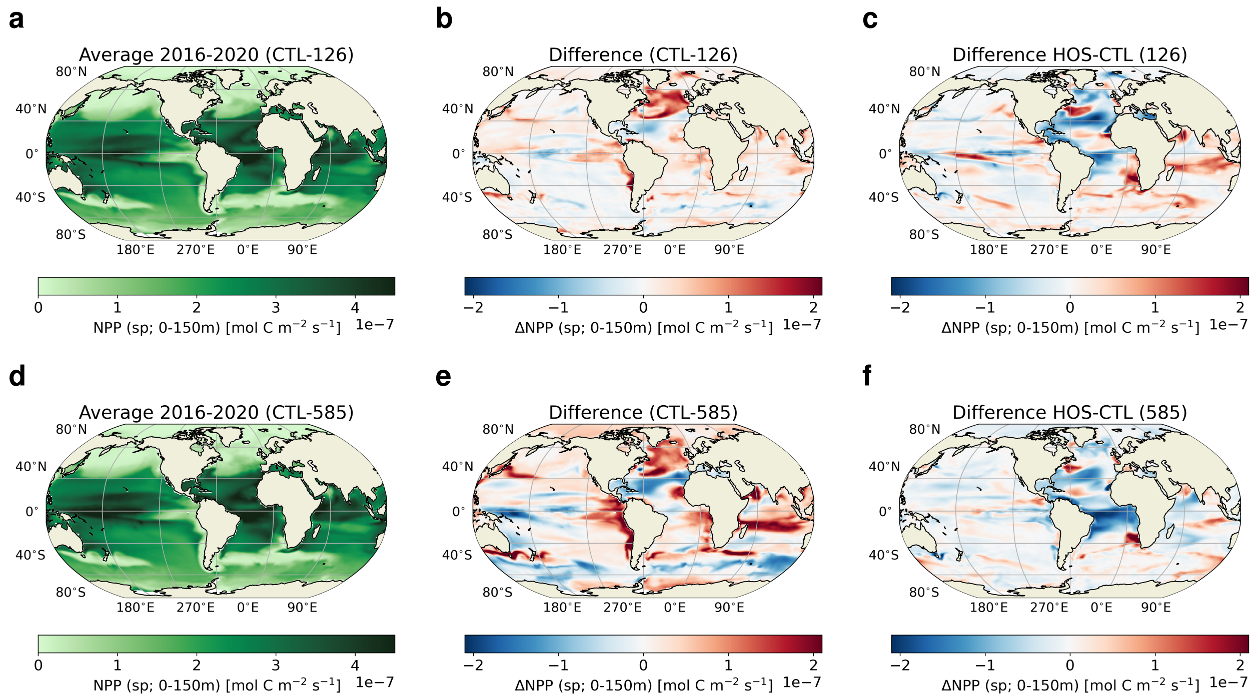

Figure S12. Net Primary Production of small phytoplankton integrated over the top 150 m in mol C m^{-2} s^{-1} for: (a) CTL-126 averaged over 2016-2020, (b) the average over 2016-2020 subtracted from the average over 2095-2099 in CTL-126, (c) CTL-126 subtracted from HOS-126 averaged over 2095-2099, and (d-f) as in (a-c) but for CTL-585 and HOS-585.

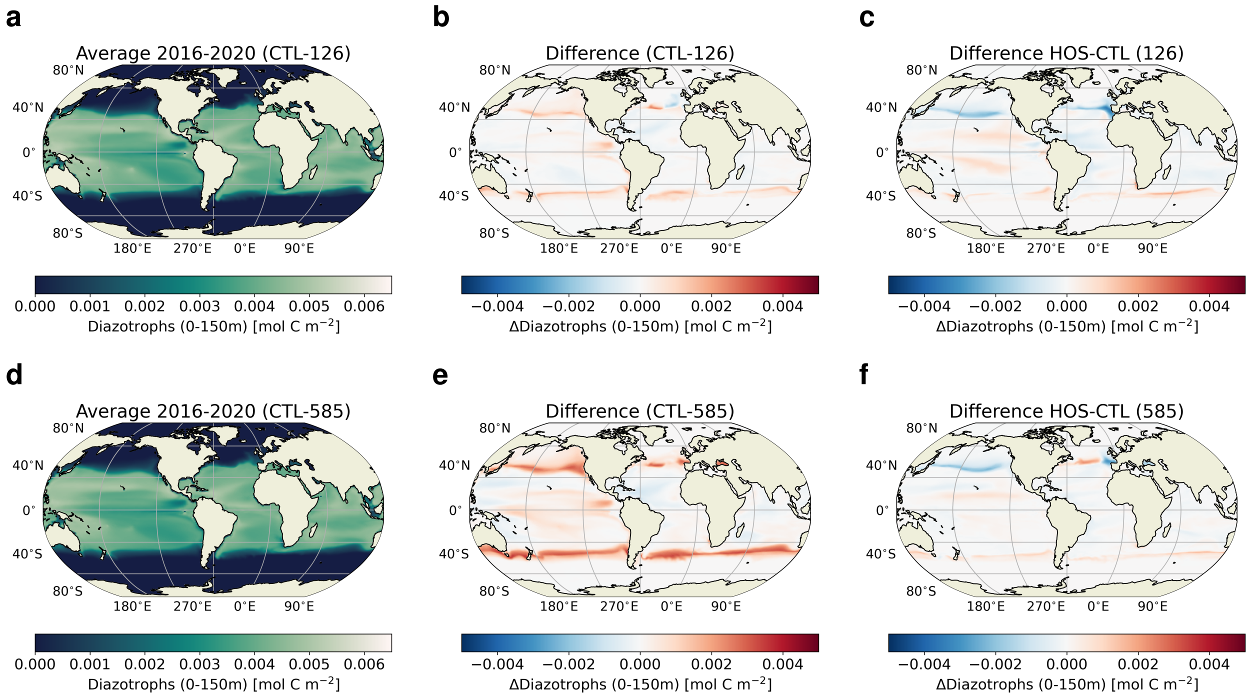

Figure S13. Diazotroph biomass integrated over the top 150 m in mol C m^{-2} for: (a) CTL-126 averaged over 2016-2020, (b) the average over 2016-2020 subtracted from the average over 2095-2099 in CTL-126, (c) CTL-126 subtracted from HOS-126 averaged over 2095-2099, and (d-f) as in (a-c) but for CTL-585 and HOS-585.

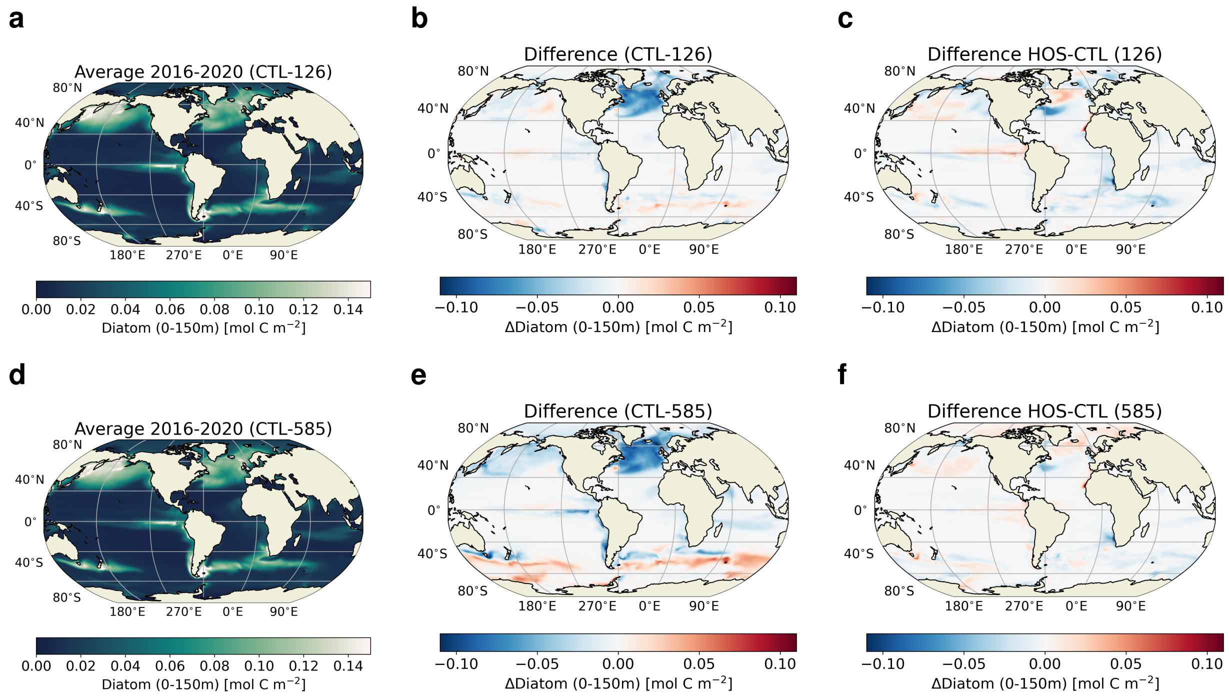

Figure S14. Diatom biomass integrated over the top 150 m in mol C m^{-2} for: (a) CTL-126 averaged over 2016-2020, (b) the average over 2016-2020 subtracted from the average over 2095-2099 in CTL-126, (c) CTL-126 subtracted from HOS-126 averaged over 2095-2099, and (d-f) as in (a-c) but for CTL-585 and HOS-585.

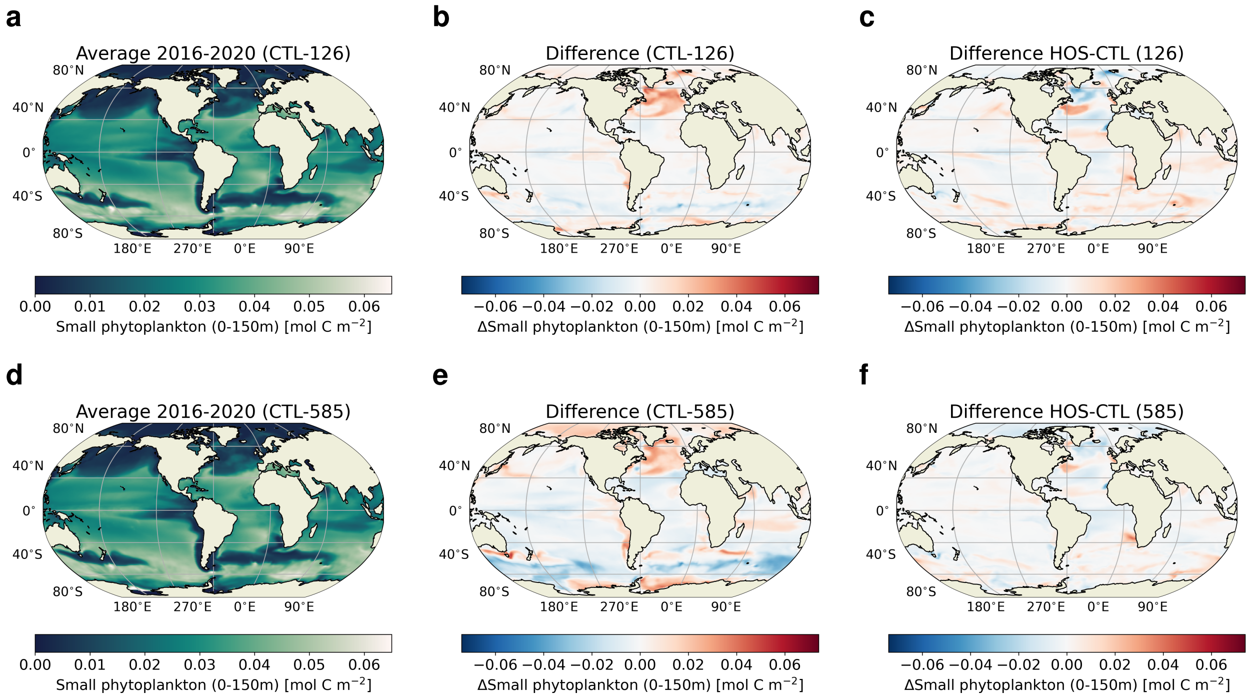

Figure S15. Small phytoplankton biomass integrated over the top 150 m in mol C m^{-2} for: (a) CTL-126 averaged over 2016-2020, (b) the average over 2016-2020 subtracted from the average over 2095-2099 in CTL-126, (c) CTL-126 subtracted from HOS-126 averaged over 2095-2099, and (d-f) as in (a-c) but for CTL-585 and HOS-585.

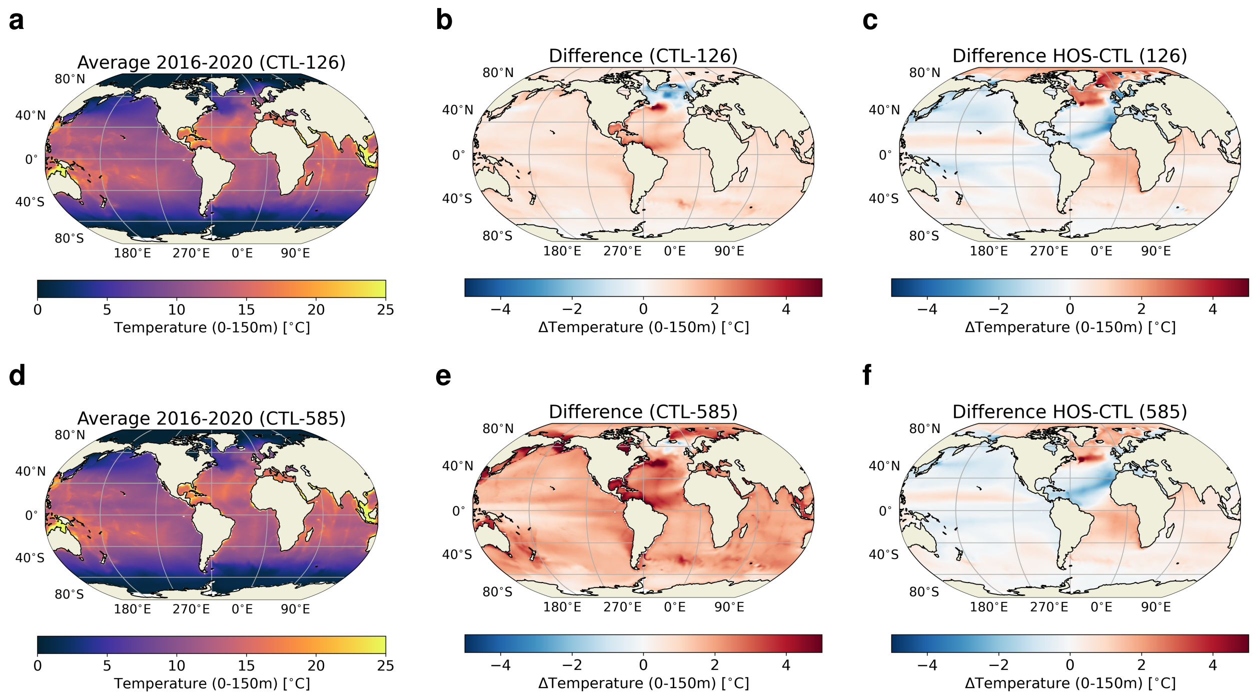

Figure S16. Temperature averaged over the top 150 m of the ocean in °C for: (a) CTL-126 averaged over 2016-2020, (b) the average over 2016-2020 subtracted from the average over 2095-2099 in CTL-126, (c) CTL-126 subtracted from HOS-126 averaged over 2095-2099, and (d-f) as in (a-c) but for CTL-585 and HOS-585.

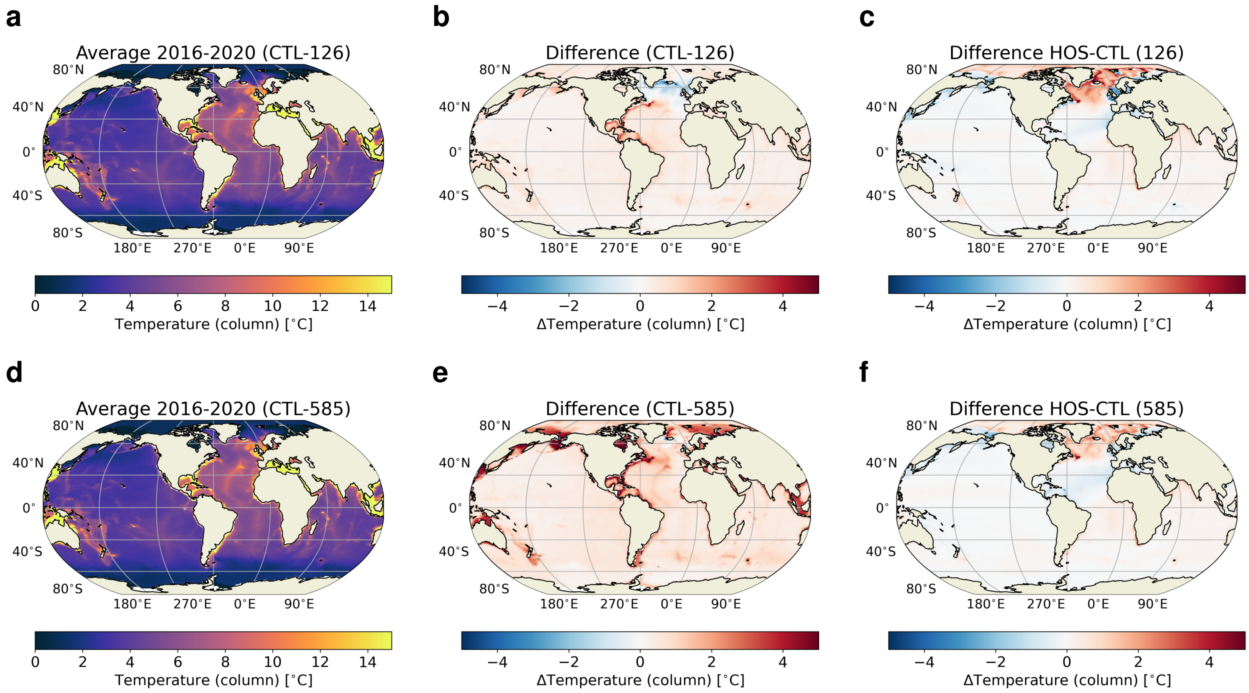

Figure S17. Temperature averaged over the entire water column in °C for: (a) CTL-126 averaged over 2016-2020, (b) the average over 2016-2020 subtracted from the average over 2095-2099 in CTL-126, (c) CTL-126 subtracted from HOS-126 averaged over 2095-2099, and (d-f) as in (a-c) but for CTL-585 and HOS-585.

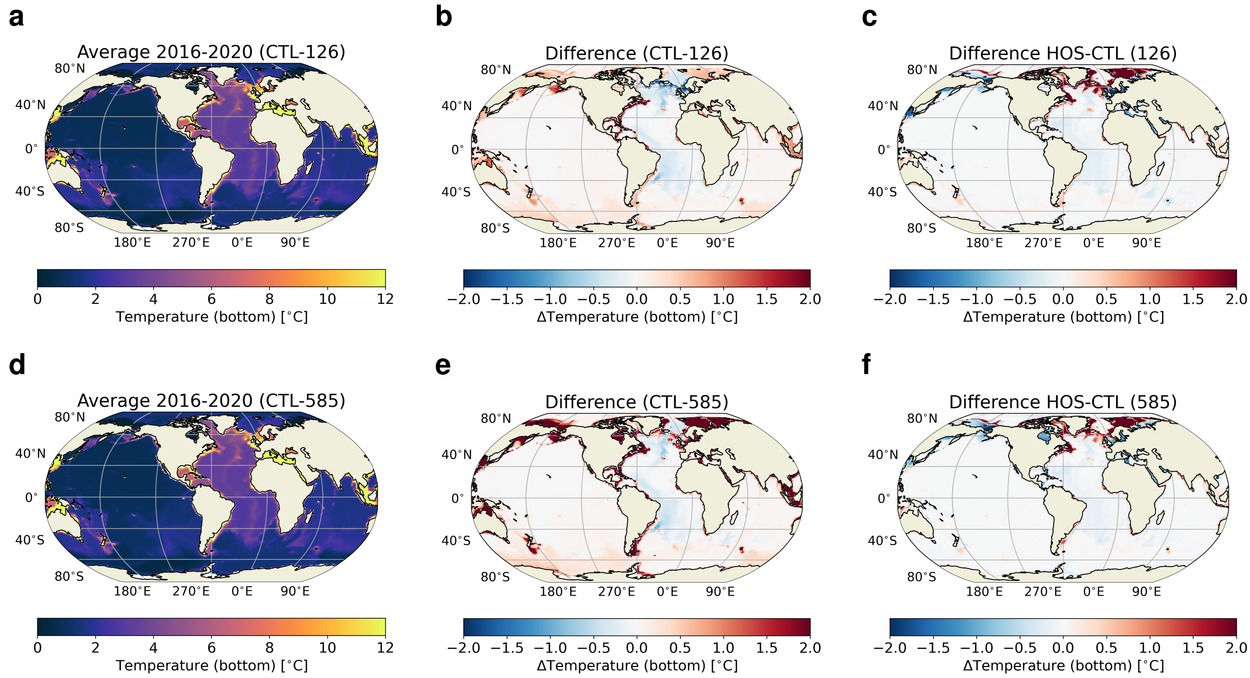

Figure S18. Bottom temperature in °C for: (a) CTL-126 averaged over 2016-2020, (b) the average over 2016-2020 subtracted from the average over 2095-2099 in CTL-126, (c) CTL-126 subtracted from HOS-126 averaged over 2095-2099, and (d-f) as in (a-c) but for CTL-585 and HOS-585.

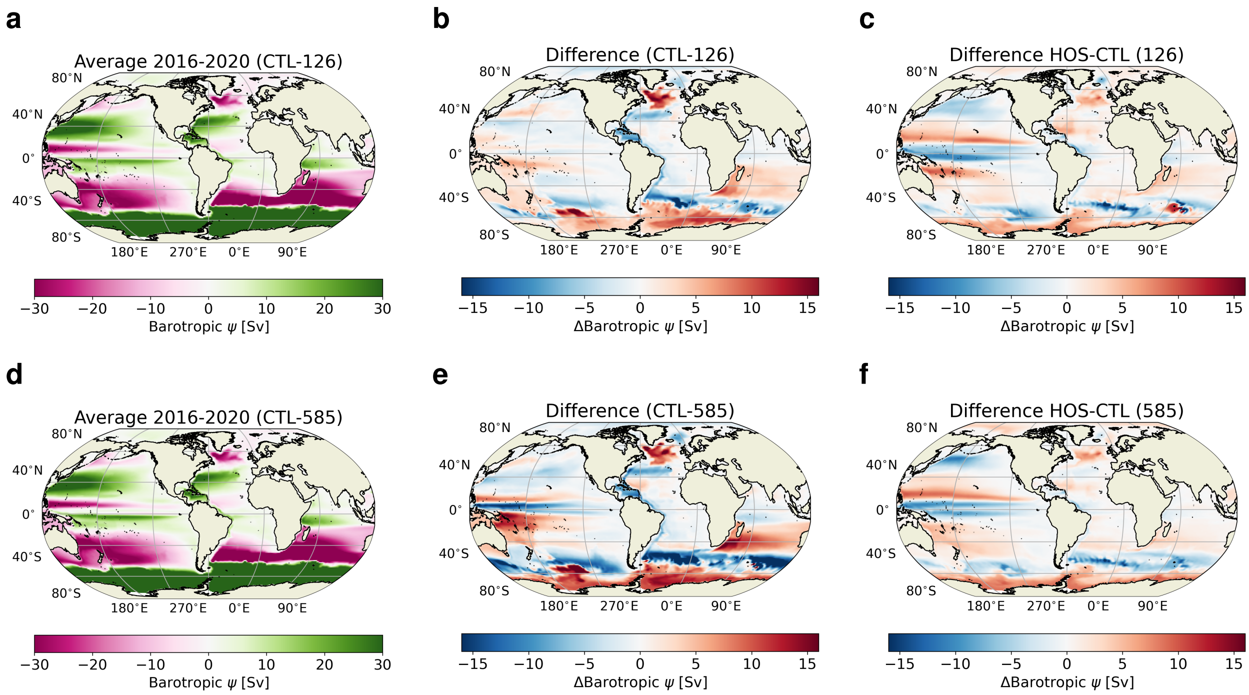

Figure S19. Barotropic stream function (BSF) in Sv for: (a) CTL-126 averaged over 2016-2020, (b) the average over 2016-2020 subtracted from the average over 2095-2099 in CTL-126, (c) CTL-126 subtracted from HOS-126 averaged over 2095-2099, and (d-f) as in (a-c) but for CTL-585 and HOS-585.

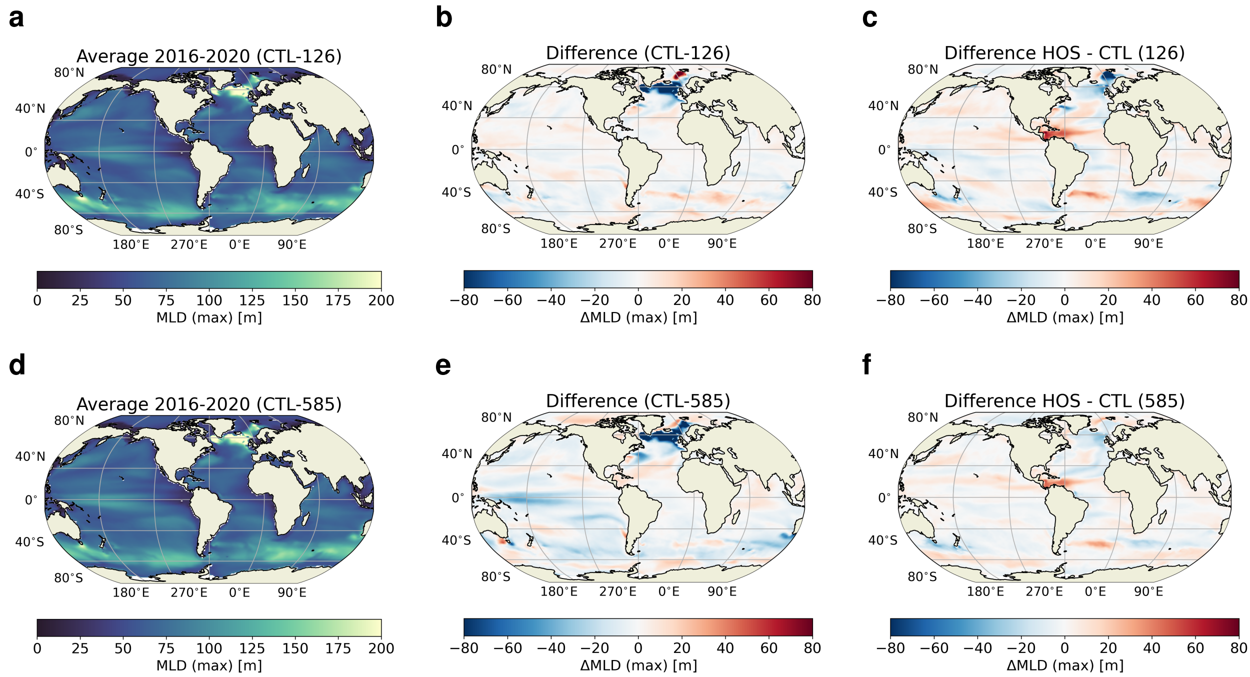

Figure S20. Maximum mixed layer depth (MLD) in m for: (a) CTL-126 averaged over 2016-2020, (b) the average over 2016-2020 subtracted from the average over 2095-2099 in CTL-126, (c) CTL-126 subtracted from HOS-126 averaged over 2095-2099, and (d-f) as in (a-c) but for CTL-585 and HOS-585.

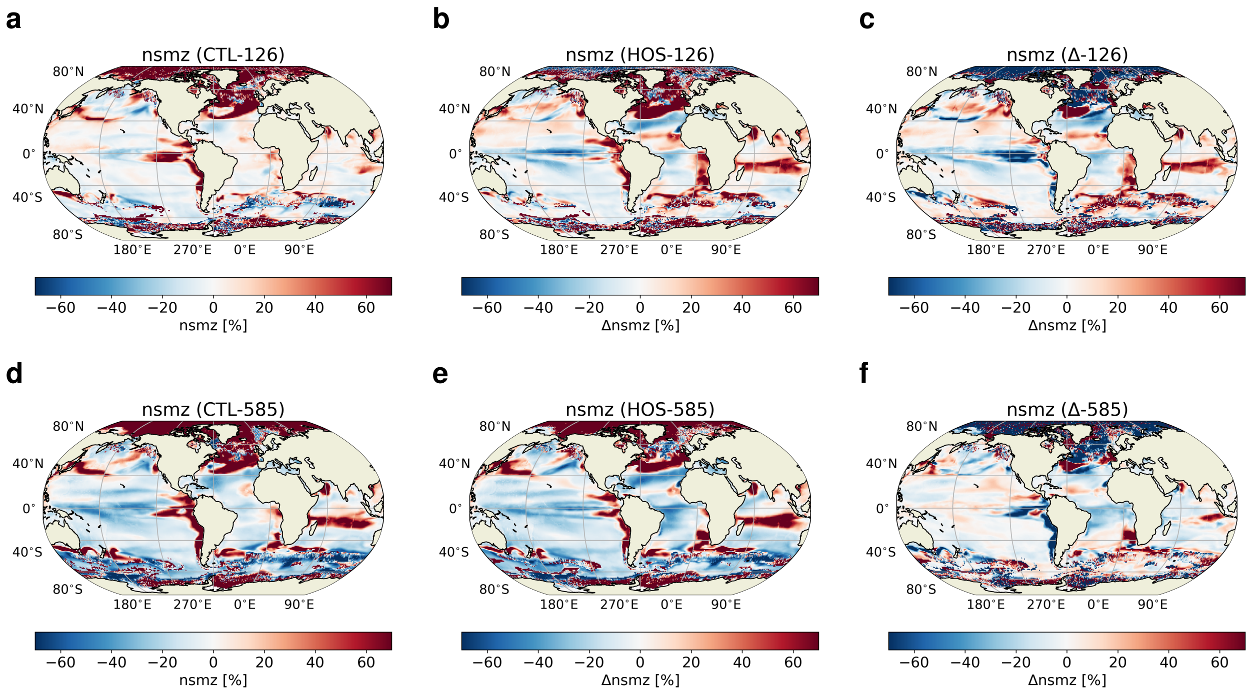

Figure S21. Relative changes averaged over 2095-2099 compared to 2016-2020 in % for microzooplankton (nsmz) in the CTL simulations (a, d), HOS simulations (b, e), and the difference between the two (c, f). (a-c) are for SSP1-2.6 and (d-f) are fore SSP5-8.5.

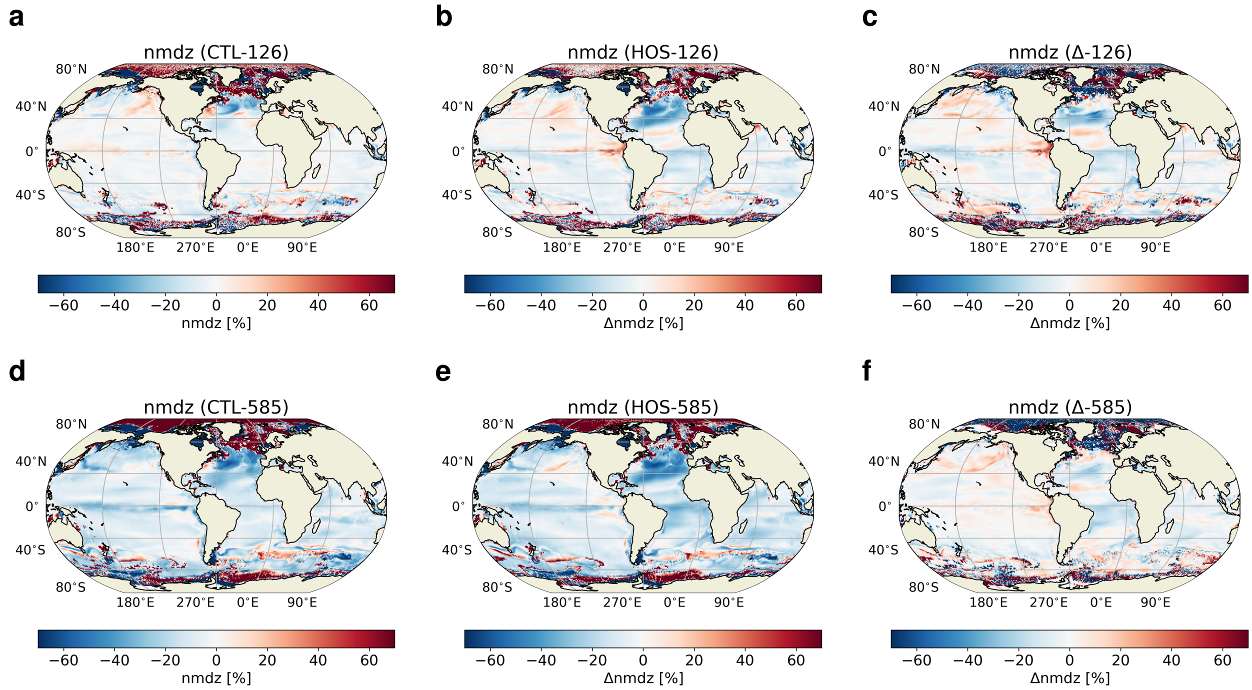

Figure S22. Relative changes averaged over 2095-2099 compared to 2016-2020 in % for meso-zooplankton (nmdz) in the CTL simulations (a, d), HOS simulations (b, e), and the difference between the two (c, f). (a-c) are for SSP1-2.6 and (d-f) are fore SSP5-8.5.

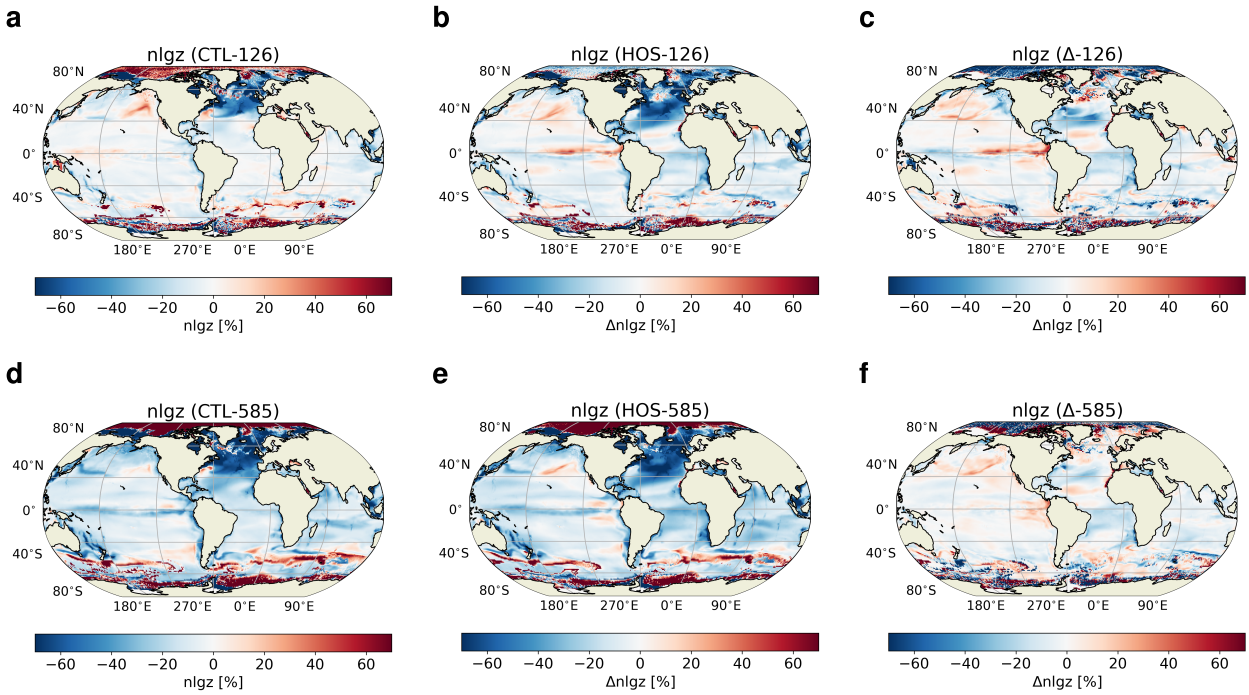

Figure S23. Relative changes averaged over 2095-2099 compared to 2016-2020 in % for large zooplankton (krill; nlgz) in the CTL simulations (a, d), HOS simulations (b, e), and the difference between the two (c, f). (a-c) are for SSP1-2.6 and (d-f) are fore SSP5-8.5.

Table S1. Relative change in % of total phytoplankton (TP), small phytoplankton (SP), diatom (DT) and diazotroph (DZ) biomass in 2099 for the difference between the HOS and CTL simulations for different regions in the ocean. Relative change is defined as in the main text as the difference in biomass between 2099 and 2015 divided by the biomass in 2015.

Region		TP		SP		DT		DZ	
		Δ-126	Δ-585	Δ-126	Δ-585	Δ-126	Δ-585	Δ-126	Δ-585
Arctic Ocean	66°N - 90°N	-21.4	7.64	-44.39	-42.35	-18.82	17.57	-4.74	83.19
Atlantic Ocean	40°N - 66°N	-4.18	-1.28	-71.06	-41.22	3.47	2.73	-45.15	10.54
	15°N - 40°N	-13.24	-5.53	-10.46	-4.24	-25.05	-9.58	-4.11	-1.97
	15°S - 15°N	-6.18	-6.56	-2.36	-10.44	-15.13	-0.12	-4.08	-2.96
	15°S - 40°S	-3.31	-6.84	17.66	10.41	-26.89	-27.84	0.12	-1.61
	40°S - 66°S	-6.27	1.32	15.53	-12.19	-15.76	7.12	16.47	9.41
Pacific Ocean	40°N - 66°N	2.13	-1.47	9.70	-1.66	1.75	-1.1	-70.96	-109.22
	15°N - 40°N	3.43	3.19	2.59	1.47	5.33	6.62	-3.76	-2.87
	15°S - 15°N	2.93	2.80	-3.08	-5.74	9.71	14.41	2.45	3.69
	15°S - 40°S	-6.74	0.17	-10.46	-1.33	0.30	4.00	1.41	0.45
	40°S - 66°S	-4.83	-1.04	2.44	-8.08	-16.36	7.23	36.93	86.38
Indian Ocean	North of 15°S	-3.49	-2.42	14.93	2.38	-31.46	-10.41	-0.50	-1.20
	15°N - 40°N	-2.30	-4.32	5.28	-3.66	-20.96	-7.57	1.03	1.37
	40°N - 66°N	-6.14	-1.86	-0.13	6.72	-14.12	-16.38	186.04	367.42
Southern Ocean	66°S - 90°S	-2.32	1.25	8.57	14.99	-18.25	-17.38	-11.16	-9.01